

Extension of the nodal code DYN3D to SFR applications

Thèse N° 7264

Présentée le 5 mars 2019

à la Faculté des sciences de base

Laboratoire de physique des réacteurs et de comportement des systèmes

Programme doctoral en énergie

pour l'obtention du grade de Docteur ès Sciences

par

EVGENY NIKITIN

Acceptée sur proposition du jury

Prof. J. Luterbacher, président du jury

Prof. A. Pautz, Dr E. Fridman, directeurs de thèse

Dr E. Shwageraus, rapporteur

Dr A. Rineiski, rapporteur

Prof. M. Quang Tran, rapporteur

2019

To my beloved wife Eszter.

Acknowledgements

First of all I would like to express my appreciation to Prof. Andreas Pautz, for supporting and overseeing my doctoral research. I owe to Dr. Emil Fridman my sincere gratitude for his guidance and encouragement from the very beginning, not only as my direct advisor, but also as my good friend.

I would like to sincerely thank Dr. Sören Kliem for his complete support, and for giving me the opportunity to work in his team. A special thanks goes to my colleagues, Dr. Yurii Bilodid, Dr. Polina Wilhelm and André Gommlich, for their willingness to help me, that they made everyday work enjoyable, and most especially, for their friendship. I am thankful to Dr. Konstantin Mikityuk for his collaboration and expert advice in fast reactor systems. I would also like to sincerely thank Cécile Tavernier for her assistance at EPFL, and that she made sure, I would not miss any important deadline.

The research was carried out at Helmholtz-Zentrum Dresden-Rossendorf and was partly supported by a project of the German Federal Ministry for Economic Affairs and Energy. The financial support is greatly appreciated.

At last but not least, I would like to thank my family for their love and unwavering support.

Lausanne, 10 October 2018

E. N.

Abstract

DYN3D is a well-established Light Water Reactor (LWR) simulation tool and is being extended for safety analyses of Sodium cooled Fast Reactors (SFRs) at the HZDR¹. This thesis focuses on the first stage of the development process, that is, the extension and application of DYN3D for steady-state and transient SFR calculations on reactor core level.

In contrast to LWRs, the SFR behavior is especially sensitive to thermal expansions of the reactor components. Therefore, a new thermal-mechanical module accounting for thermal expansions is implemented into DYN3D. At first step, this module is capable of treating two important thermal expansion effects occurring within the core, namely axial expansion of fuel rods and radial expansion of diagrid.

In order to perform nodal calculations with DYN3D, pre-generated homogenized few-group cross sections (XS) are necessarily needed. Therefore, prior to the development of thermal expansion models, a general methodology for XS generation is established for SFR nodal calculations based on the use of the Monte Carlo code Serpent.

The new methodological developments presented in this thesis are verified against the Monte Carlo solutions of Serpent. Two SFR cores are used for testing: the large oxide core of the OECD/NEA benchmark and a smaller core from the Phenix end-of-life tests. Finally, the extended DYN3D is validated against selected IAEA benchmark tests on the Phenix end-of-life experiments that contain both steady-state and transient calculations.

The contribution to the SFR-related developments at the HZDR, as presented in this thesis, makes it possible of performing steady-state and transient calculations for SFRs on reactor core level by using DYN3D. With this study, the basis of the next stage of DYN3D developments is established, that is, the up-scale of SFR analysis to system level can continue by coupling with a sodium capable thermal-hydraulic system code.

¹ Helmholtz-Zentrum Dresden-Rossendorf

Abstract

Key words: SFR, thermal expansion, group constant generation, nodal methods, spatial kinetics, Monte Carlo, Serpent, DYN3D

Kurzfassung

Der Code DYN3D ist der etablierte Kernsimulator für Leichtwasserreaktoren (LWR) am Helmholtz-Zentrum Dresden-Rossendorf (HZDR). Dieser soll für die Sicherheitsanalyse von natriumgekühlten schnellen Reaktoren (SFR) erweitert werden. Diese Arbeit konzentriert sich auf die erste Phase dieses Entwicklungsprozesses welche die Erweiterung und Anwendung von DYN3D für Berechnungen stationärer als auch transienten SFR Analysen auf Reaktorkernebene zum Inhalt hat.

Im Gegensatz zu Leichtwasserreaktoren ist das SFR Verhalten besonders empfindlich gegenüber thermischer Ausdehnung von Reaktorkomponenten. Daher wurden neue thermomechanische Modelle in DYN3D implementiert welche diese Wärmeausdehnungen berücksichtigen. Im ersten Schritt wurden diejenigen Modelle entwickelt, die die zwei wichtigsten Wärmeausdehnungseffekte innerhalb des Kerns behandeln. Dies betrifft die axial Ausdehnung der Brennstäbe und die radiale Ausdehnung der Kerntageplatte.

Um Diffusionsrechnungen auf nodaler Ebene mit DYN3D durchführen zu können, war die Erzeugung von Mehrgruppen Wirkungsquerschnittsdaten (XS) notwendig. Daher wurde, vor der Entwicklung der Ausdehnungsmodelle, eine allgemeine Methodik für die Erstellung von SFR-Querschnittsbibliotheken für nodale SFR Analysen mit Hilfe des Monte-Carlo Programm Serpent etabliert.

Die in dieser Arbeit vorgestellten Entwicklungen wurden gegen die mit Serpent berechneten Monte-Carlo Referenzlösungen verifiziert. Zum Testen wurden folgenden zwei SFR Kernkonfigurationen verwendet. Der große oxydische Kern des OECD/NEA Benchmark und ein kleinerer Kern aus den Experimenten zum Zyklusende des Phenix. Zur Validierung wurden schließlich mehrere Tests, die sowohl stationäre als auch transiente Fälle aus den Phenix-Experimenten enthalten, mit der erweiterten DYN3D Version berechnet.

Der Beitrag dieser Arbeit zur SFR bezogener Entwicklungen am HZDR ermöglicht nunmehr die Analyse von stationären und transienten SFR Fälle auf Reaktorkernebene mit Hilfe von DYN3D. Durch diese Studie wurde die Grundlage für die nächste

Abstract

Stufe der DYN3D Entwicklung geschaffen, welche die Erweiterung der SFR-Analyse auf Systemebene durch Kopplung mit einem Natrium-fähigen thermohydraulischen Systemcode beinhalten kann.

Schlüsselwörter: SFR, Wärmeausdehnung, Wirkungsquerschnittsdaten, Nodal Methoden, 3D-Neutronenkinetik, Monte Carlo, Serpent, DYN3D

Contents

Acknowledgements	i
Abstracts	iii
Contents	vii
List of figures	xi
List of tables	xiii
1 Introduction	1
1.1 The sodium cooled fast reactor technology	1
1.2 Computational analyses of SFR systems	6
1.3 The DYN3D code for SFR analyses	10
1.3.1 Extension of DYN3D to SFR applications	11
1.3.2 Preceding DYN3D developments and its application limits	11
1.4 Objectives of the study	13
1.5 Thesis outline	14
2 Generation of homogenized few-group cross sections	15
2.1 The Serpent code for XS generation	15
2.2 Reference core descriptions	17
2.2.1 Large oxide core from the OECD/NEA benchmark	17
2.2.2 Phenix End-of-Life core	18
2.3 General approach to XS generation for SFRs	21
2.4 Super-homogenization method for SFR analysis	24
2.5 Verification by means of code-to-code comparison	29
2.5.1 Results of the OECD/NEA large oxide core calculations	29
2.5.2 Cross-checking with PARCS code	33
2.5.3 Results of Phenix EOL core calculations	36
	vii

Contents

2.6	Few-group cross section generation – Summary of the results	39
3	Modeling of thermal expansions	41
3.1	Thermal expansion effects	41
3.1.1	Reactivity effect of thermally expanding materials	41
3.1.2	Thermal expansion feedbacks in SFR systems	45
3.1.3	Current trends for modeling thermal expansions	46
3.2	Thermal expansion models in DYN3D	48
3.2.1	Thermal expansion model for fuel rods	49
3.2.2	Radial thermal expansion model for the diagrid	52
3.2.3	Expansion-dependent XS treatment by DYN3D	54
3.3	Description of the test cases	57
3.4	Results of the test calculations	59
3.5	Spatial decomposition of thermal expansion effects	64
3.5.1	Axial expansion reactivity decomposition	68
3.5.2	Radial expansion reactivity decomposition	73
3.6	Modeling of thermal expansions – Summary of the results	75
4	Overall verification and validation of the extended DYN3D code	79
4.1	Phenix EOL control rod withdrawal tests	79
4.1.1	Description of the control rod withdrawal tests	80
4.1.2	Computational methodology	82
4.1.3	Numerical results	85
4.1.4	Control rod withdrawal tests – Summary of the results	93
4.2	Phenix EOL natural circulation test	94
4.2.1	Description of the unprotected stage of the transient	95
4.2.2	Computational methodology	97
4.2.3	Numerical results	98
4.2.4	Natural circulation test – Summary of the results	103
5	Summary and future work	105
5.1	Thesis summary	105
5.2	Recommendations for further research	107
	Bibliography	111
	Thesis-related publications	129

Curriculum Vitae	131
-------------------------	------------

List of Figures

2.1	References cores: radial core layout	18
2.2	Reference cores: Axial fuel rod layout	19
2.3	Radial assembly layouts of the OECD/NEA core	20
2.4	Radial assembly layouts of the Phenix EOL core	20
2.5	3D super-cell model for peripheral fuel assemblies	22
2.6	2D super-cell models for non-multiplying regions of the OECD/NEA core	23
2.7	Serpent and equivalent DYN3D models for SPH factor generation . . .	27
2.8	Radial power map of the OECD/NEA core	32
2.9	Difference in radial power of the OECD/NEA core, unrodded state . . .	34
2.10	Difference in radial power of the OECD/NEA core, rodded state	35
2.11	Radial power map of the Phenix EOL core	38
2.12	Difference in radial power of the Phenix EOL core	38
3.1	Microscopic elastic scattering cross section of ^{16}O and ^{23}Na	42
3.2	Neutron flux in PWRs and SFRs; and relevant reproduction factors . . .	42
3.3	Overview of the <i>mixing</i> model for the treatment of axial expansions . .	50
3.4	Schematic overview of the diagrid expansion	52
3.5	Schematic overview of the sodium and wrapper expansion	55
3.6	Schematic overview of the fuel rod expansion	56
3.7	Nodalization around the material interface for axial expansion modeling	60
3.8	Axial power profiles of the OECD/NEA core during axial core expansion	62
3.9	Difference in calculated axial power profiles of the OECD/NEA core . .	62
3.10	Axial power profiles of the Phenix EOL core during axial core expansion	63
3.11	Difference in calculated axial power profiles of the Phenix EOL core . .	63
3.12	Radially decomposed axial expansion effect	70
3.13	Axially decomposed axial expansion effect in OECD/NEA core	71
3.14	Axially decomposed axial expansion effect in Phenix EOL core	72
3.15	Radially decomposed radial expansion effect	74

List of Figures

3.16 Axially decomposed radial expansion effect in OECD/NEA core	76
3.17 Axially decomposed radial expansion effect in Phenix EOL core	77
4.1 Phenix EOL core: radial core layout and location of the shifted CRs . .	80
4.2 CR shift sequence	81
4.3 Schematic representation of the balancing method	82
4.4 Radial power profiles of the CR withdrawal benchmark	86
4.5 Calculated radial power deviation maps of the CR withdrawal benchmark	87
4.6 Comparison of radial deviation profiles along the diagonal	88
4.7 Comparison of control rod S-curves	90
4.8 Difference in power deviation profiles, DYN3D vs. Experiment	92
4.9 Absolute axial expansion profile of assemblies along the diagonal . . .	93
4.10 Measurements in the unprotected stage of the natural convection test	96
4.11 DYN3D results on the unprotected stage of the natural circulations test	99
4.12 Total reactivity decompositions with DYN3D	100
4.13 Averaged fuel rod temperature evolution in fissile core	100
4.14 Averaged fuel rod temperature evolution in radial blanket	100
4.15 Doppler effect decompositions with DYN3D	101
4.16 Differences in non-uniform and layer-uniform expansion models . . .	102
4.17 Change of axial expansion profiles through the transient	103

List of Tables

1.1	Number and types of operational reactors worldwide	2
1.2	Design parameters of the six Generation IV concepts	3
1.3	Fast reactors achieved criticality	4
1.4	Fast reactors for near- and mid-term deployment	5
1.5	Spatial fidelity of neutronic solvers in SFR codes or codes systems	9
2.1	Adopted 24-group energy structure	24
2.2	Group-wise SPH factors for CSD, DSD and CR follower	31
2.3	Comparison of the core integral parameters of the OECD/NEA core	31
2.4	Application of SPH correction in OECD/NEA core	32
2.5	Application of SPH correction in Phenix EOL core	37
3.1	Reactivity coefficients of typical PWR and SFR assemblies	43
3.2	Comparison of the axial expansion reactivity effects	61
3.3	Comparison of the radial expansion reactivity effects	64
3.4	Reaction- and region-wise decomposed axial expansion effect	68
3.5	Reaction- and region-wise decomposed radial expansion effect	73
4.1	Conditions used for cross section parametrization	82
4.2	Calculated core reactivities of the CR withdrawal benchmark	85
4.3	Comparison of maximal power deviations of the CR withdrawal test	89
4.4	Measured and calculated control rod worths	90
4.5	Reactivity coefficients of the Phenix EOL core	98

1 Introduction

This introductory chapter provides an overview on the Sodium cooled Fast Reactors (SFR) by summarizing the operated units of the past and pointing out the current trends for the new designs (Section 1.1). The state-of-the-art computational tools for SFR safety analyses are reviewed in Section 1.2. The reactor dynamics code DYN3D, as the selected tool for SFR calculations in this study, is presented in Section 1.3. The objectives of this study are stated in Section 1.4, while the thesis structure is introduced at the end of the chapter (Section 1.5).

1.1 The sodium cooled fast reactor technology

In 2016, the nuclear reactors provided around 14% of the total electricity generation worldwide (IAEA, 2017b). There are 454 nuclear power reactors in operation (IAEA, 2018b), from which around 85% are Light Water-cooled Reactors (LWRs), as of 2018 (Table 1.1). The rest of available types is comprised of 49 Pressurized Heavy Water cooled Reactors (PHWR), 14 Gas Cooled Reactors (GCR) and three Sodium cooled Fast Reactors (SFR). By utilizing such a LWR-dominated nuclear reactor fleet, the currently identified uranium resources would be only sufficient for over 135 years, considering uranium requirements of about 56 600 tU (NEA, 2016b).

The need to tackle this challenge of resource-ecological sustainability was one of the main motivations to form the Generation IV International Forum (GIF) (NEA, 2014). The GIF became a knowledge exchange platform on the development of next generation nuclear energy systems and serves as a guide for international and domestic research and development (R&D) programs. Additionally, the GIF sets up ambitious

Chapter 1. Introduction

Table 1.1: Operational nuclear power reactors worldwide, as of (IAEA, 2018b).

Reactor type	Descriptive name of reactor type	Number of reactors	Total net electrical capacity [MW]
LWR	Light Water Reactor	387	363933
PHWR	Pressurized Heavy Water Reactor	49	24598
GCR	Gas Cooled Reactor	14	7720
SFR	Sodium Fast Reactor	3	1400
Total		453	397651

technological goals in order to drive innovative R&D programs to obtain such economically affordable systems that are capable of efficient utilization of nuclear fuel. These systems are also required to minimize long lived radioactive waste, and meet enhanced standards of safety and proliferation resistance (NEA, 2014).

Six potential reactor concepts were selected by GIF that with further R&D could cover these goals of next generation (IV) systems (overview in Table 1.2): Sodium cooled Fast Reactor (SFR), Lead cooled Fast Reactor (LFR), Gas cooled Fast Reactor (GFR), Molten Salt Reactor (MSR), Supercritical Water cooled Reactor (SCWR) and Very High Temperature Reactor (VHTR).

Three of the selected Generation IV designs are operated in fast neutron spectrum. These reactors are capable to significantly reduce the radiotoxicity levels of the spent fuel such that the time burden of the long-term storage facilities can be lessened by several orders of magnitude to as low as couple thousand years. It has to be noted, that such progress can be only achieved by utilizing FBRs in a closed fuel cycle where plutonium of the spent fuel is reused while the minor actinides are transmuted after separation. Furthermore, the fast spectrum in the system is the base requirement for breeding of fissile fuel from fertile uranium. By utilizing such Generation IV FBRs, the uranium resources could be substantially extended and the global nuclear reactor fleet could be potentially fueled for thousands of years (NEA, 2008).

Among all innovative designs, the SFR is one of the leading concepts due to the vast operational experience accumulated since the first experimental SFR, the EBR-I, was brought to criticality in 1951 by the USA (Michal, 2001). Several experimental designs followed in the USA, while the rest of the world also picked up and produced several

1.1. The sodium cooled fast reactor technology

Table 1.2: Design parameters of the six Generation IV concepts (NERAC and GIF, 2002; Waltar et al., 2012).

Generation IV system	Neutron spectrum	Coolant material	Outlet coolant temperature (°C)	Power density (MW _{th} /m ³)
SFR	fast	sodium	550	350
LFR	fast	lead	550	77
GFR	fast	helium	850	100
MSR	fast / thermal	F ⁻ salts	700	22
SCWR	thermal / fast	water	510	100
VHTR	thermal	helium	1000	6-10

experimental reactors. Starting from the 70's, five demonstration units (>500 MWth) were built and operated by the USSR (BN-350, BN-600), France (Phenix), UK (PFR) and Japan (MONJU) (IAEA, 2006, 2012). Two commercial size SFRs were successfully built in the past. First is the Superphenix reactor with nominal power of 2990 MWth sparsely operated till 1997 in France (Schneider, 2009). Second is the recently started BN-800 in Russia with 2100 MWth nominal power (WNN, 2016a). The list of all SFRs that were able to gain operational experience so far, are presented in Table 1.3 beside the only two not Na-cooled fast reactors that ever reached criticality. One of them is the first ever-built fast reactor Clementine that was cooled with mercury, and the other is the only sodium-potassium cooled fast reactor DFR (IAEA, 2006, 2012).

Currently, several countries still consider the SFRs as one of the most promising Generation IV concepts based on their own past experience. Not just the fact that Russia, India and China are operating two experimental and three power generating SFR units (Table 1.3), but also the intentions stated by other countries for national SFR R&D programs (IAEA, 2015), confirm the dedication towards the sodium cooled technology. Table 1.4 summarizes all intended near- and mid-term deployments of fast reactors, where the majority of SFRs is clearly seen.

In EU, four Generation IV demonstrators are planned to be constructed: the SFR-prototype ASTRID (Rouault et al., 2015; Venard et al., 2015; Beck et al., 2017, 2018), the ALFRED lead cooled fast reactor (Grasso et al., 2014), the ALLEGRO gas cooled fast reactor (Stainsby et al., 2011) and the MYRRHA lead-bismuth eutectic (LBE) cooled fast reactor (Van den Eynde et al., 2015). The latter one is intended to be used in critical and subcritical mode in order to exploit both concepts at reasonable power scale for

Chapter 1. Introduction

Table 1.3: Fast reactors achieved criticality (adopted from (IAEA, 2006, 2012)).

Reactor	Type	Country	First critical	Coolant, Design	Fuel	MWth	Status
CEFR	E	CHI	2010	Na, Pool	oxide	65	In op.
Rapsodie	E	FRA	1967	Na, Loop	oxide	40	Shutdown
Phénix	D	FRA	1973	Na, Pool	oxide	563	Shutdown
Super-Phénix	C	FRA	1985	Na, Pool	oxide	2990	Shutdown
KNK-II	E	GER	1972	Na, Loop	oxide	58	Shutdown
FBTR	E	IND	1985	Na, Loop	carbide	40	In op.
JOYO	E	JAP	1977	Na, Loop	oxide	140	Suspended
MONJU	D	JAP	1994	Na, Loop	oxide	714	Suspended
BR-10	E	RUS	1958	Na, Loop	oxide carbide nitride	8	Shutdown
BOR-60	E	RUS	1968	Na, Loop	oxide	55	In op.
BN-350	D	KAZ	1972	Na, Loop	oxide	750	Shutdown
BN-600	D	RUS	1980	Na, Pool	oxide	1470	In op.
BN-800	C	RUS	2014	Na, Pool	oxide	2100	In op.
DFR	E	GBR	1959	NaK, Loop	metal	60	Shutdown
PFR	D	GBR	1974	Na, Pool	oxide	650	Shutdown
Clemen-tine	E	USA	1946	Hg, Loop	metal	0.025	Shutdown
EBR-I	E	USA	1951	NaK, Loop	metal	1.2	Shutdown
LAMPRE	E	USA	1961	Na, Loop	metal	1.0	Shutdown
EBR-II	E	USA	1963	Na, Pool	metal	65.5	Shutdown
Fermi-1	E	USA	1963	Na, Loop	metal	200	Shutdown
SEFOR	E	USA	1969	Na, Loop	oxide	20	Shutdown
FFTF	E	USA	1980	Na, Loop	oxide	400	Shutdown

E – Experimental, D – Demonstrator, C – Commercial

1.1. The sodium cooled fast reactor technology

Table 1.4: Fast reactors for near- and mid-term deployment (adopted from (IAEA, 2015)).

Reactor	Type	Country	Plan	Coolant, Design	Fuel	MWe	Status
TWR-P	D	CHI	2022 ^a	Na, Pool	metal	600	Design
TWR	C	CHI	2020s ^a	Na, Pool	metal	1150	Design
CFR-600	D	CHI	2025	Na, Pool	oxide	600	Design
CFR-1000	C	CHI	2030	Na, Pool	oxide, metal	1000	Design
ASTRID	D	FRA	2025	Na, Pool	oxide	600	Design
ALLEGRO	D	EU ¹	2030	He, Pool	oxide, carbide	75	Design
ALFRED	D	ROM	2025 ^b	Pb, Pool	oxide	120	Design
MYRRHA	E	BEL	2025 ^c	PbBi, Pool	oxide	100 _{th}	Design
PFBR	D	IND	2016 ^d	Na, Pool	oxide	1250	Under const.
JSFR	D	JAP	2025	Na, Loop	oxide	750	Susp.
Prototype SFR	D	KOR	2028	Na, Pool	metal	150	Design
SVBR-100	C	RUS	2025 ^e	PbBi, Pool	oxide, nitride	100	Design
BREST-300	D	RUS	2020 ^f	Pb, Pool	nitride	300	Design
MBIR	E	RUS	2020	Na, Pool	oxide, nitride	30	Under const.
BN-1200	C	RUS	2025	Na, Pool	nitride, oxide	1220	Postp.

R – Research, D – Demonstrator, C – Commercial

¹. Czech Republic, Hungary or Slovakia.

^a. (WNN, 2015), ^b. (WNN, 2013), ^c. (SCK•CEN, 2016), ^d. (Narasimhan, 2016),

^e. (Petrochenko et al., 2017), ^f. (WNN, 2016c).

LBE technology. In subcritical mode, it is planned to utilize an accelerator driven system (ADS) to obtain criticality. In European Union, the ASTRID is considered as the reference technology beside the lead cooled (LFR) and gas cooled alternatives (ESNII Task Force, 2010). Currently, the biggest European collaborative project on SFR systems is the ESFR-SMART (Mikityuk et al., 2017), which aims to further improve the safety of the Generation IV SFRs.

In Russia, after the recent begin of operation of the BN-800, the new multipurpose sodium cooled fast neutron research reactor (MBIR) is already under construction. BOR-60, the only in the world operating fast research reactor (WNN, 2016b) will be replaced by the MBIR. India is expecting to achieve first criticality of the Prototype Fast Breeder Reactor (PFBR) when the advanced stage of commissioning will be finally passed (Narasimhan, 2016). China plans of building the first demonstration unit based on experience of the currently operating CEFBR, moreover, the country agreed to host first travelling wave reactor (TWR), which will be cooled with liquid sodium (WNN, 2015).

Despite all the experience gained from building and operating numerous SFRs, the success of new advanced design heavily depends on the availability of sophisticated computational tools, which can accurately predict the behavior of nuclear reactors under operational and accident conditions. These codes have to have the ability to model all important physical phenomena that could affect the reactor core behavior, like temperature and density variations, or even dimensional changes through thermal expansion.

1.2 Computational analyses of SFR systems

A multitude of simulation tools are currently in use for safety analyses of SFR systems. There are specialized single codes for reactor physics, thermal-hydraulics (TH), fuel behavior or structural mechanics modeling; and there are code systems that incorporate some of the specialized codes for a more comprehensive analysis.

For a deterministic safety analysis, several codes or a code system have to be selected to cover physical phenomena that could impact the reactor behavior in operational states or in accident conditions. Each nuclear reactor research institution has its own preferences and code selections to perform such SFR analyses, and to avoid a boundless listing of codes here, only three big research organizations are highlighted

with well-defined state-of-the-art code systems:

- ANL – Argonne National Laboratory (USA)

The steady-state neutron transport calculations are done with the DIF3D code, that incorporates the finite difference diffusion (FDD) solver of the original version DIF3D (Derstine, 1984) as well as the variational nodal transport method VARIANT (Palmiotti et al., 1996). The multi-group cross sections needed for DIF3D calculations are calculated with the MC2-3 code (Lee and Yang, 2017) dedicated to fast reactor analysis, as it was also done in the EBR-II shutdown heat removal benchmark (IAEA, 2017a). The perturbation and sensitivity analyses are performed with VARI3D and PERSENT (Smith et al., 2013) that are based on the neutron flux solution of FDD and VARIANT solvers respectively.

At ANL, the reference transient simulation tool is the SAS4A/SASSYS-1 code system (Fanning et al., 2017) capable of deterministic system analysis of anticipated operational occurrences, design basis accidents and beyond-design basis accidents in liquid-metal-cooled fast reactors (LMFR). Beside the availability of the built-in point kinetics model, SAS4A/SASSYS-1 is also coupled with spatial neutron kinetics versions of the DIF3D solvers: DIF3D-K and VARIANT-K (Cahalan et al., 2000).

SAS4A/SASSYS-1 is an internationally accepted tool, which is as well used by the China Institute of Atomic Energy (CIAE) and Terrapower as was seen in the EBR-II benchmark (IAEA, 2017a). Moreover, by using the 1986's version of SAS4A, the SAS-SFR (Imke et al., 1994) was co-developed and currently used by Commissariat à l'Energie Atomique (CEA), French Radioprotection and Nuclear Safety Institute (IRSN), Japan Atomic Energy Agency (JAEA) and Karlsruhe Institute of Technology (KIT).

- CEA – Commissariat à l'Energie Atomique (France)

At CEA the reference neutronic tool for fast reactor analyses is the ERANOS code system (Rimpault et al., 2002). ERANOS consist of nuclear data libraries, solvers and procedures needed to perform reference and design calculations as well as fuel cycle calculations. The main cornerstone of the ERANOS is the ECCO cell and lattice code (Rimpault et al., 1989), which is used to generate effective cross sections and matrices for ERANOS full core calculations. Two solvers are implemented for steady-state full core calculations: the BISTRO code (Palmiotti et al., 1987) based on the SN method and the OECD version of

the variational nodal method, the TGV/VARIANT. The kinetics calculations are done with the TGV/VARIANT based KIN3D module (Rineiski and Doriath, 1997) that is capable of point- and spatial kinetics modeling as well as preparing core kinetics parameters for system analyses.

The ERANOS is also used outside of France in the European community, e.g., KIT and Paul Scherrer Institut (PSI), or even in India at Indira Gandhi Centre for Atomic Research (IGCAR) (Devan et al., 2012) and in Japan at the University of Fukui (IAEA, 2017a).

The reference system analysis tool is CATHARE (Geffraye et al., 2011), which was initially developed for Pressurized Water Reactor (PWR) safety analyses, but later it was also extended and thoroughly validated for SFRs (Tenchine et al., 2012). CATHARE is a joint development of AREVA, CEA, EDF and IRSN.

- PSI – Paul Scherrer Institut (Switzerland)

The reference tool in PSI is the FAST code system (Mikityuk et al., 2005) for static and transient analysis of SFR, GFR and LFR. The code system consists of ERANOS for static neutronic calculations, PARCS for dynamic reactor calculations, TRACE for system thermal-hydraulic modeling, and FRED for fuel behavior analysis.

PARCS (Downar et al., 2010) developed in the USA is a spatial reactor kinetics code based on nodal methods that includes multi-group diffusion and SP3 transport solvers. PARCS receives the state-dependent homogenized multi-group cross sections from ECCO module of the ERANOS code. As substitute for deterministic code ERANOS is the Monte Carlo code Serpent (Leppänen et al., 2015), which can also perform static neutronic reactor analysis, and provide kinetic parameters and homogenized cross sections for transient calculations (Ghasabyan, 2013).

TRACE is a best-estimate system code developed by U.S. Nuclear Regulatory Commission (NRC) for static and transient thermal-hydraulic analyses of LWR systems as well as for reactor systems with helium, lead-bismuth eutectic or sodium coolant. At PSI the TRACE code was extended for advanced fast reactors (Mikityuk et al., 2005) and was coupled with PARCS and fuel rod behavior code FRED (Mikityuk and Shestopalov, 2011).

By using such codes systems in deterministic safety analyses of SFR systems, it is possible to predict the outcome of anticipated operational occurrences, design basis

1.2. Computational analyses of SFR systems

accidents and beyond design basis accidents that not lead to significant core degradation. Nevertheless, it has to be noted that any proper safety analysis should include the simulation of severe accidents with the outcome of core degradation. However, this topic goes far beyond of this study, and therefore, the computational codes capable of modeling such events were not mentioned here.

Table 1.5: Spatial fidelity of neutronic solvers in codes or codes systems applied in SFR system analyses.

Neutronic solver	Code or codes system
Point kinetics	SAS4A/SASSYS-1
	SAS-SFR
	CATHARE
	TRACE
3D kinetics	SAS4A/SASSYS-1 with DIF3D-K or VARIANT-K
	TRACE/PARCS (FAST system)
	SAS-SFR/PARCS

Traditionally, in deterministic safety analysis of SFR systems, a thermal-hydraulic system code is used together with point-kinetics (PK) as neutron kinetic model (IAEA, 2013; Lázaro et al., 2014a,b). All aforementioned system codes, as summarized in Table 1.5, include an intrinsic PK solver and can be applied in stand-alone calculations. Within these codes, the thermal feedbacks on neutronic behavior of the reactor core are modeled with the help of reactivity coefficients. These coefficient are usually average over the whole core, and as pointed out by (Lázaro et al., 2014a), the point neutron kinetic modeling limits the analyses to radially core-symmetric transient scenarios.

In order to catch local effects or asymmetric core behaviors, the utilization of 3D neutron kinetics (spatial NK) codes is necessary. Such codes typically used in safety analyses of SFRs are divided between dedicated fast reactor codes (e.g., DIF3D-K or VARIANT) and adopted LWR codes such as PARCS. The utilization of an available well trusted LWR-oriented code is considered a more feasible approach than the development of completely new computer code requiring extensive expenditure of resources. Naturally, such a code has to be upgraded for SFR calculations: the physical models with LWR specific approximations have to be reconsidered, and the missing SFR system specific models have to be implemented.

The nodal diffusion codes (e.g. DIF3D-K or PARCS) can be considered attractive for coupling with thermal-hydraulic system codes because of their relatively short calculation time, not only in steady-state problems, but especially when modeling transients. Several coupling examples exist from the aforementioned codes, as listed in Table 1.5. While at ANL the dedicated fast reactor code DIF3D-K was coupled with SAS4A/SASSYS-1 (Cahalan et al., 2000), the adopted LWR code PARCS was coupled with TRACE at PSI (Chenu et al., 2010) and with SAS-SFR at KIT (Ponomarev, 2017).

At the Helmholtz-Zentrum Dresden-Rossendorf (HZDR), this kind of code-extension is an ongoing project for the in-house developed LWR code DYN3D, a reference nodal code of Germany (Kliem et al., 2017) in the European reference simulation platform NURESIM (Chauliac et al., 2011) developed currently in the framework of the NURESAFE European project (Chanaron et al., 2015; Chanaron, 2017).

1.3 The DYN3D code for SFR analyses

The reactor dynamics code DYN3D (Rohde et al., 2016) is a state-of-the-art three-dimensional reactor core simulator developed at HZDR in the last two decades. The code was initially developed for transient analysis of Russian VVER-type reactors, but was undergoing continuous improvement in order to become an advanced best-estimate tool for simulating LWR steady-states and transients. DYN3D is being continuously extended to innovative reactor designs, particularly to SFRs as the main development line.

In DYN3D, the neutron kinetics models solving the multigroup diffusion equation are based on nodal expansion methods capable of treating three-dimensional Cartesian and hexagonal-z geometries. In time-dependent calculations, the integration of the transient diffusion equation over a neutronic time step is done with the help of an implicit difference scheme and exponential transformation (Grundmann et al., 2005, p. 5). The exponent is calculated based on the flux change of previous time step. The equations of the precursor densities are integrated over time steps by assuming exponential behavior of the neutron flux and fission source (Rohde et al., 2016).

The code also contains an internal thermal hydraulic model with one- and two-phase modeling capability and a one-dimensional fuel rod model. The internal 1D fuel rod model (Rohde, 2001) can estimate realistic fuel and cladding temperature distributions and simulate the gas gap behavior. Beyond the standalone application, the

DYN3D code can be also used in coupled calculations together with thermal hydraulic system codes (Kozmenkov et al., 2001, 2015; Kliem et al., 2006), CFD and sub-channel codes (Kliem et al., 2011; Gomez-Torres et al., 2012), as well as fuel behavior code TRANSURANUS (Holt et al., 2014, 2015, 2016).

1.3.1 Extension of DYN3D to SFR applications

The availability of the hexagonal diffusion solver in DYN3D is essential for SFR calculations, since all the SFR designs utilize hexagonal lattice for the core geometry. However, a number of methodological developments are still required in order to use DYN3D for SFR analyses:

- DYN3D requires pre-generated homogenized few-group cross sections (XS) to perform any calculations.
- Through the establishment of the XS generation methodology the applicability of the nodal diffusion solver shall be demonstrated for SFR calculations.
- The thermodynamic properties of sodium coolant have to be implemented in the internal thermal-hydraulics solver. Additionally, a coupling with a system code using sodium coolant is preferable to model the reactor primary circuit.
- The DYN3D code has to be extended with a new thermal-mechanical model to account for the thermal expansion effects, which are significant feedbacks in SFR systems.
- The newly developed and verified models have to be implemented into the code, and the extended DYN3D has to be validated with real SFR measurements.

This study is a contribution to the methodological extensions of DYN3D to SFR applications as described later in Section 1.4.

1.3.2 Preceding DYN3D developments and its application limits

In contrast to usually applying fast deterministic cross section generators (e.g. ECCO from ERANOS), HZDR made efforts to utilize continuous-energy Monte Carlo methods for obtaining SFR XS. A number of studies (Fridman and Shwageraus, 2013; Rachamin

et al., 2013) presented a feasible XS generation methodology on simplified SFR cases by using the Monte Carlo code Serpent (Leppänen et al., 2015). Nevertheless, the application of this method has to be investigated on realistic SFR cores in order to demonstrate the feasibility of Serpent as a general XS generator for nodal diffusion SFR analysis.

Before this work, the thermal hydraulic solver of DYN3D was updated to include thermal-physical properties of sodium such as thermal conductivity, density, heat capacity and viscosity (Rohde et al., 2016). This allows the simulation of one-dimensional sodium flow in assembly channels. The calculations are still limited to single phase modeling and the applicability of DYN3D is restricted to cases where the sodium remains liquid during the transient. However, the liquid sodium has high transfer properties, high thermal inertia and an extensive margin till boiling conditions (>300 K), so the system safeguards (active and passive) have more time to react, avoid sodium boiling, and maintain reactor cooling even after shut-down. In order to perform two-phase flow modeling, including simulations of thermodynamic non-equilibriums or different velocities between liquid and vapor phases, additional thermal-hydraulic models are needed. These developments are out of scope of this doctoral research, and they planned for a rather later stage of DYN3D extension process.

It has to be noted, that the 1D thermal-hydraulic model of DYN3D is developed for structured parallel coolant channels. The modeling is limited to scenarios where the fuel rod cladding and the structure of the fuel bundles remain intact. Even when the modeling after fuel failure is not possible, the detection of such events was implemented for zircaloy-bounded fuels (Rohde, 2001). Nevertheless, to be this option available for SFR calculations, an extension is needed to stainless steel or oxide dispersed steel claddings. Furthermore, the modeling of core disruptive accidents is not possible with DYN3D, and the extension to this simulation domain is not foreseen in the future.

In contrast to LWRs, SFRs are especially sensitive to thermal expansion due to the combined effect of larger temperature variations and harder neutron spectrum. In fact, thermal expansions of the core and reactor components such as fuel, cladding, diagrid, control rod (CR) drivelines, vessel, etc. provide essential reactivity feedbacks under normal and transient conditions. However, since DYN3D was originally oriented to the LWRs analyses, the modeling of thermal expansion mechanisms was not considered in the code. Therefore, the development of a new thermal-mechanical

module accounting for thermal expansions has to be initiated as a part of the SFR related activities. At first step, the DYN3D code needs to be extended with the capability of treating two important thermal expansion effects occurring within the core, namely axial expansion of fuel rods and radial expansion of diagrid. Until then DYN3D is limited to steady-state calculations with uniform core expansion.

1.4 Objectives of the study

The objectives of this doctoral research can be summarized in the following:

1. Extension and verification of a few-group XS generation methodology that is applicable for nodal diffusion calculation of realistic SFR cores.
2. Development of thermal expansion models for DYN3D, which can account for the reactivity effects of the fuel rod and diagrid expansions.
3. Implementation of the new models into the DYN3D code and assessment of the code for SFR analyses by verification and validation (V&V).

The first part of the contribution is the development of the XS generation methodology for realistic SFR core designs. Two reference cores are selected for this purpose: the large 3600 MWth mixed oxide (MOX) core adopted from the OECD/NEA benchmark (NEA, 2016a) and a smaller 350 MWth MOX core of the Phenix reactor adopted from the Phenix EOL experiments (IAEA, 2013, 2014). The development of the methodology is based on the previously mentioned studies (Fridman and Shwageraus, 2013; Rachamin et al., 2013), and therefore, the continuous-energy Monte Carlo code Serpent is selected as the XS generator tool. Serpent is also used in this study as the main verification tool by providing reference full core Monte Carlo solutions for the code-to-code comparison.

In the second step of this study, the new thermal mechanical models are developed to account for thermal expansion effects. In standalone mode, DYN3D is only capable of core level simulation. Therefore, the thermal mechanic models will only cover the core-specific effects, i.e. the axial and radial thermal expansion of the core. The verification of the new models is done by using the two reference cores.

The implementation of the new models into the DYN3D source code is a significant part of the PhD work. Another important task is the overall V&V of the extended

DYN3D on reactor core level. The IAEA benchmarks on the Phenix EOL experiments, including control rod withdrawal tests (IAEA, 2014) and an initial stage of the natural circulation test (IAEA, 2013), are selected for the more detailed assessment of the extended version of DYN3D.

1.5 Thesis outline

Chapter 2 presents the methodology to generate homogenized few group cross sections for nodal diffusion analyses by using Monte Carlo code Serpent. Furthermore, the description of how to use the Super-homogenization method to improve the nodal diffusion solution in SFR cores is also described here. Nevertheless, the chapter begins with a short overview of Serpent code and is followed by the reactor core descriptions that are used for V&V purposes. The verification of the XS generation methodology is presented at the end of the chapter.

Chapter 3 provides a detailed description of the newly implemented thermal-mechanical models and presents the results of the initial verification study performed on a full core level using the two reference cores.

Chapter 4 demonstrates the overall verification and validation study of DYN3D. The extended code is validated against a selected experiments that were conducted in the Phenix reactor and were reported in the IAEA benchmarks (IAEA, 2013, 2014). The first part of the chapter (Section 4.1) presents the code assessment for steady-state analyses, whereas the second part (Section 4.2) is dedicated for the validation against a transient scenario.

The final Chapter summarizes the achieved results of the PhD study, and points out possible directions for future developments based on this study.

2 Generation of homogenized few-group cross sections

This chapter presents the general methodology on how to generate homogenized few-group cross sections (XS) for nodal diffusion analyses of SFR cores. The chapter begins with the introduction of Monte Carlo code Serpent, followed by the description of two reference SFR cores in Section 2.2. The general approach to generate XS for nodal calculation of SFRs is presented in Section 2.3. Afterwards a way to improve the nodal diffusion solution of SFR cores is introduced by using the Super-homogenization (SPH) method (Section 2.4). The presented methods are tested on the reference cores and verified against the full core Monte Carlo solution, as presented in Section 2.5.

2.1 The Serpent code for XS generation

The application of the continuous-energy Monte Carlo method for homogenized XS generation is a practice that is becoming more and more widespread, despite the usually high computational costs of such method. The main attractive attribute of the Monte Carlo method is that the interaction physics, can be simulated without major approximations typical to the traditional deterministic lattice codes. The other advantage is that Serpent applies the universe-based constructive solid geometry (CSG) builder, which makes it possible to apply the Monte Carlo method to produce XS for practically any kind of reactor design at any level of detail (Leppänen et al., 2016).

A number of attempts to adapt general purpose Monte Carlo codes for XS generation were done in the past (Redmond, 1997; Ilas and Rahnema, 2003; Pounders et al., 2005; Van der Marck et al., 2006). Nevertheless, Serpent (Leppänen et al., 2016) is a

Chapter 2. Generation of homogenized few-group cross sections

first continuous-energy Monte Carlo code particularly developed for reactor physics analysis with the high priority assigned to the development and implementation of the XS generation capabilities.

The latest versions of the Serpent code can produce a full set of homogenized parameters required by 3D full core simulators including few-group reaction cross sections, scattering matrices, diffusion coefficients and delayed neutron parameters. It is also possible to generate discontinuity factors, pin-power form factors and albedos (Leppänen et al., 2016).

Beside the XS generation, Serpent basically covers the traditional reactor analyses such as the criticality calculations, full core modeling, and fuel cycle analyses. Since the same code can be used to generate the XS for deterministic reactor simulators and to obtain the reference Monte Carlo solution, Serpent is the ideal verification tool of deterministic transport tools, because all additional discrepancies resulting from evaluated nuclear data libraries can be excluded (Leppänen et al., 2016). The elimination of such uncertainties makes it possible to better assess the physical methods of XS generation (e.g., homogenization procedure or energy group condensation), and the transport methods used in the deterministic core simulators.

A basic feasibility of using Serpent for the homogenization was demonstrated for a number of existing and innovative reactor systems. The Serpent applicability as a XS generator for Pressurized Water Reactor analysis was investigated using theoretical (Fridman and Leppänen, 2011; Fridman et al., 2013b; Hursin et al., 2013) and real-life core configurations such as one in the MIT BEAVRS benchmark (Leppänen et al., 2014; Leppänen and Mattila, 2016), the SPERT-III (Knebel et al., 2016) or the CROCUS reactor (Siefman et al., 2015; Rais et al., 2017) at EPFL. In (Herman and Shwageraus, 2011; Fridman et al., 2013a; Hall et al., 2013) the Serpent code was employed to produce XS for Resource-Renewable Boiling Water Reactor (RBWR) fuel assemblies having a strong axial heterogeneity. In (Baier et al., 2014) XS for the 3D deterministic analysis of a block-type High Temperature Reactor were computed by Serpent.

A methodology for producing XS for SFRs was also proposed by (Fridman and Shwageraus, 2013; Rachamin et al., 2013). Although the methodology was successfully tested, the verification analysis was carried out based on rather simplified SFR core models. In (Fridman and Shwageraus, 2013) a uranium startup SFR core loaded with carbide fuel of identical enrichment was considered as a reference core (Fei et al., 2011). It is worth noting that control rods were not considered in the analysis, which

is more challenging to model with diffusion codes due to the strong flux gradients around absorbers. In (Rachamin et al., 2013) only a 2D model of European SFR (ESFR) core (Fiorini and Vasile, 2011) was used to assess the Serpent performance. Such method of XS generation, developed on 2D core models, is not necessarily applicable for 3D nodal calculations, because it neglects the axial spectral effects coming from axial reflectors and possible fertile blankets. Therefore, the first objective of PhD study is to further verify the SFR XS generation methodology by applying it to a considerably more realistic and detailed SFR core configurations presented in the following section.

2.2 Reference core descriptions

In this section, two reference SFR cores are described that were used to assess all new methods and models presented in this thesis.

2.2.1 Large oxide core from the OECD/NEA benchmark

The large 3600 MWth SFR mixed oxide (MOX) core was one of the selected core designs by the SFR Expert Group Task Force of OECD/NEA Working Party on Reactor Systems for code benchmarking (NEA, 2016a). The core is loaded with 225 inner and 228 outer MOX fuel assemblies with variable Pu content and surrounded by 270 radial reflector assemblies (Fig. 2.1, left). The fuel assemblies include 271 helium bonded fuel pins with Oxide Dispersion Strengthened (ODS) steel cladding and surrounded by a hexagonal EM10 steel duct (see Fig. 2.3a). The fuel rods (bundle of pins) consist of five axial zones, namely lower gas plenum, lower reflector, fuel, upper gas plenum, and upper reflector. The lower and upper reflectors consist of the EM10 steel pellets under the fuel rod cladding. At nominal conditions, the active core height is 100.6 cm and the assembly pitch size is 21.2 cm. Fig. 2.2, left presents the axial and radial fuel rod description including the distribution of the relative Pu content.

The core is controlled by two independent reactivity control systems. The primary system contains 24 control and shutdown devices (CSD), each of which has 37 sodium bonded natural B₄C pins (Fig. 2.3b). The secondary reactivity control system comprises of the nine Diverse Shutdown Devices (DSD) with 55 sodium bonded enriched B₄C (90.0wt% of ¹⁰B) pins (Fig. 2.3c).

In order to simplify the modeling, two uniform temperatures are considered namely

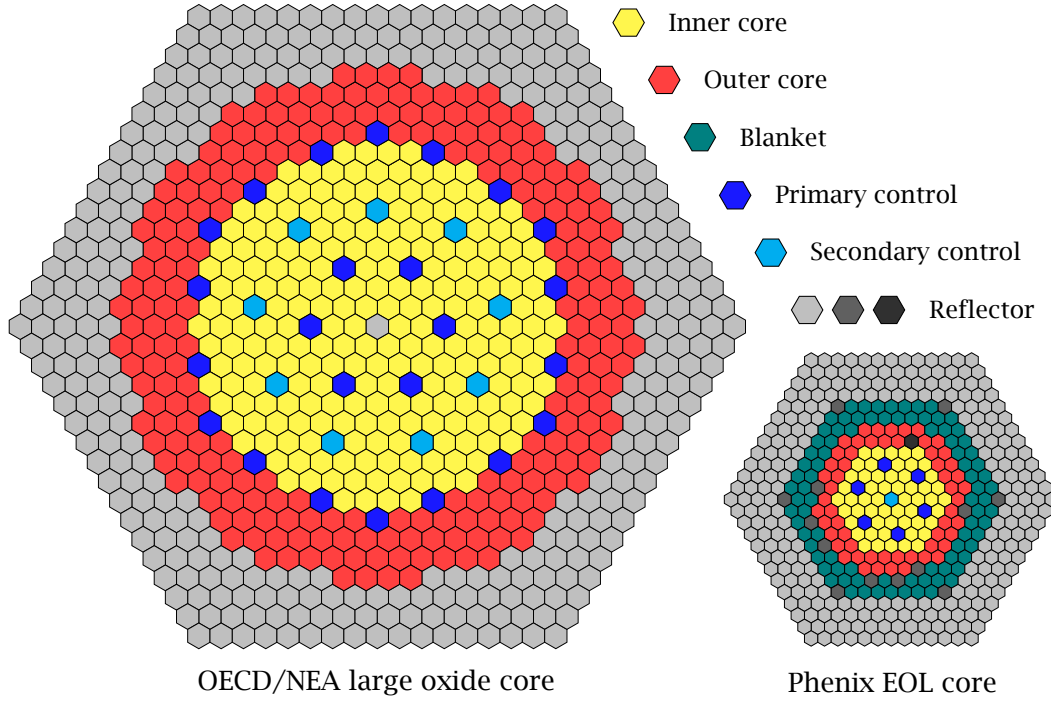


Figure 2.1: References cores: radial core layout (to scale).

1500 K for the fuel and 743 K for all structural materials, coolant, and CRs. A detailed description of the material compositions can be found in the benchmark specifications (NEA, 2016a). The fuel material compositions taken correspond to the beginning of equilibrium cycle (BOEC) state.

2.2.2 Phenix End-of-Life core

The selected Phenix EOL core is a 350 MWth SFR core using MOX fuel, and had undergone several experimental tests in 2009 before definitive reactor shutdown. From these EOL experiments two test were selected by the IAEA Working Group on Fast Reactors for code benchmarking: the natural convection test (IAEA, 2013) and the control rod withdrawal test (IAEA, 2014).

The Phenix EOL core consists of 54 inner and 56 outer MOX fuel assemblies, and firstly surrounded by 86 blanket assemblies and secondly by 252 reflector assemblies on the periphery (see Fig. 2.1, right). Furthermore, the core comprises six primary CRs, one secondary CR in the center, and 14 reflector-type (mixture of sodium and stainless steel) assemblies inside the core and blanket region as depicted in Fig. 2.1, right. The

2.2. Reference core descriptions

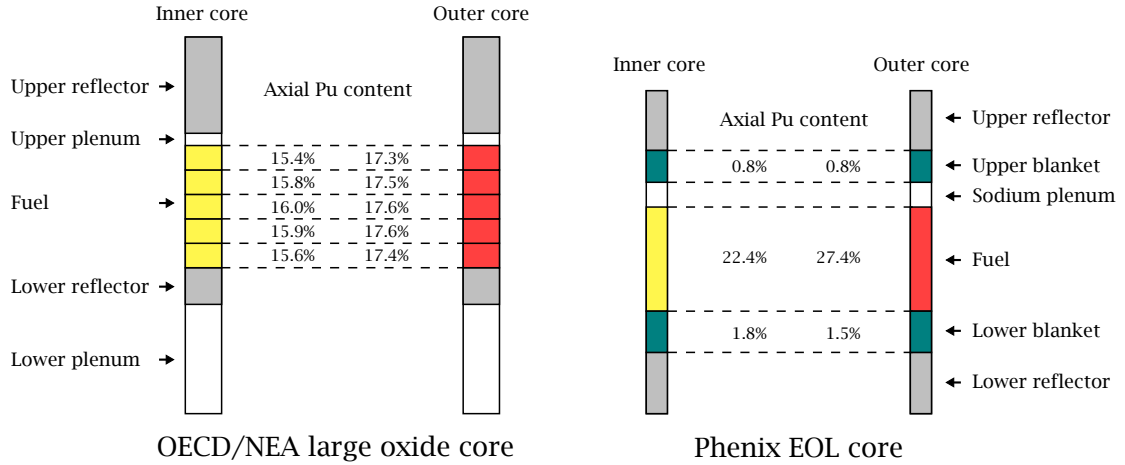
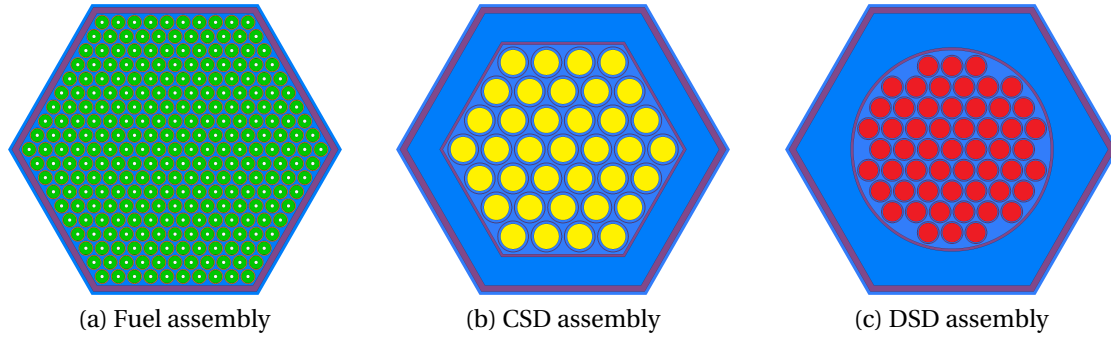


Figure 2.2: Reference cores: Axial fuel rod layout (to scale).

fuel assemblies contain 217 U-Pu MOX fuel pins with SS316 cladding in a helium bond (Fig. 2.4b). The fuel rods are subdivided into six zones including lower reflector, lower blanket, fuel, sodium plenum, upper blanket and upper reflector. Fig. 2.2, right presents the axial fuel rod description of the Phenix core including the distribution of the relative Pu content (wt%). At room temperature (293 K) the active core height is 85 cm and the assembly pitch size is 12.72 cm.

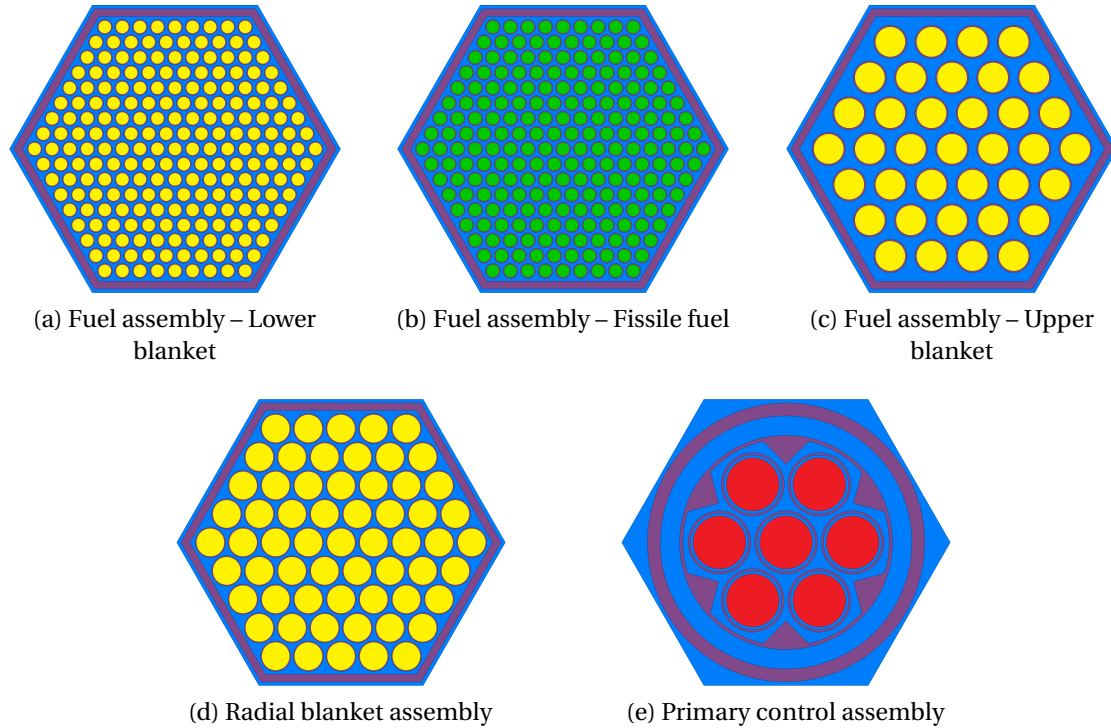
The core comprises three blanket regions containing fertile fuel pins with more than 98wt% of ^{238}U : lower blanket (Fig. 2.4a) and upper blanket (Fig. 2.4c) in the fuel assemblies, and the radial blanket assemblies (Fig. 2.4d). The primary control assemblies contain seven enriched B_4C pins (48wt% of ^{10}B) as depicted in Fig. 2.4e. For the nominal case, the CSD and DSD assemblies remain at the parking position that is the bottom of the CR pins is located at the top of the active core.

In the benchmark specifications, the EOL isotopic densities for the six average core zones were provided. However, atomic densities of the fission products (FPs) were not explicitly given but rather represented by six lumped FPs (also known as pseudo FPs) for the main actinides (i.e. ^{235}U , ^{238}U , ^{239}Pu , ^{240}Pu , ^{241}Pu and ^{242}Pu). In order to approximate the explicit FP content, single-assembly burnup calculations were performed using the Serpent code. The assembly included six “test” fuel pins each containing one of the six main actinides mentioned previously. These test fuel pins were introduced to obtain the burnup-dependent FP vector for each of the six main actinides. The final FP compositions used in the Serpent calculations were estimated by scaling the obtained FP vectors with the corresponding atomic densities of the



Blue – sodium, *green* – fuel, *purple* – EM10 steel, *yellow* – natural B4C, *red* – enriched B4C

Figure 2.3: Radial assembly layouts of the OECD/NEA core.



Blue – sodium, *green* – fissile fuel, *purple* – SS316 steel, *yellow* – fertile blanket, *red* – B4C

Figure 2.4: Radial assembly layouts of the Phenix EOL core.

pseudo FP provided in the benchmark.

In the benchmark specification, the Phenix core description is simplified in several ways for the benchmark analyses. The fuel and blanket material compositions are averaged axially and region wise. The reflector-type assemblies, sodium plenum, axial shielding and the secondary CR are modeled as homogeneous media. Three average temperatures are used to take into account the Doppler effect on microscopic cross sections namely 1500 K for the fuel, 900 K for the blanket and 721 K for structural materials, sodium coolant, and absorbers. A detailed description of the material compositions and core geometry for the Phenix EOL core can be found in the benchmark report (IAEA, 2014).

2.3 General approach to XS generation for SFRs

In this research, a study was performed to find an optimal set of lattice level models for generating XS for assembly-wise nodal calculations. The goal was to restrict the model size and heterogeneity to avoid long computational times, and actually solving the full core problem with Monte Carlo, while to get an acceptable performance of XS in nodal calculations. Starting from the simplest model of the *2D infinite assembly* model, the complexity of the model was increased by including more and more of the real environment, like the neighboring assemblies or non-multiplying axial regions. The performance of models was assessed by obtaining the k_{eff} and radial power distribution from the full core nodal calculation and comparing with the Monte Carlo reference. When a more complex model was applied, the new model was accepted if k_{eff} was improved by more than ~ 10 pcm, or the maximal power deviation by more than $\sim 0.1\%$. Otherwise, the application of the new model was rejected.

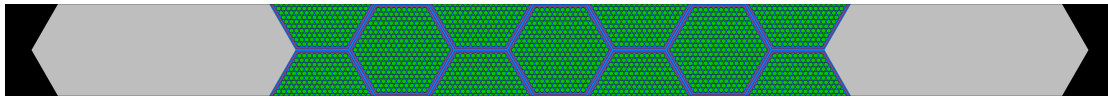
With this study the following combination of models was obtained for XS generation:

- The few-group XS for the fuel assemblies not facing radial reflector were calculated using a 3D single assemblies model with reflective radial and black (zero incoming neutron current) axial boundary conditions (BC). This model allows for a simultaneous generation of XS for several axial fuel zones. The XS were generated for the fuel region only. Furthermore, the 3D model that includes all axial regions (e.g., plenums, axial blankets and shielding) accounts for the axial self-shielding and spectral effects in the fuel XS. By accounting for the axial environment, these fuel XS perform significantly better in full core nodal

Chapter 2. Generation of homogenized few-group cross sections

diffusion calculations, than just using a simple 2D infinite fuel model.

- As demonstrated by (Aliberti et al., 2004; Rachamin et al., 2013), the reflector assemblies soften the neutron spectrum in the outermost fuel assemblies. These spectral effects can be accounted for in the outermost fuel assemblies and the power can be improved by using the 3D fuel-reflector model depicted in Fig. 2.5. The cross sections are homogenized over the peripheral fuel assemblies facing the radial reflector only. This model was upgraded from the 2D model originally proposed by (Fridman et al., 2013c). The 3D version allows a simultaneous XS generation for all axial layers while accounting for the spectral and spatial self-shielding effects from the immediate surroundings.
- The XS for blanket assemblies and all non-multiplying regions (i.e. reflectors, sodium plenum, control rods and their empty channels) are prepared using 2D super-cell models depicted in Fig. 2.6. All super-cells are constructed as central hexagonal region of interest surrounded by the fuel assemblies. The XS are homogenized over the central hexagonal region only.



Gray – radial reflector, black – vacuum

Figure 2.5: 3D super-cell model for peripheral fuel assemblies.

The few-group energy structure used for the generation of the XS is a 24-group subset of the ERANOS 33-group energy structure (Ruggieri et al., 2006) obtained by collapsing last 10 energy groups (from 24 to 33) into a single thermal group (Table 2.1). This modification was proposed by (Fridman and Schwageraus, 2013; Rachamin et al., 2013), because Serpent calculations present large statistical uncertainties in the neutron flux in thermal groups. For OECD/NEA large oxide core and the Phenix EOL core, the XS were generated from ENDF/B-VII and JEFF-3.1 nuclear libraries, respectively.

In order to remain consistent in the MC calculations, all Serpent results were obtained with not higher than 3 pcm uncertainty in the k -eigenvalue. Each set of XS was generated by using 640 million neutron histories, i.e. 1000 active and 100 skipped cycles with 640,000 neutrons per cycle. The skipped cycles are to ensure that the initial transport simulations are excluded from the results, before the fission source distribution is converged (Brown, 2006; Leppänen, 2007). The computation took

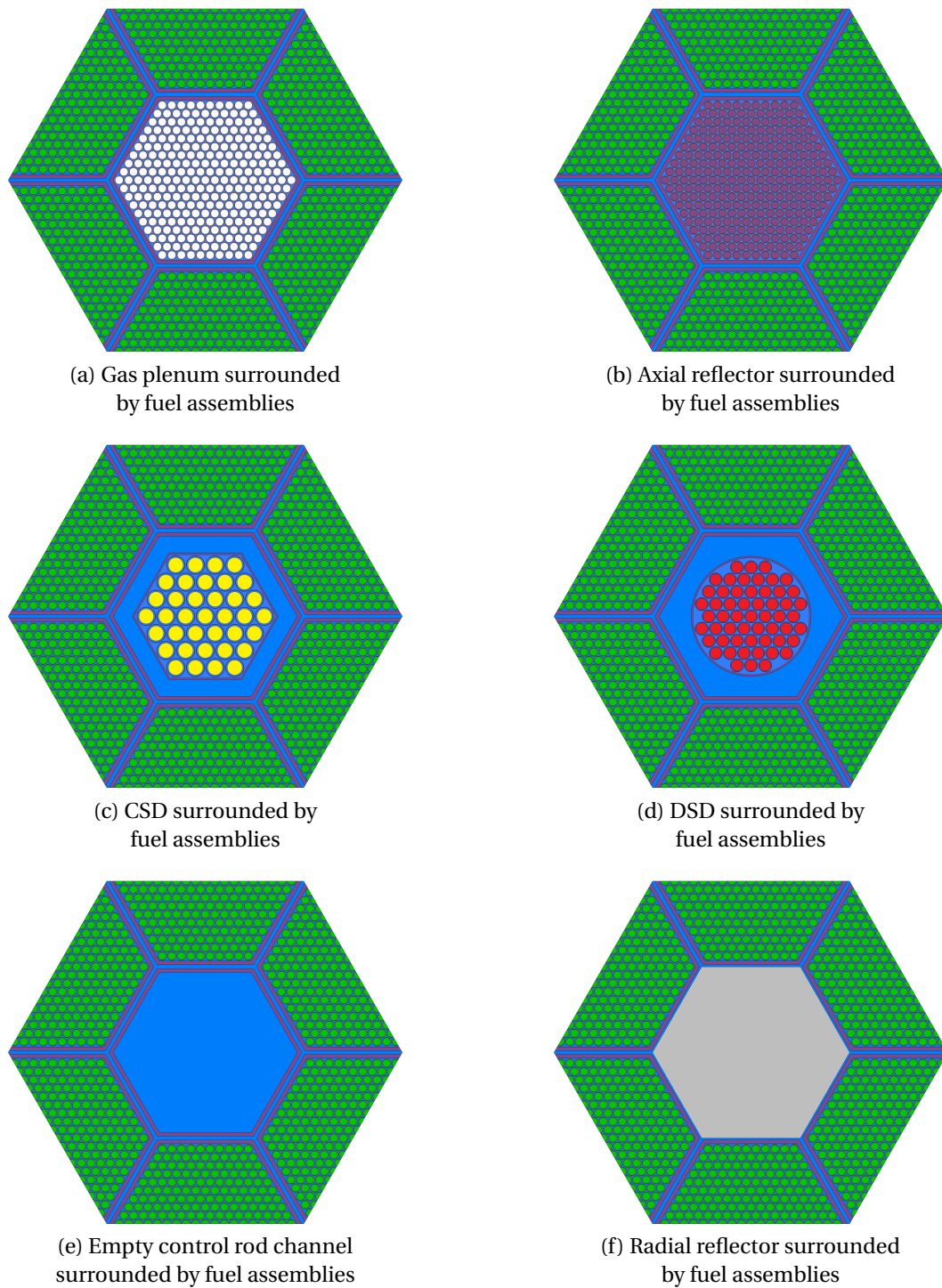


Figure 2.6: 2D super-cell models for non-multiplying regions of the OECD/NEA core.

Chapter 2. Generation of homogenized few-group cross sections

Table 2.1: Adopted 24-group energy structure.

Group #	Upper energy limit (MeV)	Group #	Upper energy limit (MeV)
1	2.0000E+01	13	4.0867E-02
2	1.0000E+01	14	2.4787E-02
3	6.0653E+00	15	1.5034E-02
4	3.6788E+00	16	9.1187E-03
5	2.2313E+00	17	5.5308E-03
6	1.3533E+00	18	3.3546E-03
7	8.2085E-01	19	2.0346E-03
8	4.9787E-01	20	1.2341E-03
9	3.0197E-01	21	7.4850E-04
10	1.8315E-01	22	4.5399E-04
11	1.1109E-01	23	2.7536E-04
12	6.7379E-02	24	1.6701E-04

in average from 2 to 4 hours depending on the type of computational architecture used. Currently at HZDR cluster, two main types of computational architectures are available for reactor physics application, either the 4×16 -core AMD Opterons or the 2×16 -core Intel Xeons (Schulz, 2017), where the later has the better performance. The most optimized computation was achieved by using the hybrid parallelization model, where 4 MPI processes were used together with 8 or 16 OpenMP threads for Intel or AMD nodes, respectively.

2.4 Super-homogenization method for SFR analysis

The drawback of the lattice level XS generations is that, it does not consider the full core configuration. The spatial homogenization is done on assembly level in symmetric and infinite configurations, where the leakage effect of the real environment is not completely modeled.

A traditional leakage correction is to use critical spectrum for collapsing the homogenized cross sections. The critical spectrum can be obtain by solving, e.g., B_1 , P_1 or fundamental mode equations (Stammler and Abbate, 1983; Choi et al., 2017). The B_1 method is available in Serpent (Leppänen et al., 2016), and by default, the B_1 -leakage corrected XS are generated beside the XS that are condensed with the *infinite* spectra.

2.4. Super-homogenization method for SFR analysis

The B_1 method is typically used to account for the leakage effects in infinite fuel lattice calculations. However, the B_1 method relies on certain approximations, in cases such as fuel surrounded by non-fuel regions, the correction can lead to non-physical results, as also warned by (Smith, 2016; Leppänen et al., 2016). In addition, B_1 is not applicable for non-multiplying regions by definition.

In this research, the energy condensation with infinite spectra was rather selected in Serpent, and for more problematic regions, a post-correction of the XS was done depending on its environment. A correction is usually desired when the neutron balance is not preserved between the heterogeneous transport and the homogenized diffusion solutions, e.g., between control rod and fuel assemblies. In order to preserve the multiplication factor and different reaction rates with the homogeneous calculation, the *equivalence theory* was introduced by (Koebeke, 1978). Two broadly used methods were developed based on the equivalence theory: the General Equivalence Theory (GET) by (Smith, 1980) and the Superhomogenization (SPH) method by (Kavenoky, 1978).

In the GET method, the so-called *discontinuity factors* are calculated for the nodal surfaces as the ratio of the homogeneous and heterogeneous surface flux. When applying these factors in nodal diffusion calculations, the homogeneous flux becomes discontinuous at the nodal interface, but in the mean time the homogeneous flux distribution of the node becomes the same as the heterogeneous one. This leads to the simultaneous preservation of reaction rates and the net surface currents (Smith, 1986).

In practice, the GET is mostly applied for two general cases: the infinite single-node and the super-cell homogenization problems. The procedures for both of these cases are incorporated in Serpent. In the infinite single-node problem, the whole lattice model is homogenized for XS with reflective boundary conditions. In this case, the net boundary currents are reduced to zero and the homogenized flux distribution becomes uniform. This means that the homogeneous surface flux equals to the node-average flux that can be used to obtain the discontinuity factor. In order to calculate the discontinuity factors for infinite single-node problem, the homogeneous and heterogeneous surface fluxes are calculated by Serpent using surface and cell flux tallies, respectively (Leppänen et al., 2016). However, infinite single-node models were not proposed in the XS generation methodology of this research (Section 2.3).

In the super-cell problem, the region intended for homogenization is modeled to-

Chapter 2. Generation of homogenized few-group cross sections

gether with its immediate surroundings. The net surface currents at homogenization boundaries can not be assumed zero as well as the homogeneous diffusion flux can not be assumed uniform within homogenization boundaries. In order to obtain the homogeneous surface flux, the diffusion equation has to be solved for the homogeneous media by applying the net surface currents of lattice calculation as boundary conditions. In Serpent, the net currents for the surface boundaries are calculated with standard surface current tallies, and a two-dimensional diffusion flux solver is implemented to calculate the homogeneous surface flux. However, the Serpent method has limitations and can produce non-physical results when the net surface currents are close to zero. In such cases, the statistics of this estimate are very poor, and to reach convergence may not be feasible, especially for higher number of energy groups applied in the diffusion calculation (Leppänen et al., 2016).

The SPH method, initially proposed by (Kavenoky, 1978) and extended by (Hebert and Benoist, 1991; Hebert and Mathonniere, 1993), is typically used to produce few-group XS for pin-by-pin transport and diffusion calculations of LWR cores (Courau et al., 2008; Grundmann and Mittag, 2011; Lemarchand et al., 2012). The aim of the method, is to preserve the reaction rates of reference heterogeneous transport solution in homogeneous diffusion calculation. In this method, the ratio of the heterogeneous and homogeneous node-average fluxes is used to correct XS. As compared to GET, the calculation of boundary net currents is not needed, but only the estimation of node-average multi-group fluxes. Obtaining such estimates with Serpent is statistically more simple task, especially for lattice models. On the other hand, the SPH method needs an iterative procedure to obtain the correction factors, while GET does not.

Several other techniques have been applied in order to improve the accuracy of the control rod few-group cross sections. For example, in the ERANOS code, the transport–transport reactivity equivalence method is routinely used for the treatment of regions containing control rods (Rimpault et al., 2002). More recently, the nodal equivalence theory was applied to produce discontinuity factors for the interfaces between a control assembly and surrounding fuel assemblies (Heo and Kim, 2014). The method, however, requires the conversion of heterogeneous X–Y control rod geometry into a simplified multi-ring R–Z model.

Although, several methods exist to further improve the accuracy of the nodal diffusion solutions, the goal in this research was to assess the potential of the SPH method for SFR cores. A very similar technique was used by (Takeda et al., 2005; Takeda, 2011),

2.4. Super-homogenization method for SFR analysis

but the improvement in nodal results (e.g., reactivity, radial power distribution and CR worth) due to the use of this equivalence method was not assessed.

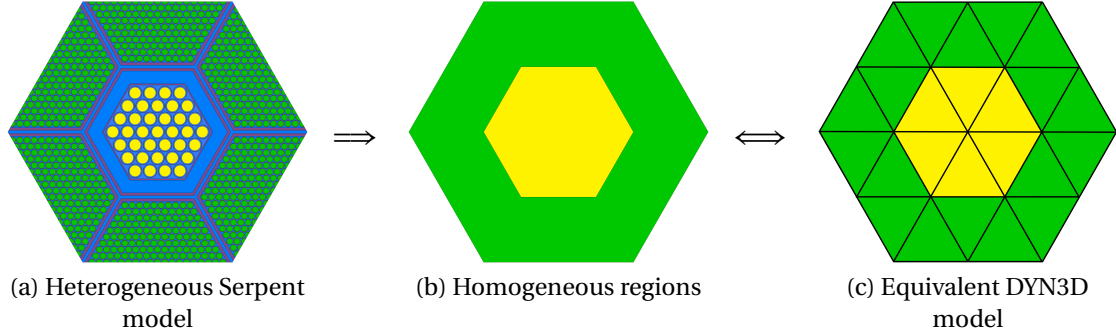


Figure 2.7: Serpent and equivalent DYN3D super-cell models for the evaluation of SPH factors.

The application of the SPH method in this study was inspired by the experience gained in the pin-by-pin calculations of LWRs with DYN3D at HZDR (Grundmann and Mittag, 2011; Baldova et al., 2014). The SPH factors were calculated using the Serpent and DYN3D codes in the following manner:

1. Previously specified heterogeneous super-cell Serpent models of non-multiplying regions (Fig. 2.6) were used to produce reference transport solution. The few-group XS and fluxes were calculated for the two homogeneous regions, e.g., fuel and control rod as shown in Fig. 2.7b.
2. The homogeneous super-cell DYN3D model equivalent to the heterogeneous super-cell model was constructed as shown in Fig. 2.7c. Since it is impossible to build the homogeneous super-cell model using hexagonal elements, the fuel and non-multiplying regions were sub-divided into triangular nodes (Fig. 2.7c). For this purpose, the trigonal diffusion version of the DYN3D code was used (Duerigen et al., 2013).
3. The SPH factors were obtained with the following standard iterative procedure to which the description was adopted from (Baldova et al., 2014):
 - (a) The diffusion solution is calculated with DYN3D for the super-cell model (Fig. 2.7c) employing few-group XS generated by Serpent. Then the neutron fluxes are averaged over the fuel and non-multiplying regions (green and yellow colors in Figs. 2.7b and 2.7c).

Chapter 2. Generation of homogenized few-group cross sections

- (b) The SPH factors μ for every region r ($r = 1, 2$) and energy group g ($g = 1, \dots, 24$) are calculated as:

$$\mu_{r,g} = \frac{\bar{\phi}_{r,g}^{Het}}{\phi_{r,g}^{Hom}} N_g, \quad (2.1)$$

where $\bar{\phi}_{r,g}^{Het}$ and $\phi_{r,g}^{Hom}$ are the average heterogeneous and homogeneous neutron fluxes in region r and group g obtained from heterogeneous Serpent transport solution and homogeneous DYN3D diffusion solution respectively. N_g is a normalization factor calculated as:

$$N_g = \frac{\sum_r V_r \phi_{r,g}^{Hom}}{\sum_r V_r \bar{\phi}_{r,g}^{Het}}. \quad (2.2)$$

- (c) Modified cross sections, $\Sigma_{r,g}^{Mod}$ are calculated for every region and energy group using the SPH factors generated according to Eq. (2.1):

$$\Sigma_{r,g}^{Mod} = \mu_{r,g} \Sigma_{r,g}. \quad (2.3)$$

- (d) The two-region super-cell diffusion problem is solved again by the code DYN3D using the modified cross sections. The obtained homogeneous neutron fluxes are used for the calculation of a new set of the SPH factors. This iterative process is terminated after n iteration when the convergence criterion is satisfied for every r and g :

$$\max \frac{|\mu_{r,g}^n - \mu_{r,g}^{n-1}|}{\mu_{r,g}^{n-1}} < 10^{-6}. \quad (2.4)$$

The SPH method was applied to correct the flux-volume weighted few-group XS of non-multiplying and blanket regions. The iteration of SPH factors was performed simultaneously for both regions: the region of interest (e.g., CR) and the surrounding fuel. This implies that, instead using XS obtained from the 3D single assembly model, the SPH-corrected fuel XS has to be used for neighboring fuel assemblies of the problematic region in the full core nodal calculation. Applying the SPH-corrected fuel XS improves the full core nodal diffusion solution (k_{eff} and radial power distribution) in respect to the case when the uncorrected fuel XS were obtained with 2D infinite assembly model.

2.5. Verification by means of code-to-code comparison

However, the fuel XS generated in a 2D model does not account for the spectral and spatial self-shielding effects of the axial environment. It was found in this study that by keeping the correction on the non-multiplying XS, but omitting the corrected fuel XS from the 2D super-cell model, provides consistently and significantly better results (improvement in $\Delta\rho$ is more than ~ 100 pcm) in all full core nodal diffusion calculations presented in this thesis. The XS obtained from the 3D single assembly model are applied to all fuel assemblies, including fuel assemblies neighboring to the problematic regions (e.g., CRs).

2.5 Verification by means of code-to-code comparison

By using the methods described previously (Sections 2.3 and 2.4), the homogenized few-group cross sections were generated with Serpent for both reference cores on the 24 energy group structure. The 3D full core nodal diffusion solution of the reference cores was calculated with DYN3D by using the Serpent XS.

The DYN3D results, such as core integral parameters and radial power distributions, were compared against the full core Monte Carlo solutions of Serpent, as presented in this section. The reference full core solutions were obtained by the averaging the results of the 20 independent Serpent calculations each of which was executed with an overall 960 million neutron generations (i.e. 1500 active and 200 skipped cycles with 640 thousand neutrons per generation). This is in order to obtain a more realistic estimate of the real variance of the radial power values.

In order to demonstrate the effect of the SPH correction on the accuracy of the results the DYN3D calculations were repeated twice: (1) without using the SPH correction and (2) using SPH-corrected few-group cross sections on some selected regions. In case of the OECD/NEA core the generated cross sections were also cross-checked with another nodal diffusion code PARCS (subsection 2.5.2) with the help of Konstantin Mikityuk from the Paul Scherrer Institute (PSI).

2.5.1 Results of the OECD/NEA large oxide core calculations

In the comparison of the OECD/NEA core solutions the following parameters were evaluated: core multiplication factor (k_{eff}), effective delayed neutron fraction (β_{eff}), Doppler constant (K_D), sodium void worth ($\Delta\rho_{Na}$), total CR worth ($\Delta\rho_{CR}$), and radial

Chapter 2. Generation of homogenized few-group cross sections

power distribution.

The $\Delta\rho_{Na}$ was estimated as the reactivity change between the sodium voided and nominal states: $\Delta\rho_{Na} = \rho_{\text{void}} - \rho_{\text{nominal}}$. In the benchmark, the sodium voided state is defined by voiding sodium in the active core only. Doppler constant was calculated as:

$$K_D = \frac{(\rho_2 - \rho_1)}{\ln \frac{T_2}{T_1}}, \quad (2.5)$$

where T_1 and T_2 are the nominal and perturbed fuel temperatures and ρ_1 and ρ_2 are corresponding reactivity values. According to the benchmark specifications, the perturbed fuel temperatures is a factor of two of that of the nominal average fuel temperature and is equal to 3000 K. The $\Delta\rho_{CR}$ was calculated as the reactivity change between the roddeed and nominal states: $\Delta\rho_{CR} = \rho_{\text{roddeed}} - \rho_{\text{unroddeed}}$, while for the roddeed case all the CSD and DSD assemblies were fully inserted to the bottom of the active core. In the calculations utilizing the SPH method, the SPH-corrected cross sections were generated only for the control assemblies (CSD and DSD) and the CR followers. The SPH factors are summarized in Table 2.2.

The integral core parameters evaluated by Serpent and DYN3D are presented and compared in Table 2.3. As compared to Serpent, DYN3D without the SPH correction underestimate k_{eff} by 128 pcm in the unroddeed state. However, the difference is reduced to 64 pcm when SPH-corrected XS are used by the code. In the roddeed state, without the SPH correction, DYN3D k_{eff} values deviate from the reference by 255 pcm. This difference is noticeably higher than for the unroddeed state. The use of the SPH correction significantly reduces the discrepancy to 107 pcm. The application of the SPH correction noticeably improves the prediction of the total CR worth, while the deviation from the reference value reduces from 127 to 43 pcm for DYN3D.

Table 2.4 shows a more detailed decomposition of the reactivity effects induced by treating DSDs and CSDs with and without SPH corrections. For the both unroddeed and roddeed states, the largest improvement in the reactivity prediction of ~70% can be attributed to the SPH correction applied to CSDs.

Effective delayed neutron fraction and Doppler constant calculated by DYN3D agree within few pcm with those of Serpent. DYN3D overestimates the sodium void effect by about 90 pcm. The prediction accuracy for K_D and $\Delta\rho_{Na}$ is not improved with the

2.5. Verification by means of code-to-code comparison

Table 2.2: Group-wise SPH factors for CSD, DSD and CR follower.

Group #	CSD	DSD	Follower	Group #	CSD	DSD	Follower
1	0.7587	0.8180	0.8353	13	1.0043	0.9243	1.0278
2	0.7931	0.8130	0.8303	14	0.9969	0.9596	1.0082
3	0.8410	0.8538	0.8636	15	0.9911	0.9211	1.0067
4	0.8755	0.8817	0.8963	16	0.9855	0.8794	1.0161
5	0.9487	0.9531	0.9681	17	0.9807	0.9037	0.9685
6	0.9860	0.9806	0.9741	18	0.9301	0.7795	0.8405
7	0.9525	0.9373	0.9668	19	0.8854	0.9249	1.0817
8	1.0046	0.9971	1.0262	20	0.8912	0.9166	1.0808
9	0.9771	0.9516	0.9828	21	0.8916	0.9096	1.0488
10	0.9941	0.9676	1.0121	22	0.8686	0.8914	1.0578
11	1.0013	0.9639	1.0045	23	0.9077	0.9643	1.0737
12	0.9960	0.9398	0.9824	24	0.8977	1.0445	1.0659

Energy group numbering according to Table 2.1.

Table 2.3: Comparison of the core integral parameters of the OECD/NEA core.

		Serpent *	Difference (pcm)			
			vs. DYN3D	+ SPH	vs. PARCS	+ SPH
k_{eff}	Unrodded	1.01070	-128	-64	-84	-21
	Rodded	0.95249	-255	-107	-264	-121
Feedbacks (pcm)	$\Delta\rho_{CR}$	-6046	-127	-43	-180	-100
	K_D	-852	-15	-15	-15	na.
	$\Delta\rho_{Na}$	1864	87	90	81	na.
β_{eff} (pcm)		358	-2	-2	-2	-2

* Standard deviation of $k_{eff} = 2$ pcm.

Chapter 2. Generation of homogenized few-group cross sections

use of SPH correction on the control assemblies.

Table 2.4: Application of SPH correction in OECD/NEA core: decomposition of the reactivity effects.

State	SPH application	DYN3D vs Serpent (pcm)	Improvement (pcm)	Contribution (%)
<i>Unrodded</i>	No SPH	−128	ref	
	<i>All CRs</i>	−64	64	100.0
	Only CSD	−86	42	65.6
	Only DSD	−106	22	34.4
<i>Rodded</i>	No SPH	−255	ref	
	<i>All CRs</i>	−107	148	100.0
	Only CSD	−152	103	69.6
	Only DSD	−210	45	30.4

The full core normalized radial power distribution calculated with Serpent for unrodded and rodded states are depicted in Fig. 2.8. The relative difference in radial power distribution between Serpent and nodal diffusion codes is shown in Figs. 2.9 and 2.10 for unrodded and rodded states respectively. Subfigures *a* and *b* show the DYN3D results obtained without and with SPH factors, respectively.

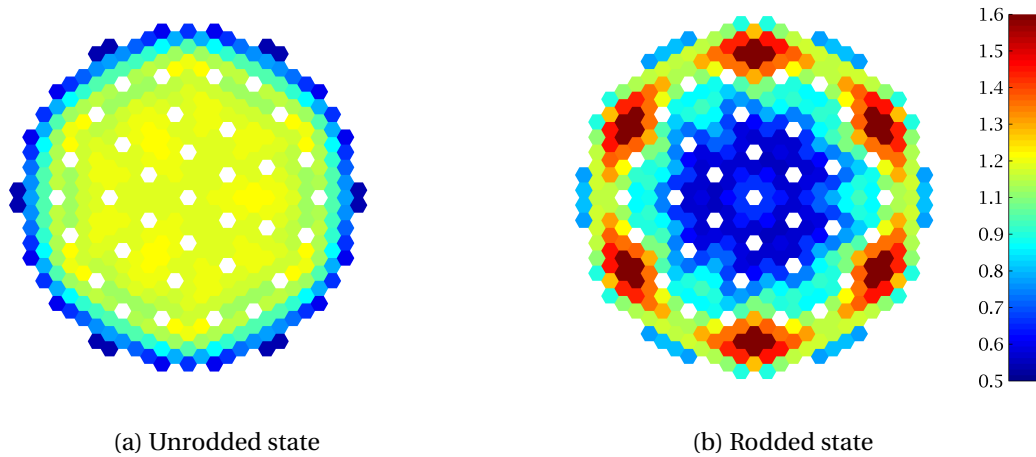


Figure 2.8: Normalized radial power map of the OECD/NEA core, Serpent full core Monte Carlo.

The radial power distribution predicted by DYN3D without the SPH correction for

2.5. Verification by means of code-to-code comparison

unrodded state is already in a very good agreement with the reference Monte Carlo solution while the average/maximum differences are about 0.25/0.66%. The use of the SPH correction only slightly improves the prediction accuracy (Fig. 2.9b), while the deviations are reduced to 0.21/0.59%. However, for the rodded state, the use of the SPH correction significantly reduces the deviation from the reference Monte Carlo solution (Fig. 2.10b). In this case the average/maximum difference drops from 1.74/4.67% to 0.32/1.41%.

2.5.2 Cross-checking with PARCS code

The same calculations done on the OECD/NEA oxide core were also performed with PARCS code (Downar et al., 2010) by using the same homogenized few-group cross sections as in the DYN3D calculations. This was done in order to demonstrate that this XS generation methodology is not limited to DYN3D, but can be applied for practically any nodal diffusion code. The PARCS calculations were carried out by Kontstantin Mikityuk at PSI, while the XS and the SPH factors were provided by the author.

The PARCS results on the OECD/NEA core are presented side-by-side with DYN3D results in the preceding subsection. The integral core parameters are presented and compared with Serpent and DYN3D in Table 2.4 in the previous subsection. The presented results show generally the same good agreement between PARCS and Monte Carlo solution, as for DYN3D. As compared to Serpent, PARCS without the SPH correction underestimates k_{eff} by 84 pcm. However, the difference drops to 21 pcm when SPH-corrected XS are used. Without the SPH correction, PARCS k_{eff} value deviates from the reference by 264 pcm. The use of the SPH correction significantly reduces the discrepancy to 121 pcm. Similarly to the DYN3D results, the SPH factors noticeably improve the prediction of the total CR worth of PARCS, while the deviation from the reference value is reduced by ~ 80 pcm to 100 pcm. The Doppler constant and the sodium void worth calculated with PARCS are in complete agreement with the ones of DYN3D.

The power prediction of PARCS is also in the same good agreement with the Monte Carlo reference as DYN3D. As seen in Figs. 2.9 and 2.10 the differences compared to the Serpent solution are consistent with DYN3D differences. Furthermore, the application of the SPH method provides a similar improvement in the nodal diffusion solution of PARCS, as for DYN3D. In the unrodded case, without the SPH correction, the average/maximum differences are about 0.35/1.07% for PARCS. The use of the SPH

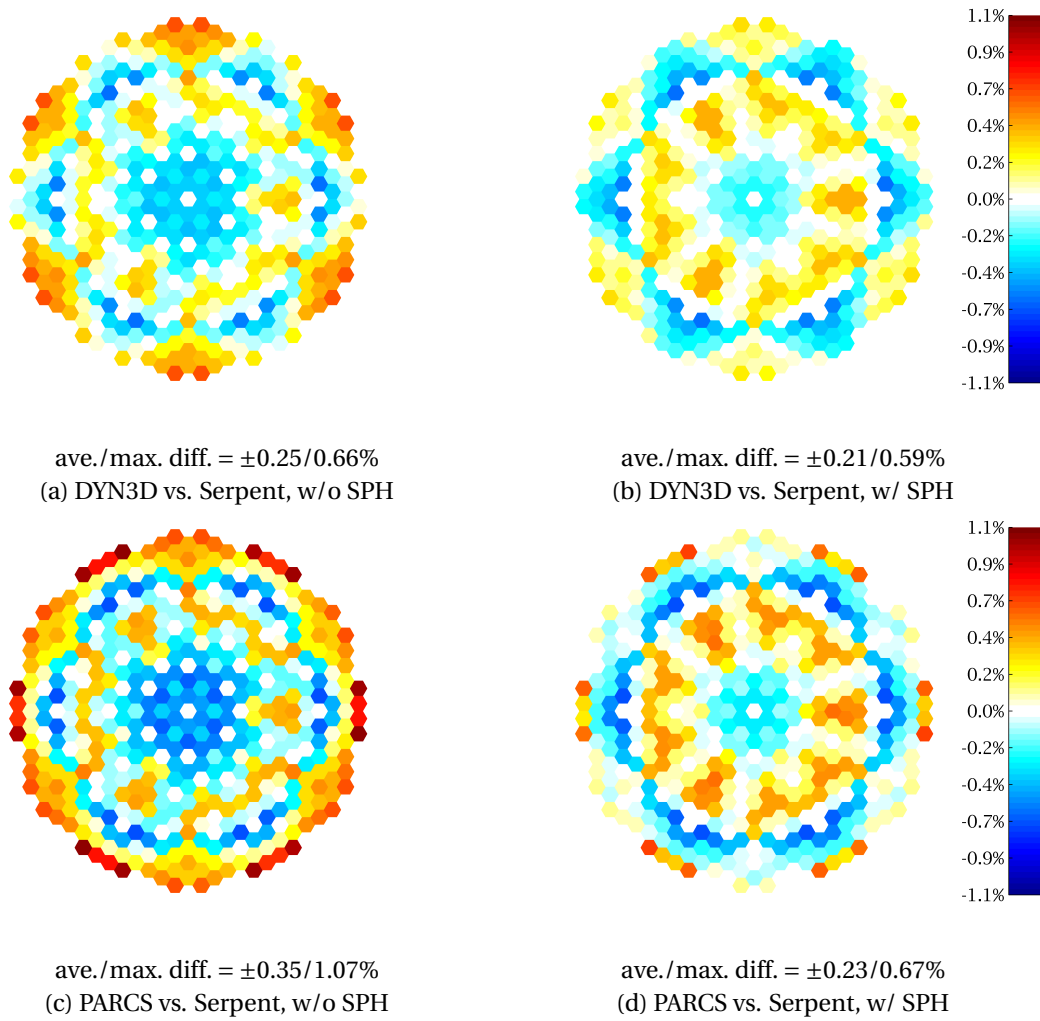


Figure 2.9: Relative difference in radial power distribution of the OECD/NEA core, unrodded state.

2.5. Verification by means of code-to-code comparison

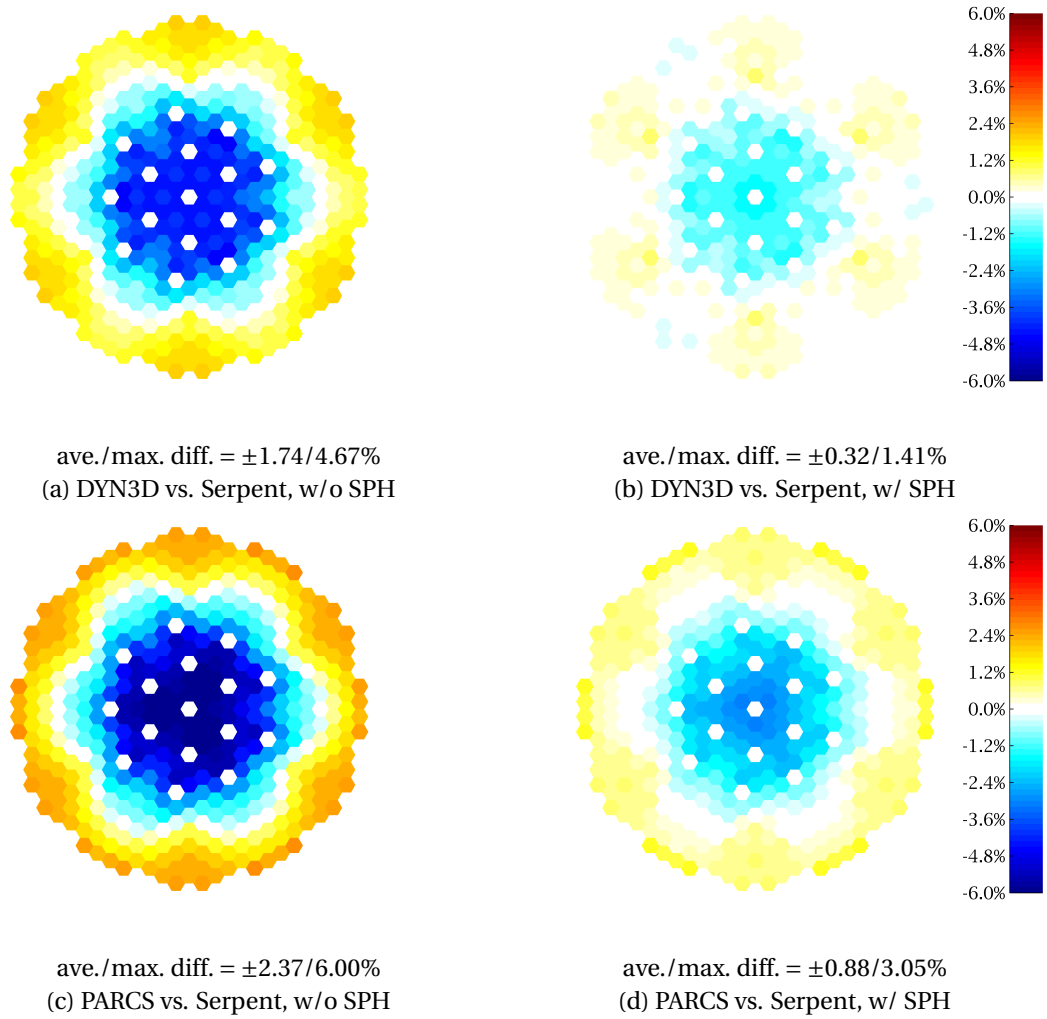


Figure 2.10: Relative difference in radial power distribution of the OECD/NEA core, rodged state.

correction slightly reduces the deviation from the reference solution to 0.23/0.67%. The significant improvement due to the use of SPH factors in the rodded state is also present in the PARCS results, while the originally predicted average/maximum difference drops from 2.37/6.00% to 0.88/3.05%.

2.5.3 Results of Phenix EOL core calculations

The Phenix EOL core was also calculated with the Serpent-DYN3D codes sequence for further verification of the XS generation method. For this calculation the reference state of the control rod withdrawal benchmark was selected (IAEA, 2014), where the primary control rods are partially inserted in the core (~558 mm) while the secondary rod is in withdrawn position.

In this subsection, deterministic DYN3D and Monte Carlo Serpent solutions, the core eigenvalue (the $\Delta\rho$ in Table 2.5) and the radial power distributions are compared. The normalized radial power distribution of the Phenix core calculated with Serpent is presented in Fig. 2.11.

As it is also seen in the radial power distribution (Fig. 2.11), the Phenix core is much smaller than the OECD/NEA core, moreover, it has a significantly stronger radial power gradients in the core, and at the beginning of the low power region of blanket assemblies the radial peaking factor drops from around 1.0 to 0.3. At such regions as around the blankets, where the flux and power gradients are large, the modeling with nodal diffusion methods is inherently more challenging due to diffusion approximation of the transport equation. This strongly reflects on the DYN3D solution when the Super-homogenization method is not yet applied, as shown in Table 2.5, where the difference in the multiplication factor in respect to the Serpent reference is as high as 569 pcm. While the deviation in normalized radial power from the reference solution is in good agreement in the fissile core with average/maximum difference of 0.52/1.10%, but the discrepancies in the fertile blanket region are significantly higher with values of 2.16/5.80% (Fig. 2.12).

The use of the SPH method on different regions of the core, consequently improves the nodal solution of the Phenix core. Table 2.5 presents the overall reactivity improvement and the decomposed contribution by regions. As it shows, the application of SPH factors on all blanket and non-multiplying regions reduces the difference in reactivity from 569 to 162 pcm. The main contributors to the improvement are the

2.5. Verification by means of code-to-code comparison

SPH factors applied on the control assemblies with $\sim 40\%$ of the total effect. In some regions, like in the upper blanket and the radial reflector assemblies, the use of SPH method does not affect the core reactivity. Significant improvement is only seen when the first-neighbor regions to the fissile fuels are corrected with the SPH factors.

While the average difference in radial power between DYN3D and Serpent solutions did not change much with application of the SPH method (Fig. 2.12b), but noteworthy improvement is seen in the maximal deviation. In the fissile core the maximal difference in radial power is dropped from 1.10 to 0.68%, whereas in the radial blanket assemblies it reduced from 5.80 to 4.54%, as presented in Fig. 2.12.

Table 2.5: Application of SPH correction in Phenix EOL core: decomposition of the reactivity effects.

SPH application	DYN3D vs Serpent (pcm)	Improvement (pcm)	Contribution (%)
No SPH	-569	ref	-
All SPH	-162	407	100.0
Control assemblies	-408	161	39.6
Radial blanket	-473	96	23.7
Inside core reflectors	-509	60	14.8
Lower axial blanket	-514	55	13.5
Sodium plenum	-534	35	8.6
Upper axial blanket and outside core reflectors	-569	0	0.0

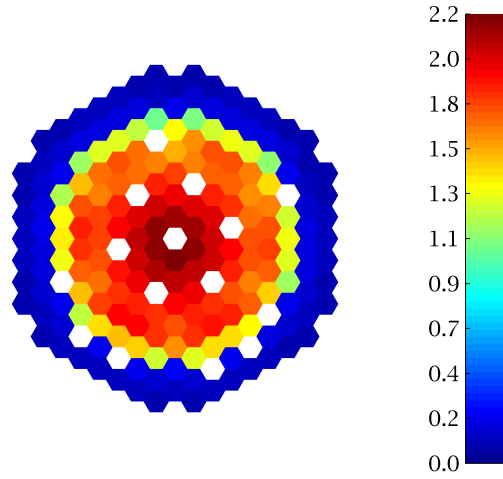


Figure 2.11: Radial power map of the Phenix EOL core, Serpent full core Monte Carlo.

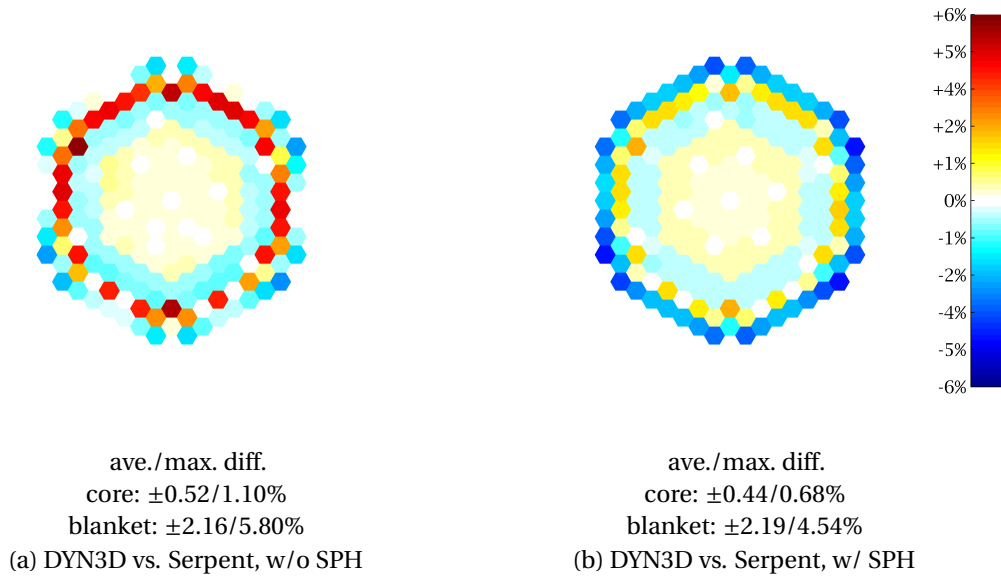


Figure 2.12: Relative difference in radial power distribution of the Phenix EOL core.

2.6 Few-group cross section generation – Summary of the results

The two-step methodology, previously applied to the analysis of simplified SFR cores, was successfully utilized by the author for more realistic and detailed SFR core configuration: the large 3600 MWth oxide core from the OECD/NEA benchmark, and the smaller 350 MWth oxide core from the Phenix EOL experiments. Firstly, the homogenized few-group cross sections were generated on lattice level with Monte Carlo code Serpent, and secondly, these were used in the nodal diffusion code DYN3D in the full core modeling.

The prediction accuracy of the deterministic core simulator was assessed by comparing the results against the full core Serpent solution as reference. The results of DYN3D models were in a very good agreement with the reference solution. This implies that such computational sequence can be applied for the static neutronic analysis of detailed SFR cores.

Then in this chapter, the Super-homogenization method was tested in order to improve further the accuracy of the nodal diffusion solution. The SPH method together with the Serpent-DYN3D codes sequence was verified against the full core Serpent solution. The presented results show that application of the SPH correction leads to a better agreement between the nodal diffusion and the Monte Carlo solutions. It is worth noting that the improvement in k -eff and radial power distribution is significantly more pronounced in the case of the rodded core. The SPH factors applied on blankets and non-multiplying regions, that are first-neighbors to the fissile fuels assemblies, were the main contributors to the improvement of the solution. In summary, the generation of the SPH factors, while poses relatively minor additional computational burden, can noticeably improve the accuracy of the nodal diffusion codes applied to the analyses of SFR core.

In order to cross-check the few-group cross section generation methodology and the SPH method, the OECD/NEA large oxide core calculations were repeated with the PARCS nodal diffusion code by applying the same XS library. The PARCS solutions were in very good agreement Serpent, and basically the results were aligned with DYN3D solution. It was demonstrated that practically any other nodal diffusion code can be also used for realistic SFR core calculations by applying the XS generation and the SPH methodology presented in this chapter.

3 Modeling of thermal expansions

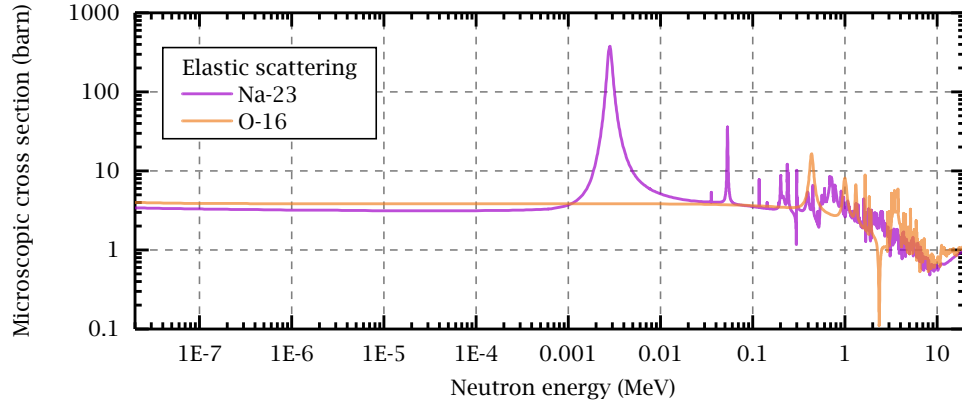
This chapter starts with an overview on the significance of modeling thermal expansions in SFR calculations. Section 3.2 provides a detailed description of the thermal expansion models that were implemented in DYN3D by the author. The test cases used for the preliminary verification of the models are described in Section 3.3. The numerical results are summarized in Section 3.4 demonstrating an adequate performance of the newly implemented models. Section 3.5 introduces a spatial decomposition method for the thermal expansion reactivity effects based on the nodal diffusion solution.

3.1 Thermal expansion effects

3.1.1 Reactivity effect of thermally expanding materials

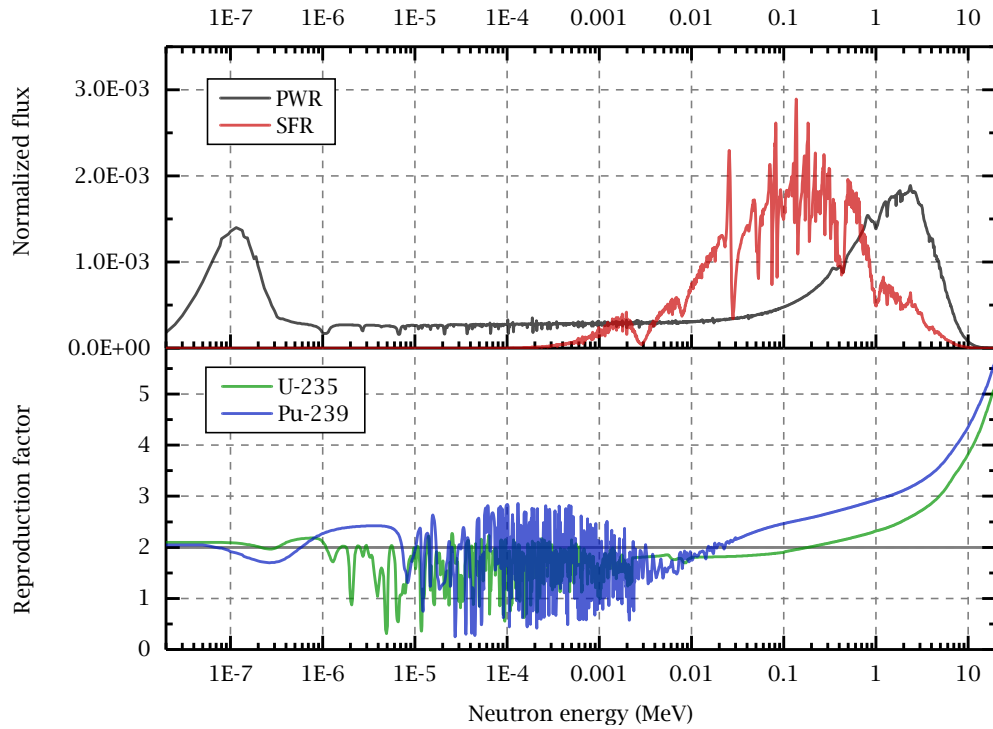
The reactivity effect arising from thermally expanding materials in SFR cores can be decomposed into the temperature effect on the microscopic cross sections and the effect of dimensional/density changes of the materials in respect to the surroundings.

In SFRs utilizing oxide fuels, both fuel- and coolant temperature effects is mainly attributed to the elastic scattering of neutrons on ^{16}O and ^{23}Na (Fig. 3.1). In nominal operation the elastic scattering, especially the large ^{23}Na resonance at ~ 3 keV, suppresses the neutron flux to the lower energies where the ^{238}U capture cross section are higher (Sun et al., 2011). The increase in fuel temperature broadens the capture resonances of ^{238}U and ^{240}Pu (Doppler effect), therefore increasing the parasitic capture and providing a negative feedback to the system. The density reduction of the



Extracted from JANIS (Soppera et al., 2014).

Figure 3.1: Microscopic elastic scattering cross section of ^{16}O and ^{23}Na .



Reproduction factors extracted from JANIS (Soppera et al., 2014).

Figure 3.2: *Top*: Neutron flux distribution in PWR and SFR fuels; *Bottom*: the energy-dependent reproduction factor of ^{235}U and ^{239}Pu .

3.1. Thermal expansion effects

fuel material increases the mean free path of neutrons, i.e. it increases the chance of escaping the fuel matrix. These neutrons are more likely to slow down and being captured in the surroundings (e.g., cladding, coolant, etc.), or completely leaking from the system. Therefore, the density effect is additionally strengthening the negative temperature feedback of the fuel.

The thermally expanding coolant reduces its own density, which decreases the scattering and capture events on ^{23}Na and hardens the neutron spectrum. The spectrum hardening is always a positive feedback in SFRs, not only because of the lessening neutron capture events at lower energies, but mainly because of the increase of neutron population due to the threshold fission in ^{238}U at high energies and the increasing reproduction factor (η – number of neutrons produced per neutron absorbed) of ^{235}U and ^{239}Pu above 0.1 MeV, as shown in Fig. 3.2.

Table 3.1: Reactivity coefficients of typical PWR and SFR assemblies.

(pcm/K)	Doppler coeff.	Coolant temp. coeff.	Axial exp. of the fuel	Axial exp. of cladding	Radial exp. of the core
PWR ^a	-2.114	-56.903	-0.001	-0.062	+0.647
SFR ^b	-0.500	+0.675	-0.032	+0.073	-0.332

^a MOX 4.0% fuel assembly from (Kozłowski and Downar, 2007, p. 43).

^b MOX fuel assembly from the large oxide core (Blanchet et al., 2011, p. 7).

In contrast to LWRs, the reactivity effects of expanding structures in SFRs play a major role in reactor behavior and thus have to be considered in safety calculations. This can be attributed to the following reasons. Firstly, the coolant density effect and the Doppler effect are less dominant in SFRs. Secondly, the coolant temperature excess from nominal to boiling onset conditions is an order of magnitude higher (around 30 K in LWRs and more than ~300 K in SFRs, relatively to the typical core outlet temperature), and the thermal expansion effects become relevant before the overwhelming voiding effect takes over.

The former reason was investigated by comparing the reactivity effects of two typical MOX fuel assemblies (see in Table 3.1). The calculations were done with the Serpent code in 2D assembly model. Reflective boundary conditions were used and thus the leakage effect was ignored. The outcome of the comparison is summarized in Table 3.1. In case of the SFR, the Doppler effect is smaller by a factor of four, while the coolant temperature effect by two orders of magnitude. The amplitude of thermal expansion

Chapter 3. Modeling of thermal expansions

effects in the SFR are more comparable to the Doppler and coolant feedbacks, while in the typical PWR remain minor. Therefore, the thermal expansion effects have high potential in SFRs to influence the neutronic behavior, whereas they remain unnoticed in PWRs beside the coolant and Doppler effect.

It has to be emphasized, that the values presented in Table 3.1 consider only the spectral component of the feedback. In order to account for the additional leakage component, a full core calculations would be necessary. However, it is known that the smaller core size and higher neutron mean free path makes the SFRs more leaky to the neutrons. Due to the same reasons, the leakage is more sensitive to the increase in active core dimensions and decrease in fuel material densities. Therefore, the axial and radial fuel expansion effects become even more negative and more pronounced in the SFR cores.

Furthermore, the SFRs encounter significantly larger temperature variations during the operation. The typical temperatures of the Generation IV SFR designs range between 640-670 K and 780-820 K for inlet and outlet temperatures, respectively (Waltar et al., 2012). Moreover, the temperatures and temperature gradients can drastically increase further in transient conditions, e.g. in the accident scenario of the Unprotected Loss Of Flow (ULOF) transient, the peak coolant temperature can rise several hundred of degrees in just a few tens of seconds (Cahalan et al., 1990).

Nevertheless, the wide temperature range from normal operation till the condition of boiling onset provides an extensive margin (around 300-500 K), where the reactivity feedbacks could act as system safeguards, and the reactor could be passively shut down before the strong coolant voiding effects become predominant. For instance, the self-protective mechanisms of thermal expansions were demonstrated in the start-up tests of the MOX fueled Superphenix (Bergeonneau et al., 1990) or the heat removal tests of metallic core of EBR-II (Planchon et al., 1986).

It is worth mentioning that in ULOF accidents, because of the positive reactivity contribution of the Doppler effect, the thermal expansion feedback may not reduce the power fast enough to avoid loss of coolant and fuel rod failure. The metallic fuels have higher thermal conductivity, and so the temperature difference in respect to coolant (~ 100 -200 K) is significantly smaller than in oxide cores (~ 700 -800 K). This means that the total effect of Doppler is more modest in metallic cores, when the fuel temperature is reduced close to the coolant temperature during power decrease. This allows the power to reduce fast enough to avoid sodium boiling, which cannot be said

in the case of oxide cores as the sodium boiling conditions (~ 1150 K) can be reached within a minute (Cahalan et al., 1990; Lázaro et al., 2014b). Additional safety measures were proposed in the past to avoid boiling in oxide fueled SFRs during ULOF, like increasing the inertia of pumps to prolong the coastdown or implementing passive shut down devices such the gas expansion module (GEM) successfully applied in FFTF (Burke, 1998).

3.1.2 Thermal expansion feedbacks in SFR systems

The net thermal expansion feedback is a combination of the effects coming from the expansion of different system components. The most important contributors can be distinguished by the driving temperatures (Hummel and Okrent, 1970; Rouault et al., 2010; Waltar et al., 2012):

1. Fuel expansion

The temperature increase of the fuel material expands the dimensions of the fuel matrix, while the fuel material density proportionally decreases in order to preserve the mass. Because of to the elongation of the fuel pins, the surrounding mass of sodium is increased, therefore spectrum softening effect due to scattering will be also increased, and so the reactivity will be reduced. Moreover, the axial elongation of the fuel will increase the radial neutron leakage, and lower the reactivity further. The radial fuel expansion without coolant displacement is normally negligible, since it does not change the effective core radius.

2. Cladding expansion

The increase in cladding temperature reduces the material density, therefore reducing the scattering and parasitic capture of neutrons. The radially expanding cladding forces out some of the surrounding sodium, i.e. reducing the neutron scattering macroscopic cross section of sodium in the assembly. Both effects will harden the spectrum and therefore increase the core reactivity.

3. Wrapper expansion

The hexagonal sheet covering the fuel assemblies, i.e. the wrapper behaves in the same way as the cladding when it expands.

4. Diagrid expansion

The diagrid structure is located below the core holding each fuel assembly end-

fitting (Gallet and Venot, 1977). The radial expansion of the diagrid increases the distance between fuel assemblies, thus increasing sodium fraction in the core, which finally introduces negative reactivity. The diagrid temperature is driven by the averaged inlet sodium temperature.

5. Differential expansion between core, vessel and control rod drivelines

In pool-type SFRs, the core is sitting on the bottom of the vessel, and it can expand upwards depending on its temperature. The vessel and the control rod drivelines are fixed above the core and hanging down, therefore they can only expand downwards depending on the inlet and outlet sodium temperature, respectively. The relative expansion between the three components basically determines the control rod position change in respect to the core, i.e., the magnitude and the direction of the reactivity effect.

All these expansion phenomena significantly affect the core reactivity, and therefore, the modeling of thermal expansion effects cannot be neglected. Nevertheless, the standalone DYN3D is not capable of modeling the whole primary system, and calculate the thermal expansion of all system components. Therefore, only the axial and radial thermal expansion of the core will be accounted for in this thesis by modeling the first four of the aforelisted contributors in DYN3D calculations.

3.1.3 Current trends for modeling thermal expansions

In traditional transient analyses of SFRs, TH system codes are used along with point kinetics solvers (Lázaro et al., 2014a,b), where the thermal expansion effects are simply represented by the reactivity coefficients provided as input parameters. In case of spatial NK, while the density changes can be easily taken into account during the few-group XS generation procedure, supplementary models capable of handling changes in physical dimensions are required. Two main approaches are currently observed in the literature to model core deformations in spatial neutron kinetics, be it either thermal expansion or local displacement (e.g., assembly bowing):

1. Development of neutron kinetic solvers that are capable of solving the spatial neutronics on deforming meshes, e.g., the GeN-Foam from PSI/EPFL (Fiorina et al., 2015) and the CAST3M from CEA (Patricot et al., 2016).
2. Using an available neutron kinetics solver with fixed regular meshes, but manip-

ulating the homogenized few-group cross sections in the mesh cells in such a way, that the thermal expansion effects will be taken into account in the neutron kinetic solution.

For instance, in case of the axial expansion of fuel rods (i.e. bundle of fuel pins in assembly), the difficulty in the modeling with existing spatial NK codes can be attributed to the inflexibility of the regular mesh. Since all cells in a same axial layer have to be of an identical height, the direct use of the fixed-mesh codes restricts the modeling to a simplified case of the radially uniform axial expansion.

To overcome this limitation, several approaches based on the manipulation of homogenized few-group XS have been proposed and implemented in fixed-mesh spatial NK solvers so far (second approach). Some techniques have been developed (Reed et al., 2014; Andriolo et al., 2015; Gentili et al., 2015) based on the similarity theory proposed by (Shikhov, 1960) to calculate local deformation or expansion reactivity coefficients by using first order perturbation theory.

In an other technique, developed by (Ponomarev, 2017) in the SAS-SFR/PARCS codes system, the σ_0 -model (Pelloni and Mikityuk, 2011) is utilized to calculate XS *on the fly* from temperature-dependent self-shielded microscopic cross section libraries. These microscopic multi-group cross sections are generated beforehand with the deterministic cell-code ECCO. The isotopic densities necessary to obtain the XS are computed in this technique by considering the temperature and density effects as well as the axial material relocations due to thermal expansions.

Aside from the axial expansion modeling, the pixelation (Patricot et al., 2014) technique was developed with the second approach to calculate assembly bowing and flowering effects by considering the anisotropic inter-wrapper gap change between the assemblies.

The PARCS code, a nodal diffusion code similar to DYN3D, was extended with capabilities to model core thermal expansions as already mentioned before. In the FAST code system, PARCS can model axial and radial core expansion by physically expanding the nodal mesh, but it is limited to uniform core expansions. While the non-uniform expansion of fuel rods is possible to model in the coupled SAS-SFR/PARCS codes system, the radial core expansion is not yet available. For both code systems the main XS generation tool for SFR analyses is the deterministic code ERANOS. In case of modeling uniform core expansions, this can be replaced with MC code Serpent as it was done at

PSI (Ghasabyan, 2013). Although, Serpent is not applicable for the non-uniform axial expansion modeling in SAS-SFR/PARCS, which relies on the ECCO-based σ_0 -model.

3.2 Thermal expansion models in DYN3D

As compared to the developments done for PARCS, a different approach was selected for DYN3D to tackle thermal expansion modeling. First of all, instead of the deterministic code ERANOS, the XS generation procedure is based on using the MC code Serpent (see Chapter 2). Furthermore, any XS manipulation to account for material relocations is done with the homogenized macroscopic XS obtained from Serpent. This is also different to the method used in SAS-SFR/PARCS, where the “smeared geometry” approach (Ponomarev and Sanchez, 2014) uses microscopic cross section libraries to obtain homogenized XS on the fly during simulation. Secondly, the axial fuel rod expansion model in the FAST system (PARCS) is restricted to uniform cases. In DYN3D, the option to model non-uniform axial expansion cases is desired in order to catch asymmetric and local effects in the calculations.

In the process of XS generation for the DYN3D calculations, the thermal expansion of the structure is modeled explicitly. That is, the temperature and density effects as well as the change of dimensions are accounted for in the produced XS. Those components of expansion that *do not change* the nodal boundaries can be modeled in DYN3D *without modifying* the code. For instance, after radial expansion of the fuel pins, the expanded geometry does not exceed the initial nodal boundary, so the node remains same size. Such kind of expansion can be simulated with the proper XS directly in DYN3D.

On the other hand, the nodal boundaries are affected when the fuel pins expand axially or the diagrid increases the inter-assembly pitch size. In these cases, the utilization of proper XS is not sufficient, and additional thermal-mechanical models are needed to treat the deformation of the nodal mesh. Therefore, two new models were developed for DYN3D: the axial fuel rod expansion model (subsection 3.2.1) and the radial diagrid expansion model (subsection 3.2.2).

Beside these two new models, a new parametrization of XS was introduced that covers all core level thermal expansions. This also includes the radial expansion of fuel pins, and the volumetric expansion of the assembly wrapper and sodium coolant. The parametrization and dynamic reactivity decomposition is described in

subsection 3.2.3.

3.2.1 Thermal expansion model for fuel rods

The new axial expansion model of DYN3D is designed to be flexible to resolve the constraints of the nodal mesh. The idea of the model was to preserve the axial size of the nodes and to account for the axial expansion effects by manipulation of homogenized cross sections.

The axial movement of materials due to thermal expansion through fixed mesh is a similar problem to the control rod movement. In most cases, when the control assembly is introduced, the absorber material is only partially inserted in some nodes. For such cases, DYN3D computes the node-average XS by geometrical or flux weighting (Grundmann et al., 2005, p. 53).

The approach used to *mix* XS for the axial expansion modeling is based on the geometrical weighting model. As compared to the available approach, a completely new procedure had to be implemented into DYN3D that accounts for axial temperature profiles and for shifting of upper materials due to the expansion of lower ones. In DYN3D code the modeling of axial thermal expansion can be summarized as follows:

1. Initial axial discretization is specified to account for the material boundaries at some reference temperature (e.g. room temperature) as shown in Fig. 3.3, left.
2. The obtained axial nodes are further subdivided into a smaller node with a height of the anticipated maximal possible axial expansion of the lower node and into a bigger one as shown in Fig. 3.3, right.
3. For each assembly, local nodal temperatures are used for the estimation of the axial expansion and new material interface levels. It should be noted that all new material levels are located within the *stripped* regions as depicted in Fig. 3.3, right.
4. When a new material interface within the *stripped* regions is detected, the mixing of the XS is performed using volumetric weighting:

$$\Sigma_{\text{mixed}} = \frac{h_1 \Sigma_1 + h_2 \Sigma_2}{h_1 + h_2}, \quad (3.1)$$

where the indices 1 and 2 represent the lower and upper materials, h is the height of the material inside the *mixing* sub-node, Σ are the original XS, and Σ_{mixed} is the final XS for the *mixing* sub-node. The Σ includes all macroscopic reaction cross sections, group-to-group scattering matrices, and diffusion coefficients.

5. The nodal XS are generated before the calculation by taking into account the local thermal expansion effects (e.g. reduced material density) at given node temperatures. This is also done in case of the *mixing* sub-nodes. That is the Σ_1 and Σ_2 are computed according to the local node temperatures before the volumetric weighting is done.

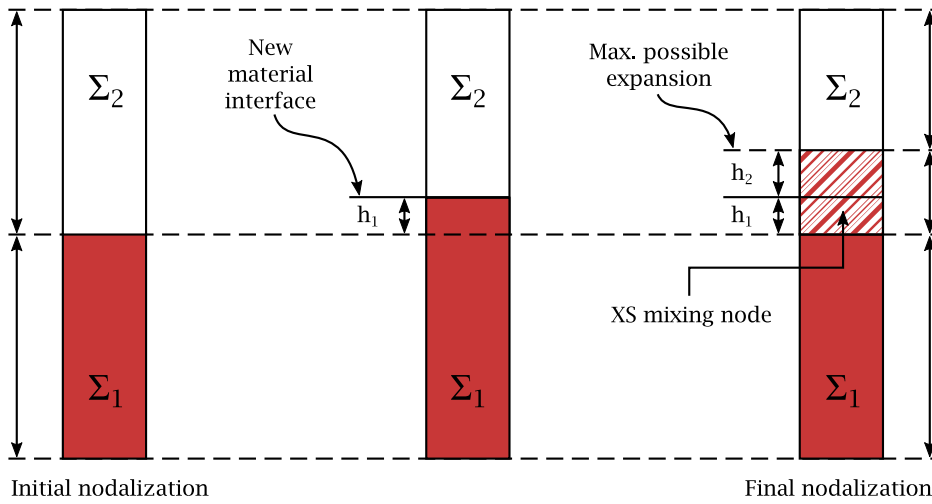


Figure 3.3: Overview of the *mixing* model for the treatment of axial expansions.

It has to be noted that adding extra nodes for mixing is completely up to the DYN3D user. After calculation of the new material interfaces, the program performs *mixing* in each node having more than one material. This is done regardless of the node size, and even when the material shrinks below the initial boundary.

In principle, the XS mixing can be performed without specifying additional *mixing* sub-nodes. However, axial expansion is relatively small compared to the height of the node. The XS mixing over entire *initial* nodes can lead to a so-called cusping effect (Lee et al., 1998; Dall'Osso, 2002) typical for the modeling of partially inserted control rods. This is especially problematic for the nodes with significantly different neutronic properties (e.g. adjacent fuel and sodium plenum nodes). The introduction of smaller *mixing* nodes is suggested to reduce this dilution and smearing effect.

The size of the *mixing* node can be limited to the anticipated maximal expansion. This value depends on the selection of the coldest and hottest state in the simulation. A reasonable choice is to use the isothermal state (e.g., 250°C) as the coldest and the melting temperature as the hottest state. In this thesis, the hottest state was always selected around the cladding melting temperature. Such size proved to be sufficiently small to avoid significant smearing effect, as presented later in Section 3.4.

Alternatively, when the modeling accuracy becomes insufficient, other weighting approaches for XS *mixing* can be applied in the later stage of code extension. Naturally, the first option would be to use the flux weighting approach of DYN3D control rod model (Grundmann et al., 2005, p. 53), which was also proposed in (Gehin, 1992). In this model, two additional calculations are needed per node to obtain nodal fluxes for weighting. In case of CR modeling, one calculation is done with totally roded and one with rod-free node. Then, these two different node-average fluxes are used for weighting. Such approach is less realistic for thermal expansions without using additional *mixing* nodes, since the fuel material does not intrude into the upper node more than ~5% of typically used node size.

Several other approaches were proposed in the past to reduce cusping effects in nodal diffusion calculations. The most relevant ones are summarized in (Lee et al., 1998; Dall’Osso, 2002). It has to be noted that most of these require additional computations to obtain the weighting factors by using, e.g., fine mesh fluxes, adjoint fluxes or axial discontinuity factors. Furthermore, by utilizing a nodal solver that can treat heterogeneous nodes would allow an implicit treatment of the mixing. For instance, the heterogeneous node technique was implemented in the 3D VARIANT code by (Marchetti, 2017, p. 87). However, an implementation of a different nodal solver into DYN3D is far beyond of this research, and currently, not aligned with the development strategy at HZDR.

The estimation of the axial expansion is done assuming a predefined gas gap condition (i.e. closed or open gap between fuel and cladding). In case of a closed gap, the expanding cladding is dragging the fuel pellets upwards, i.e., the fuel and cladding expand simultaneously driven by the cladding temperature. If the gap exists, then one can assume that the axial expansion of the fuel and the cladding is taking place separately driven by their own temperatures. In such case, the new material interface (h_1 in Fig. 3.3) is determined by the fuel pellet expansions only. In any case, the density reduction of the cladding is taken into account in XS generation step according to the

given nodal cladding temperature.

For a more accurate modeling of fuel rod deformation, a coupling with structural-mechanical model and fuel performance code is needed. Then it would be possible to simulate additionally: e.g., fuel-cladding interaction to determine local gas gap conditions, *ballooning* of the cladding at prompt power rise, pin-to-pin or pin-to-wrapper interactions through the pin wires, etc. However, such development is only envisaged for the later stage of code extension.

3.2.2 Radial thermal expansion model for the diagrid

The diagrid located below the core acts as a sodium flow distributor and a support structure for core assemblies. The radial expansion of diagrid driven by an increase of inlet sodium temperature extends the distance between fuel assemblies (assembly pitch) whereas the size of the assemblies (flat-to-flat distance) remains unchanged, as presented in Fig. 3.4. Consequently, the effective core radius is increased (while obviously keeping the total fissile amount) as well as the total sodium amount in the core. The larger effective core radius increases the axial neutron leakage, and the higher sodium fraction in fuel assemblies induces a higher ^{238}U capture rate through the down-scattering effect of ^{23}Na . Both effects introduce a negative reactivity feedback.

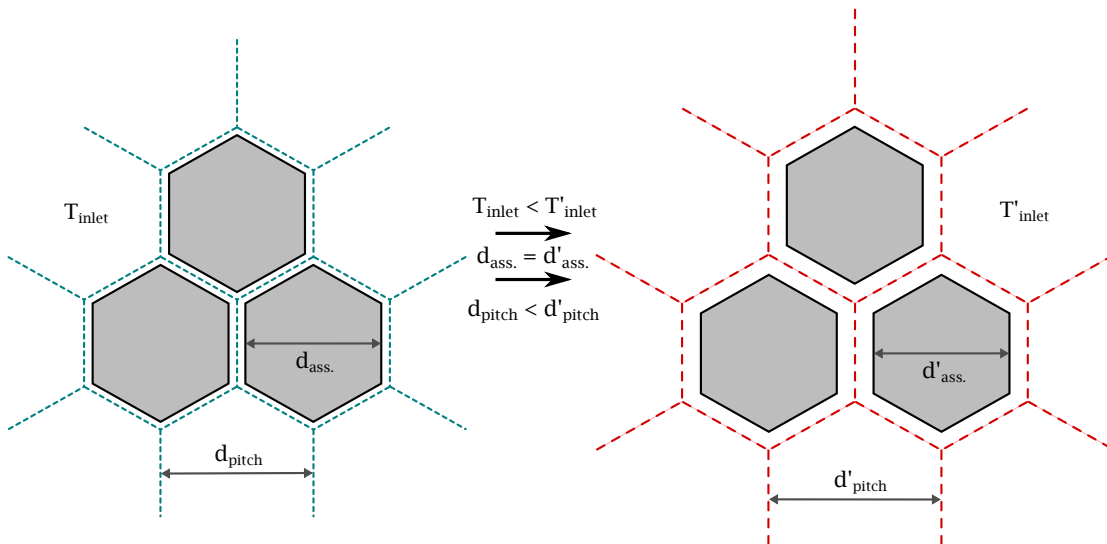


Figure 3.4: Schematic overview of the diagrid (assembly pitch) expansion.

The new radial thermal expansion model (hereinafter diagrid model) assumes a uni-

form radial expansion driven by the average inlet sodium temperature. During calculations, DYN3D updates the radial hexagonal assembly pitch based on the current diagrid temperature and the corresponding linear expansion coefficient. The XS data library format utilized by DYN3D was modified to introduce the assembly pitch as a new independent state parameter, which can be accounted for in the few-group XS generation process. The new diagrid model, DYN3D can simulate the time-dependent diagrid heat-up or cool-down, and is able to apply, respectively, the expanded or contracted assembly pitch size in the steady-state and transient core calculations.

The diagrid expansion model assumes that only the gap between the assemblies is increased. In the mean while the material densities, fuel rods dimensions, pin-to-pin pitch size, and the dimensions of hexagonal wrapper remain unchanged. This means that the amount of sodium inside the assembly wrapper is unchanged and only the amount of inter-wrapper sodium is increased (Fig. 3.4). It should be kept in mind that at the stage of XS generation the volume used for homogenization has to be extended accordingly in order to be applied in the radially expanded nodal mesh. The radial expansion of the fuel rods and assembly wrapper is treated separately, and these are driven by other state parameter, as described in subsection 3.2.3.

When the coolant temperature at pump inlet is known instead of the core inlet, a heat structure model can be applied to calculate the diagrid temperature by accounting for it's thermal inertia. The time-dependent diagrid temperature can be estimated with the one-dimensional cylindrical heat structure model additionally implemented into DYN3D. The model solves the Fourier heat conduction equation with constant properties (k thermal conductivity, ρ density and c specific heat):

$$\frac{\partial T}{\partial t} = \frac{k}{\rho c} \frac{1}{r} \frac{\partial}{\partial r} r \frac{\partial T}{\partial r}, \quad (3.2)$$

by using $\left(\frac{\partial T}{\partial t} = 0\right)$ and surface convection boundary conditions at the cylinder center and surface, respectively. The Crank-Nicolson method (Crank and Nicolson, 1996) is used for discretization that provides a numerically stable implicit second order method to solve Eq. (3.2). The system of linear equations is computed with the tridiagonal matrix algorithm.

The numerical implementation of the heat structure model was verified with the approximate analytical solution of the transient heat-up of an infinitely long cylinder (Baehr and Stephan, 2006, p. 167). By default, the cylindrical model is divided into ten

Chapter 3. Modeling of thermal expansions

rings and the stainless steel type 316 was selected for diagrid material. The thermal-physical properties were implemented from (Chawla et al., 1981).

The simplified heat structure model has to be used with caution, because the sodium flow regime is much more complicated in reality than it is typically modeled in system codes. The liquid sodium, after entering the diagrid structure, flows between very densely positioned assembly end-fitting columns. Then, it enters the columns through elongated slots and streams upwards in the assembly end-fittings. Only after that, the sodium reaches the core, as described in (Gallet and Venot, 1977). This kind of geometry provides a large contact area and turbulent flow regimes. Usually, a detailed specification of the diagrid structure is not available, and the decision on the heat transfer area is often based on simplified models and engineering judgment.

In system analyses, the coolant behavior in the diagrid is often modeled with 0D models. As reported in (IAEA, 2013), such modeling overestimates the thermal inertia of the diagrid, and calculates a much lower temperature. In the case of Phenix core, it was demonstrated in (Chenu et al., 2012) that the assumption of a very low thermal inertia in the diagrid provides a good agreement between the simulation and experiment. It also presented an almost synchronous evolution of the diagrid expansion reactivity contribution and the core inlet temperature. This suggests that applying the core inlet temperature for direct expansion of the diagrid is a good approximation, when this temperature is known and the diagrid specification is insufficient.

3.2.3 Expansion-dependent XS treatment by DYN3D

Before using DYN3D, state-dependent XS for each material type have to be generated to encompass all relevant reactor operation conditions. DYN3D uses multi-dimensional tables that cover the full parametric space of the XS. To acquire the nodal data of a current state, a multi-dimensional interpolation is performed between the available states. Since these tables contain XS for all possible combinations of parameter variations, the correlations between state variables are implicitly considered.

Parametrization of XS for SFR calculations

A new set of state parameters is proposed for SFR calculations that also cover the core level thermal expansion effects, as described in the following:

- Fuel temperature

The change in fuel temperature is considered to account for the Doppler effect. The node-average fuel temperature is obtained by DYN3D with the 1D fuel rod model.

- Sodium coolant temperature

Depending on the coolant temperature, the change of sodium temperature and density is considered, i.e. the thermal expansion of sodium is modeled. The thermal expansion of the assembly wrapper is assumed to be driven by the sodium temperature, and so the change in wrapper dimensions, temperature and density is also accounted for (Fig. 3.5). In DYN3D, the coolant flow inside and outside of the wrapper is modeled together as one thermal-hydraulic channel. Therefore, all sodium and the wrapper temperatures are modeled as equal. The node-average coolant temperature is obtained by DYN3D with the thermal-hydraulic model.

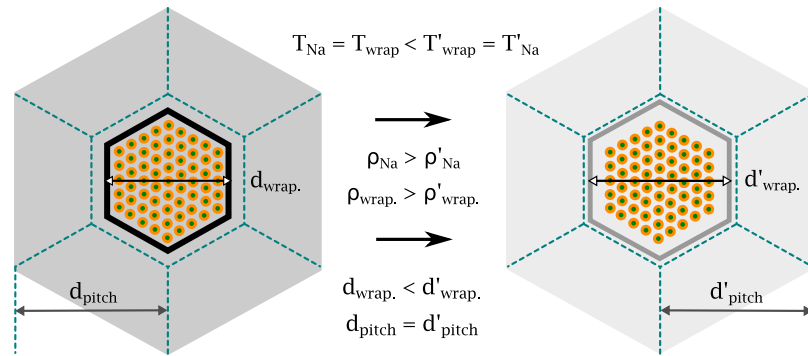


Figure 3.5: Schematic overview of the sodium and wrapper expansion.

- Diagrid expansion

When the diagrid-expansion-dependent XS are generated, the difference in models between different diagrid expansion states is only the inter-assembly sodium gap width (Fig. 3.4). This means that the geometry within the assembly (fuel pins, pin pitch size, wrapper, etc.) is unchanged between two diagrid expansion states. Therefore, only the surrounding sodium amount is increased with expansion, i.e. the sub-assembly pitch size.

- Fuel rod expansion

When the fuel rods are expanded, not only the axial but also the radial expansion

of the fuel and cladding is considered in the XS model. In other words, the material density is changed inversely proportional *not* to the linear change in axial direction but to the volumetric change. Furthermore, the explicit expansion of the pin dimensions in the radial direction will automatically consider the reduction in the liquid sodium amount between the fuel pins (Fig. 3.6).

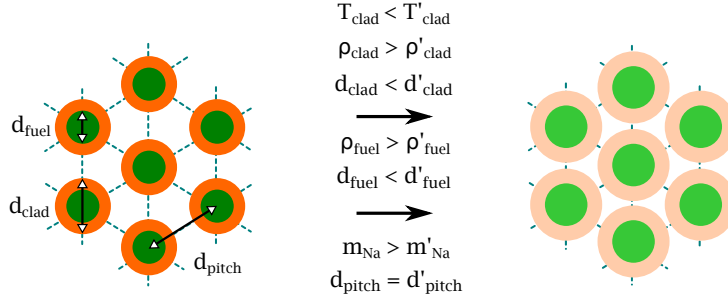


Figure 3.6: Schematic overview of the fuel rod expansion.

The calculation of the expansion coefficients and the expansion dependent XS is done with DYN3D in the following manner:

1. The temperature driving the thermal expansion is obtained from the TH module of DYN3D. In case of fuel rod expansion, this can be either the node-average temperature of the cladding or the fuel. In case of the radial core expansion, the temperature is taken from the diagrid model.
2. The expansion coefficient is calculated as:

$$\varepsilon(T) = \frac{L(T)}{L(T_0)} = 1 + \alpha(T) \cdot (T - T_0), \quad (3.3)$$

where L is the linear dimension and α is the linear expansion coefficient corresponding to the temperature T , and T_0 is the reference temperature of the used linear expansion correlation. The correlation can be arbitrary selected by the user prior to the calculation.

3. The expansion-dependent cross section Σ are calculated from the library and the expansion coefficient ε by using linear interpolation:

$$\Sigma = \Sigma_i + \frac{\varepsilon - \varepsilon_i}{\varepsilon_{i+1} - \varepsilon_i} \cdot (\Sigma_{i+1} - \Sigma_i), \quad (3.4)$$

where $\varepsilon_i < \varepsilon < \varepsilon_{i+1}$ and $\Sigma_i = \Sigma(\varepsilon_i)$ are the pre-generated XS in the library.

4. In case of fuel rod expansion, the “mixing” model is called after step 3 (see subsection 3.2.1).

Dynamic reactivity decomposition for SFR calculations

In transient calculations, the main algorithm to calculate the change of core reactivity (i.e. dynamic reactivity) is based on the weighted spatial integration of the time-dependent diffusion equation (Grundmann et al., 2005; Rohde et al., 2016). By applying the perturbation theory, DYN3D calculates the dynamic reactivity from changes of the XS weighted with the adjoint flux of initial state and with the normal flux of the actual state. First the weighting is done for each node, then integrated over the whole core to get the dynamic reactivity.

The steady-state adjoint flux is obtained by DYN3D with the same procedure as the normal flux just before the transient calculation. The solved adjoint equation is constructed to be the same type as the steady-state diffusion equation by redefining the cross sections (Grundmann et al., 2005, p. 37).

Since the XS are parametrized, the contribution of each perturbed parameter to the total XS change, and therefore, to the total reactivity effect can be obtained separately. In this doctoral research, new computational routines were added to calculate the SFR specific reactivity components, i.e. the fuel rod and diagrid expansion effects. The extension was based on the already available model that calculates LWR specific reactivity effects in DYN3D (Grundmann et al., 2005, p. 41).

SFRs usually have different fissile regions and fertile blankets, like Phenix and Superphenix. These regions behave differently in respect to fuel temperature change. This is especially true for the blanket region, since it has lower average temperature and almost pure ^{238}U -oxide pins. In order to have a better analyses of the core behavior, a region-wise reactivity decomposition of the Doppler effect was added to the code.

3.3 Description of the test cases

The OECD/NEA and Phenix EOL cores presented in Section 2.2 were used to test the new thermal-mechanical models. The references cores were expanded either axially or radially using different linear expansion coefficients. For every expansion state, a steady-state DYN3D calculation has been performed while applying the new

Chapter 3. Modeling of thermal expansions

thermal-mechanical models. The nodal diffusion results were compared to the full core MC solutions of Serpent. In the Serpent calculations the thermal expansion was modeled explicitly, i.e. the material boundaries were physically increased and the densities of the expanded materials were reduced accordingly. A superimposed mesh, equal to the nodal mesh used in DYN3D, was applied in Serpent calculations to obtain the power distribution.

For the axial expansion modeling, it was assumed that the gas gap between the fuel pellets and cladding is closed, i.e. the expansion of fuel and cladding is driven by the cladding temperature. The fuel rods were uniformly expanded along heat-generating part in axial direction by 0.25%, 0.45%, 0.65%, and 0.85% relatively to the reference state. When preparing the XS with Serpent, the fuel and cladding densities were reduced according to the linear expansion in order to preserve the total mass. The wrapper tube of the assemblies was assumed to have the same temperature as the sodium coolant (averaged value of the inlet and outlet), so the wrapper dimensions and density were calculated accordingly that remained unchanged in all states. For every expansion state, the thermal expansion reactivity worth ($\Delta\rho_{\text{exp}}$) and axial power distribution were calculated with Serpent and DYN3D. The thermal expansion reactivity worth was estimated as the change in reactivity between the expanded and reference states:

$$\Delta\rho_{\text{exp}} = \rho_{\text{exp}} - \rho_{\text{ref}}. \quad (3.5)$$

For every expansion state, the corresponding temperature was calculated using temperature dependent linear expansion coefficient and the current value of the relative thermal expansion. In this test, the linear expansion coefficients of the ODS (Hamilton et al., 2000) and SS316 (IAEA, 2014) were applied for the OECD/NEA and Phenix EOL cores respectively.

For the OECD/NEA core, the nominal state with the average core temperature of 743 K served as a reference state. Only the active core was axially expanded during the test. For the Phenix EOL core, the isothermal state (523 K) served as a reference state. The whole fuel rods including the axial blankets and axial reflectors were expanded. In order to reduce the effect of relative CR insertion due to the upward expansion of fuel rods, the CR positions were adjusted in each expansion state to maintain the level difference between the top of the fuel rods and bottom of CRs. In both reference cores, the CRs were modeled in the complete withdrawn position, as indicated in the

corresponding benchmark specification.

For both reference cores, the diagrid was radially expanded by 0.3% and 1.0%. The corresponding reactivity effects were estimated from Serpent and DYN3D solutions using Eq. (3.5). A larger assembly pitch size results in a higher volumetric ratio of sodium, which was also considered in regions containing homogeneous mixtures (e.g., reflectors).

3.4 Results of the test calculations

In order to test the XS mixing model, the axial expansion reactivity worth and the shift in axial power profile were calculated by the DYN3D code and compared to the MC reference. The test cases were computed with the two methods for a better assessment of the new expansion model:

- *Direct mesh expansion method* – The nodal boundaries are physically expanded according to the expansion states (Fig. 3.7a). All material interfaces are aligned with the nodal mesh. This method is limited to uniform axial expansions.
- *New expansion model* – The nodal mesh is fixed at the reference state and is used in all expanded states (Fig. 3.7b). Mixing sub-nodes are added after each material interface. In case of expansion, DYN3D mixes two different XS in the sub-nodes as described in subsection 3.2.1.

The total height of the modeled OECD/NEA and the Phenix EOL cores at reference state are 311.160 cm and 264.853 cm respectively. In DYN3D, the assemblies were axially divided into the nodes of about 10 cm height. The mixing sub-nodes, used with the new expansion model (Fig. 3.7b), had the size from about 0.1 cm to about 2 cm starting from bottom along the axial direction. It should be noted that in all simulations, numerical instabilities were not observed.

The axial expansion reactivity effects predicted by Serpent and DYN3D are presented in Table 3.2. It can be observed that the magnitude of the axial expansion reactivity effect in the Phenix EOL core is noticeably higher than in the OECD/NEA core due to the much smaller size of the former. For both reference core designs and all expansion states, the axial expansion reactivity worths predicted by DYN3D show a reasonably good agreement with those calculated by Serpent. The difference between diffusion

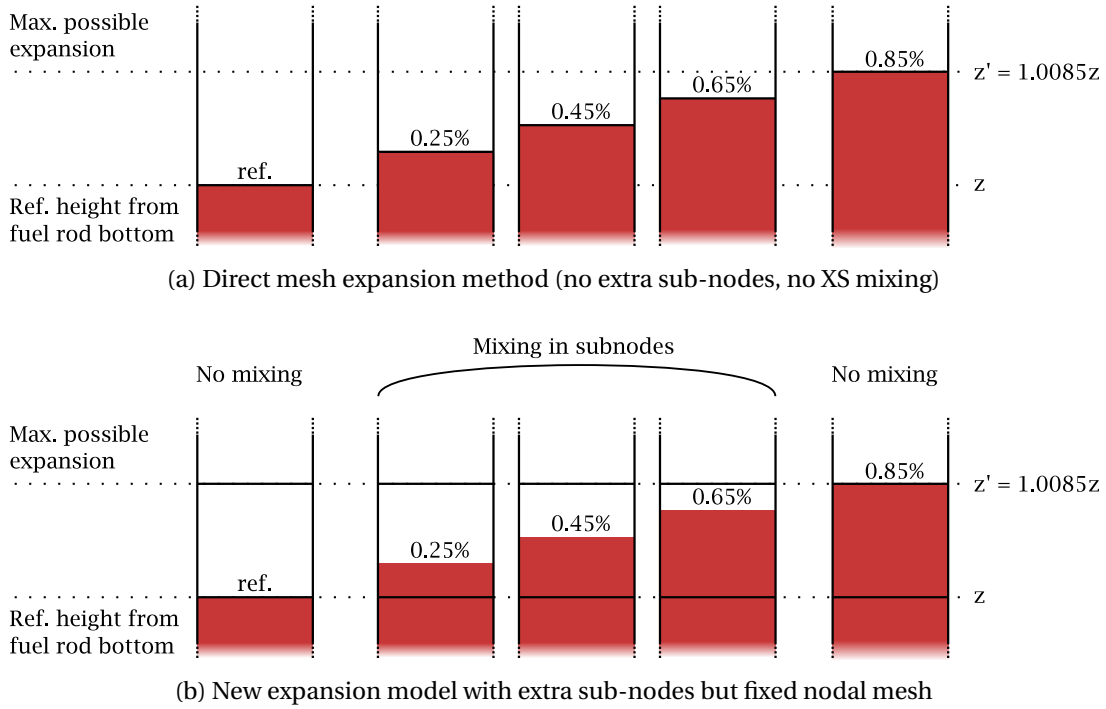


Figure 3.7: Nodalization around the material interface in DYN3D in direct mesh expansion method (a) and with new expansion model (b).

and MC solutions typically stays within one standard deviation and does not exceed few pcm. It should be noted that the actual XS mixing is performed only for the expansion states of 0.25%, 0.45% and 0.65% because in case of the 0.85% expansion, the mixing sub-nodes are completely filled with expanding material (Fig. 3.7b, right). The difference between the two applied methods is limited to 3 pcm in all cases demonstrating a very satisfactory performance of the mixing model.

The shift in axial power distributions due to axial expansion as calculated by Serpent is presented in Figs. 3.8 and 3.10. The radially averaged axial power profiles for all expansion states are shown in upper panels and the shift in axial power profiles are shown in lower panels. The power deviation curves clearly indicate an upward shift of the axial power profile resulting from the axial fuel rod expansion. As compared to the reference state, the sodium plenum (white background in Figs. 3.8 to 3.11) also gains power due to the introduction of the expanded fuel material into the fixed sodium plenum node. A power reduction in the lower part of the active core is more pronounced in the lowest active node of the Phenix EOL core (Fig. 3.10). This can be explained by the fact, that the lower axial blanket expands into the active core, pushes

3.4. Results of the test calculations

Table 3.2: Comparison of the reactivity effects (pcm) related to the axial fuel rod expansion.

<i>OECD/NEA large oxide core</i>						
dL/L ref.	T* (K) 743	Serpent	Direct mesh expansion		New expansion model	
			DYN3D	vs. Serpent	DYN3D	vs. Serpent
0.25%	924	-13 ± 3	-10	3	-10	3
0.45%	1056	-27 ± 3	-29	-2	-30	-3
0.65%	1176	-43 ± 3	-44	-1	-46	-3
0.85%	1287	-60 ± 3	-57	3	-57	3
<i>Phenix EOL core</i>						
dL/L ref.	T* (K) 523	Serpent	Direct mesh expansion		New expansion model	
			DYN3D	vs. Serpent	DYN3D	vs. Serpent
0.25%	657	-48 ± 3	-51	-3	-48	0
0.45%	759	-90 ± 3	-88	2	-85	5
0.65%	860	-123 ± 3	-129	-6	-126	-3
0.85%	958	-165 ± 3	-165	0	-164	1

*Cladding temperature needed to reach the corresponding expansion (dL/L). The TH feedbacks are neglected.

out a certain amount of fuel, and, finally, reduced the power even more than in case of the OECD/NEA core (Fig. 3.8).

As demonstrated in Figs. 3.9 and 3.11, the axial power profiles predicted by DYN3D with the new expansion model are in a very good agreement with the Serpent solutions. The maximum relative difference between Serpent and DYN3D is smaller than 0.50% and 0.25% for the OECD/NEA core (Fig. 3.9) and Phenix EOL core (Fig. 3.11) respectively. In general, Figs. 3.9 and 3.11 shows a comparable magnitude of the relative error for the 0.85% expansion state, where no XS mixing due to expansion is done, and the rest of the expansion states. Therefore, it can be concluded that the smearing effect of the mixing model is relatively small. The results of the direct mesh expansion method were omitted in Figs. 3.9 and 3.11 due to no visible differences, and that would only overlap the results obtained with the new expansion model.

The calculated diagrid radial expansion reactivity worths are presented in Table 3.3. As compared to the reference MC, the radial expansion reactivity worth calculated

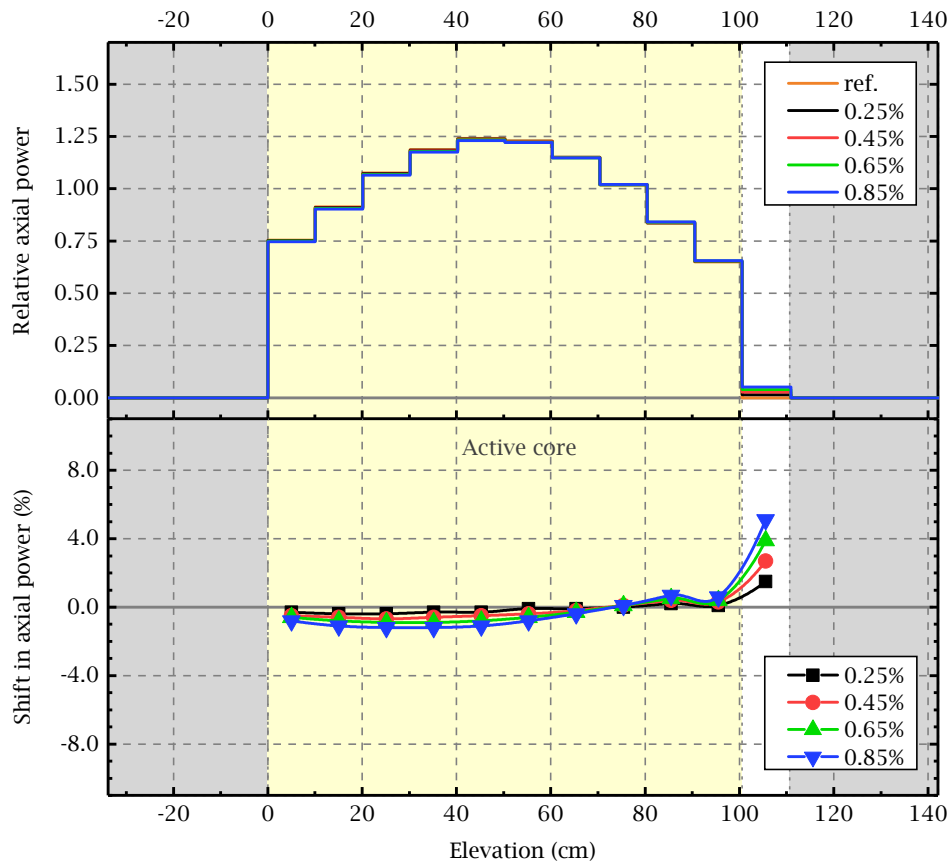


Figure 3.8: OECD/NEA core. *Top*: radially averaged axial power profiles for different axial expansion states; *Bottom*: shift in axial power profiles relative to the reference state. Serpent results.

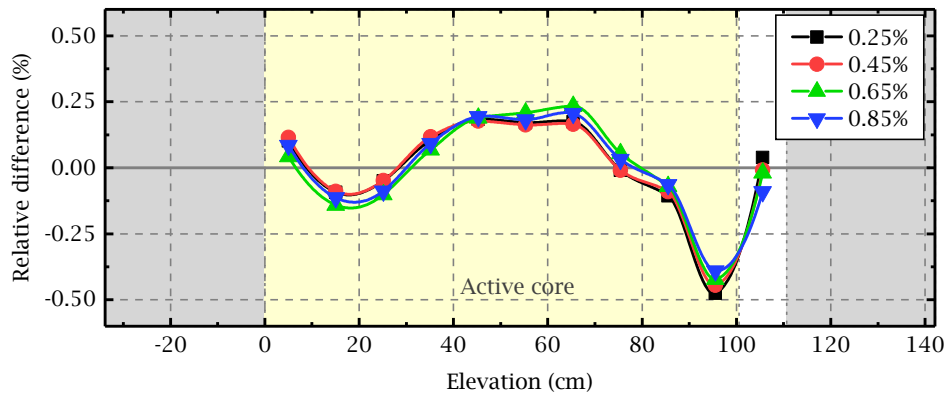


Figure 3.9: OECD/NEA core. Relative difference in the axial power profiles for different axial expansion states, Serpent vs. DYN3D.

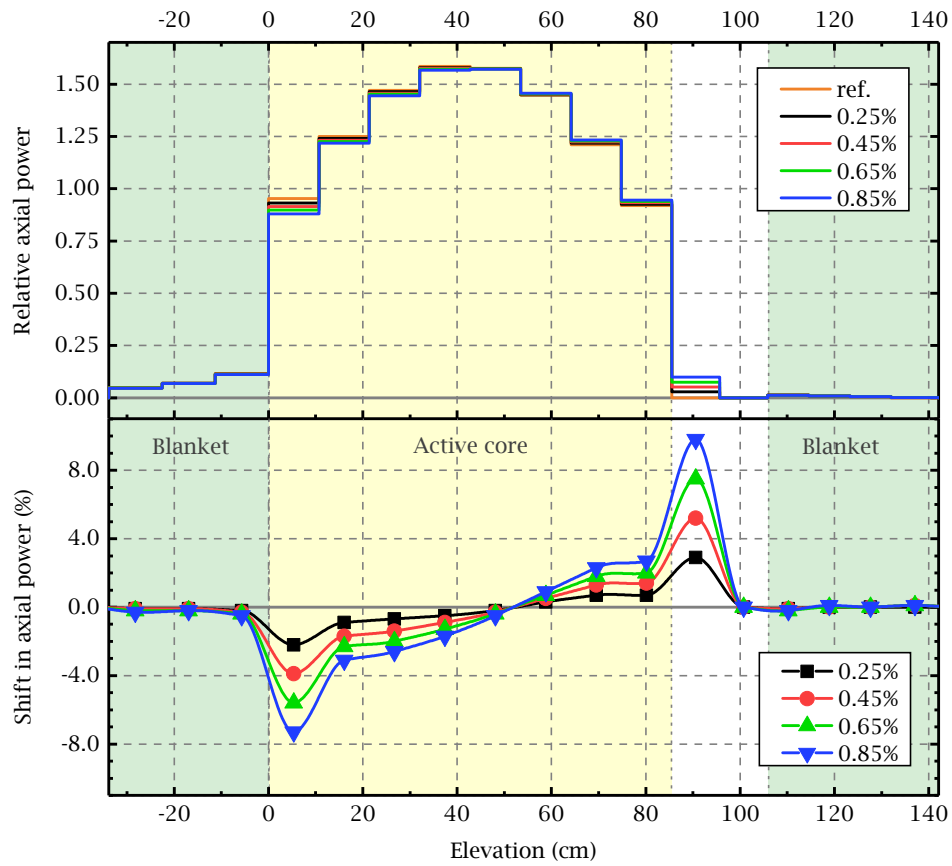


Figure 3.10: Phenix EOL core. *Top*: radially averaged axial power profiles for different axial expansion states; *Bottom*: shift in axial power profiles relative to the reference state. Serpent results.

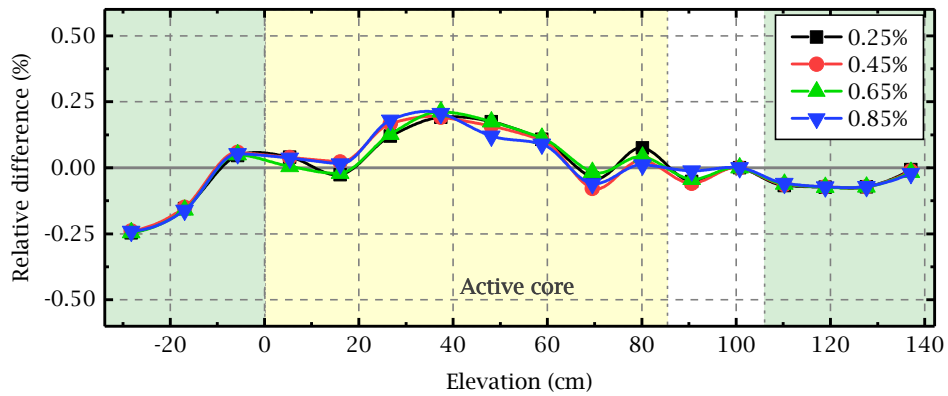


Figure 3.11: Phenix EOL core. Relative difference in the axial power profiles for different axial expansion states, Serpent vs. DYN3D.

Chapter 3. Modeling of thermal expansions

by DYN3D deviates up to about 20 pcm in both OECD/NEA and Phenix EOL cores. Nevertheless, the radial expansion coefficients remain in a good agreement, while roughly covering the temperature range of the liquid sodium between nominal and boiling states.

Table 3.3: Comparison of the reactivity effects (pcm) related to the radial expansion of the diagrid.

<i>OECD/NEA large oxide core</i>				
dL/L ref.	T* (K) 668	Serpent	Direct mesh expansion DYN3D vs. Serpent	
0.30%	818	-124 ± 4	-136	-11
1.00%	1153	-429 ± 4	-428	1
<i>Phenix EOL core</i>				
dL/L ref.	T* (K) 523	Serpent	Direct mesh expansion DYN3D vs. Serpent	
0.30%	683	-159 ± 4	-148	11
1.00%	1032	-529 ± 4	-507	22

*Diatrid temperature needed to reach the corresponding expansion (dL/L). The TH feedbacks are neglected.

3.5 Spatial decomposition of thermal expansion effects

The reactivity coefficients, calculated in Section 3.4, represent only the global neutronic behavior of the SFR system when the reactor core thermally expands. One may wonder, why is the magnitude of the axial expansion effect different in the two reference cores (Table 3.2). In order to have a better understanding of the consequences of the core thermal expansion, the total change in reactivity has to be spatially decomposed. In this way, it can be identified which regions of the core are more or less neutronicly influenced by thermal expansions. Additionally, a reaction-wise decomposition would quantify the contribution of each reaction type, namely the neutron absorption, leakage and production.

The spatial decomposition of the thermal expansion reactivity effect is possible to do in simple manner by looking into the neutron balance of the system at thermally expanded state and comparing it with the reference state. Since the procedure is

3.5. Spatial decomposition of thermal expansion effects

done with the nodal diffusion solution of DYN3D, the description of the method is introduced with the steady-state one-group diffusion equation:

$$D\nabla^2\Phi - \Sigma_a\Phi + \nu\Sigma_f\Phi = 0, \quad (3.6)$$

where the one-group formulation is used to simplify the notation. Nevertheless, Eq. (3.6) represents the balance between the number of produced neutrons and the lost ones due to leakage and absorption, in any given unit volume of a critical system (Okumura et al., 2014).

For the sake of reactivity calculation, the neutron balance is expressed as an eigenvalue (k_{eff}) problem:

$$k_{eff} = \frac{\nu\Sigma_f\Phi}{(-D\nabla^2\Phi) + \Sigma_a\Phi} = \frac{\nu\Sigma_f\Phi}{\nabla\vec{J} + \Sigma_a\Phi} = \frac{P}{L + A}, \quad (3.7)$$

where P , L and A denote neutron production, leakage and absorption rates, respectively. The leakage term is replaced “back”, according to Fick’s law, to the expression using the net neutron current (\vec{J}). This is done due to the practical reason of applying the net surface currents provided by DYN3D to calculate the nodal leakages directly.

The multiplication factor can be substituted for reactivity of the system:

$$\rho_{sys} = 1 - \frac{1}{k_{eff}} = 1 - \frac{L_{sys} + A_{sys}}{P_{sys}} = \frac{P_{sys}}{P_{sys}} - \frac{L_{sys} + A_{sys}}{P_{sys}} = \frac{P_{sys} - L_{sys} - A_{sys}}{P_{sys}}, \quad (3.8)$$

where the last expression will allow us to quantify the local change in production rates.

The reactivity change between the reference and thermally expanded state can be expressed with the help of Eq. (3.8), so that the reaction rates are integrated over energy and space:

$$\Delta\rho_{sys} = \rho_{sys}^{exp} - \rho_{sys}^{ref} = \frac{P_{sys}^{exp} - L_{sys}^{exp} - A_{sys}^{exp}}{P_{sys}^{exp}} - \frac{P_{sys}^{ref} - L_{sys}^{ref} - A_{sys}^{ref}}{P_{sys}^{ref}}. \quad (3.9)$$

The neutron leakage, absorption and production terms can be calculated with the few-group node average fluxes Φ_{ig} and net neutron currents J_{ig} of the nodal surfaces

Chapter 3. Modeling of thermal expansions

obtained from the DYN3D solution:

$$\begin{aligned}
 L_{sys} &= \sum_{i=1}^N L_i = \sum_{i=1}^N \int_{V_i} \nabla \vec{J}_i = \sum_{i=1}^N \oint_{S_i} \vec{J}_i = \sum_{i=1}^N S_i \sum_{g=1}^G J_{ig}^{\text{out}}, \\
 A_{sys} &= \sum_{i=1}^N A_i = \sum_{i=1}^N \int_{V_i} \Sigma_{a,i} \Phi_i = \sum_{i=1}^N V_i \sum_{g=1}^G \Sigma_{a,ig} \Phi_{ig}, \\
 P_{sys} &= \sum_{i=1}^N P_i = \sum_{i=1}^N \int_{V_i} \nu \Sigma_{f,i} \Phi_i = \sum_{i=1}^N V_i \sum_{g=1}^G \nu \Sigma_{f,ig} \Phi_{ig}.
 \end{aligned} \tag{3.10}$$

In Eq. (3.10) V_i and S_i denote the volume and surface of node i in the N node system. The J_{ig}^{out} indicates net currents for the outer direction at the node surface. The absorption ($\Sigma_{a,ig}$) and neutron production ($\nu \Sigma_{f,ig}$) homogenized cross sections are taken from the XS library generated with Serpent and used in the DYN3D modeling. As noted on the right-hand side of Eq. (3.10), the one-group node-wise reaction rates are condensed from the G -group energy domain.

The reactivity effect of Eq. (3.9) can be decomposed node-wise by substituting the total absorption and leakage rates with the second terms of Eq. (3.10):

$$\Delta \rho_{\text{sys}} = \sum_{i=1}^N \left(\frac{P_i^{\text{exp}} - L_i^{\text{exp}} - A_i^{\text{exp}}}{P_{\text{sys}}^{\text{exp}}} - \frac{P_i^{\text{ref}} - L_i^{\text{ref}} - A_i^{\text{ref}}}{P_{\text{sys}}^{\text{ref}}} \right) = \sum_{i=1}^N \Delta \rho_i. \tag{3.11}$$

Moreover, the contribution of each node can be further decomposed by reaction types. This can be achieved by simply reorganizing the numerators of Eq. (3.11):

$$\Delta \rho_i = \underbrace{\left(\frac{P_i^{\text{exp}}}{P_{\text{sys}}^{\text{exp}}} - \frac{P_i^{\text{ref}}}{P_{\text{sys}}^{\text{ref}}} \right)}_{\text{production}} + \underbrace{\left(\frac{L_i^{\text{ref}}}{P_{\text{sys}}^{\text{ref}}} - \frac{L_i^{\text{exp}}}{P_{\text{sys}}^{\text{exp}}} \right)}_{\text{leakage}} + \underbrace{\left(\frac{A_i^{\text{ref}}}{P_{\text{sys}}^{\text{ref}}} - \frac{A_i^{\text{exp}}}{P_{\text{sys}}^{\text{exp}}} \right)}_{\text{absorption}} = \Delta \rho_i^P + \Delta \rho_i^L + \Delta \rho_i^A. \tag{3.12}$$

These three terms characterize the thermal expansion reactivity effect in respect to the change in neutron production, leakage and absorption rate of the node i . It should be noted that summing up the production term over all nodes produces zero due to the normalization to total production rate.

During axial- and radial expansion of the core, a significant increase is expected in the radial- and axial leakage, respectively. To investigate this statement, the nodal leakage reactivity contribution of Eq. (3.12) is resolved further into the axial and radial component. In case of hexagonal prism node, the leakage from Eq. (3.10) is simply

3.5. Spatial decomposition of thermal expansion effects

decomposed as:

$$L_i = S_i^{\text{axi}} (J_{i,\text{top}} + J_{i,\text{bot}}) + S_i^{\text{rad}} \sum_{s=1}^6 J_{i,s} = L_i^{\text{axi}} + L_i^{\text{rad}}. \quad (3.13)$$

The first term contains the axial leakage through the top and bottom faces of the node, while the second term sums over the six side faces to obtain the radial leakage. The directional component of the leakage effect can be expressed, when Eq. (3.13) is applied in Eq. (3.11):

$$\Delta\rho_i = \Delta\rho_i^P + \Delta\rho_i^{L_{\text{axi}}} + \Delta\rho_i^{L_{\text{rad}}} + \Delta\rho_i^A. \quad (3.14)$$

When the directional leakage component of reactivity is calculated for all nodes of the reactor, the direction of leakage change from node to neighboring nodes can be mapped. Whereas, the total sum of this components will provide the global reactivity effect due to the increased core leakage. For demonstration purposes, this procedure is applied on the two reference cores in the following subsections.

It has to be mentioned that beside the neutron balance method, the calculation of sensitivity coefficients with perturbation theory is an alternative method for reactivity effect decomposition. However, this method requires an additional adjoint flux calculation for the reference state. In this doctoral research, the direct fluxes and currents were already available for both reference and perturbed states from the verification study (Section 3.4), and it was more practical to apply instantly the neutron balance method.

The perturbation theory method and the neutron balance method was previously compared in (Sun et al., 2011) by decomposing the coolant voiding reactivity effect reaction-, isotope and energy-group-wise. The research presented that both methods are quite consistent with each other. The principal difference between these two methods was well-formulated by (Sun et al., 2011): while the former provides a measure of the *causes* for a given reaction, the latter provides better understanding of the *consequences* of that reaction. In this thesis, the main motivation for the decomposition was to understand the consequences of the same thermal expansion on the reactivity for different core designs. Therefore the balancing method was well suited for spatial reactivity decomposition.

3.5.1 Axial expansion reactivity decomposition

The neutronic behavior of both reference cores during axial fuel rod expansion was assessed with the reactivity decomposition method. The intentions of this test was to acquire a better understanding of the axial expansion feedbacks in general, and to see what are the effect driving mechanisms in different core designs. From the DYN3D solutions presented in Section 3.4, the cores expanded by 0.85% were selected for comparison. In the both OECD/NEA and Phenix EOL cores the reactivity effects were region- and reaction-wise decomposed, as summarized in Table 3.4.

Table 3.4: Reaction- and region-wise decomposed axial expansion effect (pcm) at 0.85% axial core expansion.

<i>OECD/NEA large oxide core</i>					
Effect	Inner fuel	Outer fuel		Rest of ass.	Full core
<i>Total</i>	-31	-25		0	-57
– Production	+127	-127		0	0
– Absorption	-155	+85		+19	-51
– Leakage	-3	+16		-19	-6
<i>Phenix EOL core</i>					
Reaction	Inner fuel	Outer fuel	Blanket	Rest of ass.	Full core
<i>Total</i>	-89	-69	-7	0	-165
– Production	-30	0	+30	0	0
– Absorption	+13	-13	-87	-65	-152
– Leakage	-72	-56	+50	+65	-13

Table 3.4 presents that, in both cores, around 90% of the total full core effect is due to the significant increase in absorption rates and only ~10% due to the increased neutron leakage from the system. While the absorption rate increase is localized in the inner fuel region of the OECD/NEA core, the effect is rather dominant in the radial blanket and reflector zones of the Phenix EOL core. The reason for this difference should be sought in the leakage component of the effect, as shown in Table 3.4.

In the OECD/NEA core, the leakage component is negligible on full core level as well as locally in each region. The assembly- and reaction-wise decomposed reactivity effects are presented in Fig. 3.12a. It also demonstrates that the total contribution of each

3.5. Spatial decomposition of thermal expansion effects

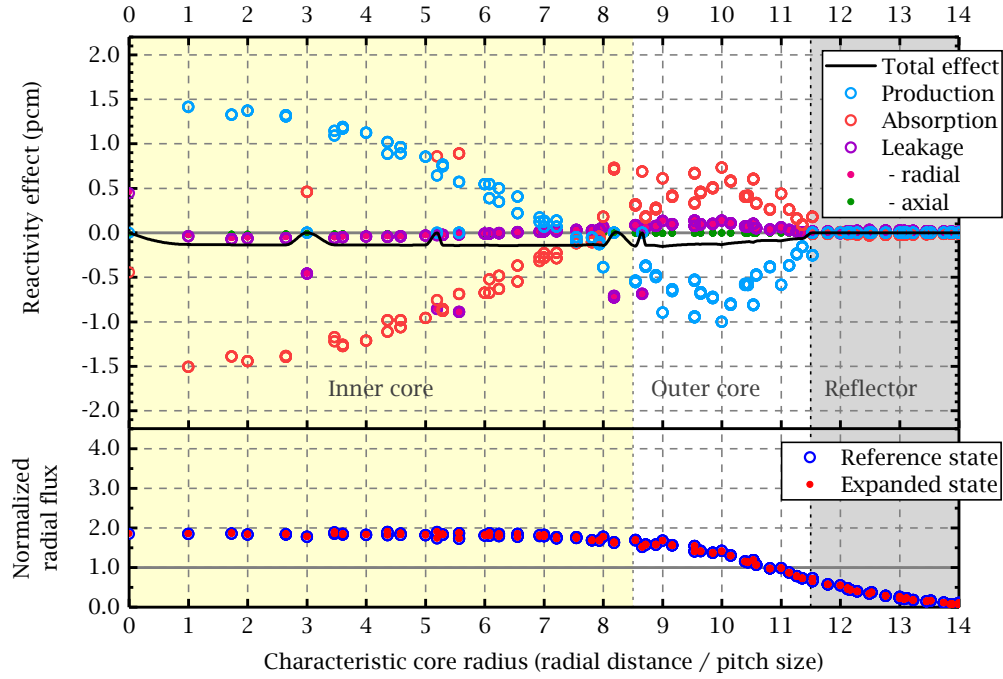
assembly is clearly driven by the change in neutron absorption rates while the leakage effect remains minor. In the fissile regions, the positive assembly-wise contribution of the absorption terms is always overcompensated with stronger production term.

Furthermore, the axial expansion effect in the OECD/NEA core was decomposed axially and presented in Fig. 3.13. Since each region had a distinctive contribution to the full core effect, the decomposition was done on the radially averaged assemblies of each region. In the averaged inner- and outer fuel an up-ward shift of absorption rates is observed. In the lower main part of the active core, the absorption rate in the fuel is decreased due to density reduction induced by the fuel rod expansion. This contributes a positive absorption term, as seen in Fig. 3.13. In the upper plenum, to where the fuel material intrudes by thermal expansion, the production rate is increased while contributing a local positive feedback. As seen in the non-fuel assemblies (Fig. 3.13, bottom), the absorption and leakage effects are negligible to that of the fuel assemblies.

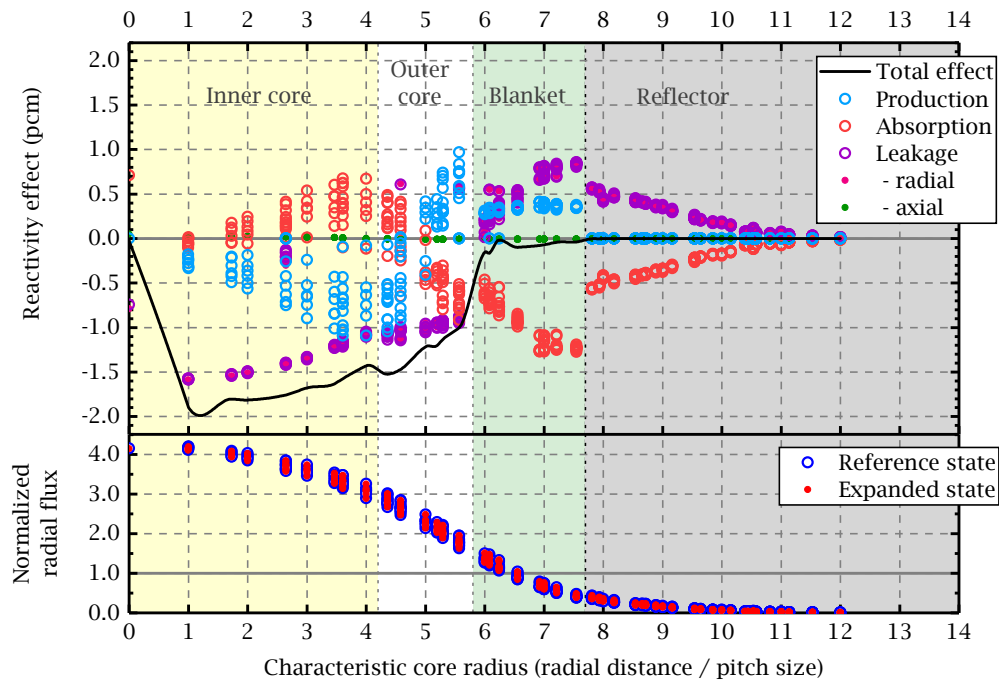
While in the Phenix core the full core leakage effect is also small, the region-wise components are significant, even if on full core level these cancel each other out. Table 3.4 shows a strong negative effect in the fissile zones and a compensating positive effect in the radial blankets and reflectors. The neutron leakage has increased inside, while reducing the production rate, and it has reduced on the outside of the core, i.e. the neutrons tend to migrate from the core to the periphery as compared to the non-expanded state. The large absorption terms on the core periphery indicate that the neutrons leaked from core are almost all absorbed here, and only a small portion escapes the whole system. This fact is also confirmed by the small ratio of full core leakage- and total reactivity effect, that is 13 over 165 pcm.

The smaller size of the Phenix core and the high flux gradient along radial direction is the cause for the significant change of the leakage rates inside the core (Fig. 3.12b, bottom). In the OECD/NEA core the flux profile is flat (zero gradient) until the outer core periphery, and so the neutron leakage rates are less likely to change at small density perturbations. Whereas, the non-flat profile of the Phenix core makes it more radially leaky during axial fuel rod expansion. By looking at the radial decomposition (Fig. 3.12b), it can be seen that the negative axial expansion effect is driven by the radial leakage, but the increased absorption in the whole core determines the magnitude of the effect (Table 3.4).

The axial reactivity decomposition in Phenix EOL core (Fig. 3.14) presents a similar



(a) OECD/NEA core



(b) Phenix EOL core

Figure 3.12: Radially decomposed axial expansion effect at 0.85% axial core expansion (*top*) and normalized radial flux (*bottom*).

3.5. Spatial decomposition of thermal expansion effects

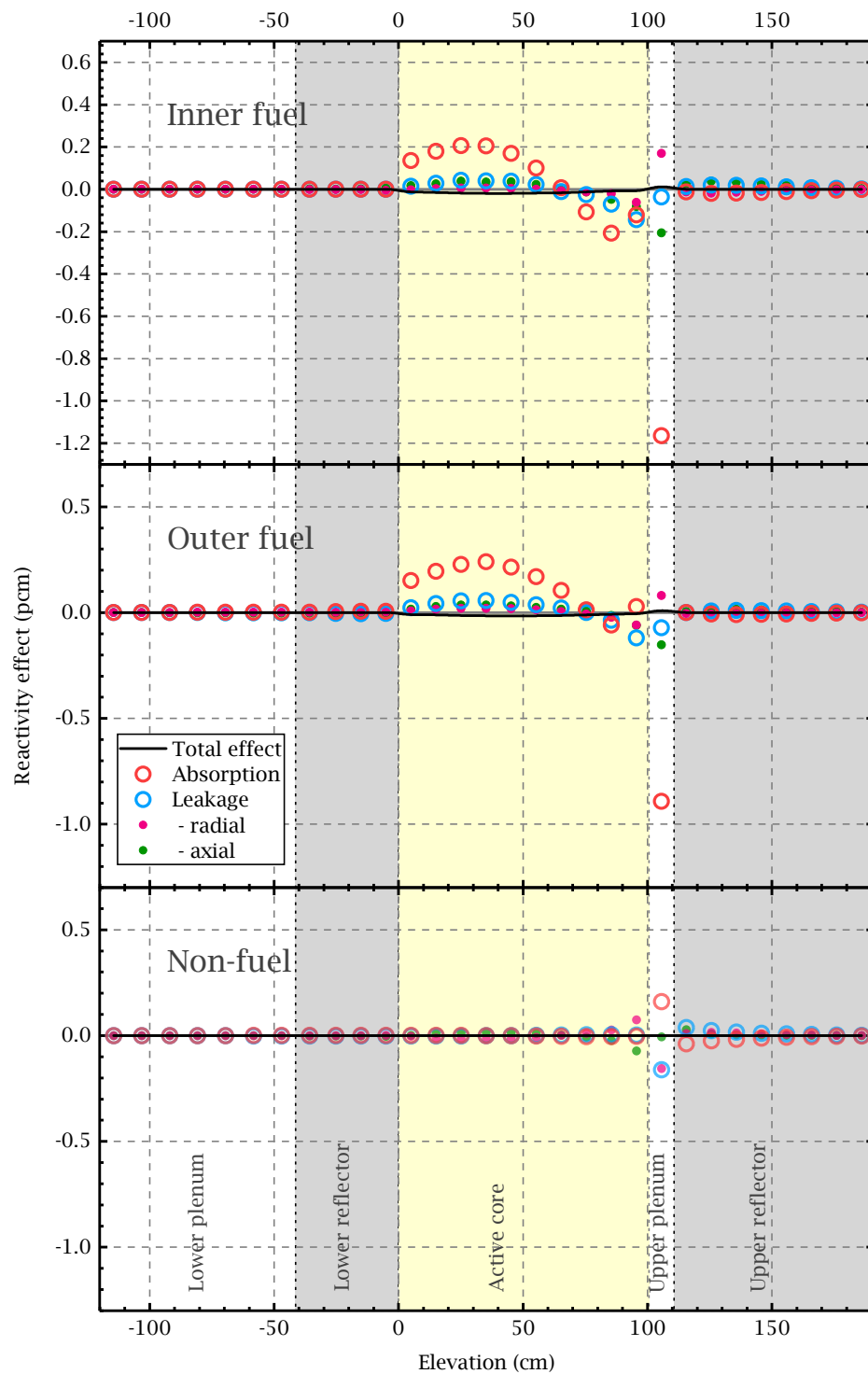


Figure 3.13: Axially decomposed axial expansion effect of the region-wise averaged assemblies in OECD/NEA core.

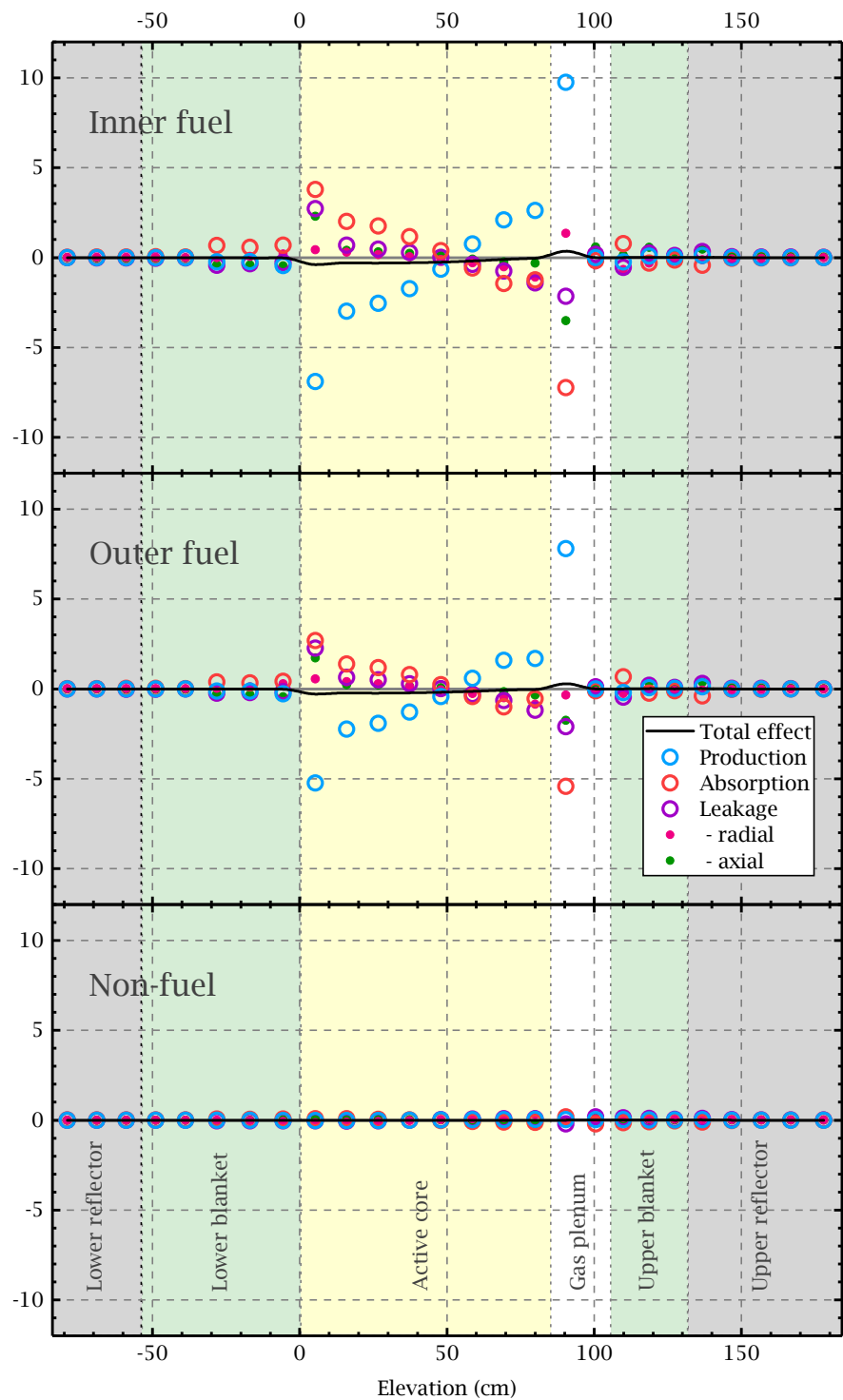


Figure 3.14: Axially decomposed axial expansion effect of the region-wise averaged assemblies in Phenix EOL core.

3.5. Spatial decomposition of thermal expansion effects

behavior as in the OECD/NEA core, i.e. the absorption rate profile is shifted upwards in the fissile cores. Besides, a positive peak is also present in the top fissile node, because the fissile material expands into the plenum. The production is increased in this node and provided a positive feedback.

3.5.2 Radial expansion reactivity decomposition

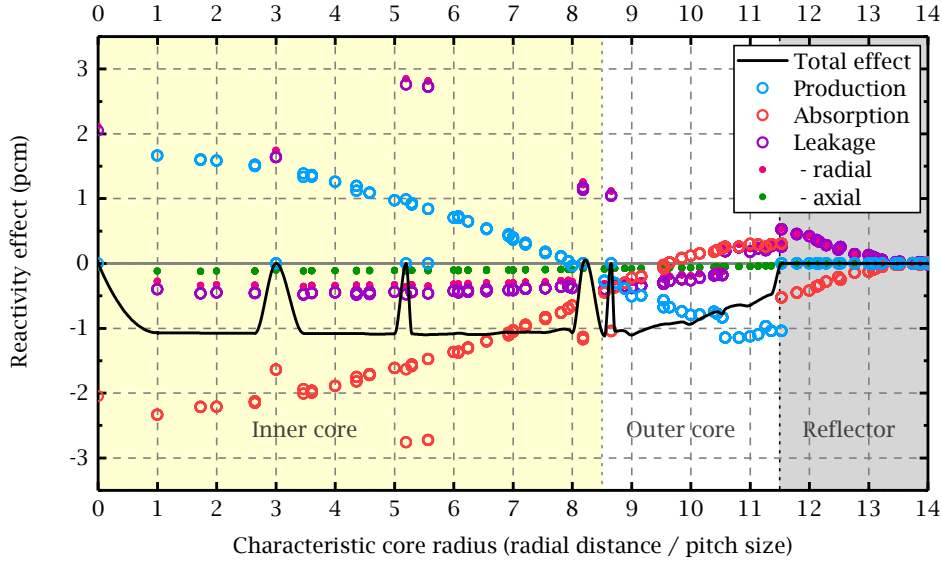
The radial diagrid expansion reactivity decomposition was performed identically to that of the axial expansion effect presented in the previous subsection. The DYN3D solutions of Section 3.4, where the cores were radially expanded by 1.00%, were selected for comparison. In these cases, the reactivity of the OECD/NEA and Phenix EOL cores was reduced by 428 and 507 pcm, respectively. The region- and reaction-wise decomposed reactivity effects are summarized in Table 3.5.

Table 3.5: Reaction- and region-wise decomposed radial expansion effect (pcm) at 1.00% radial core expansion.

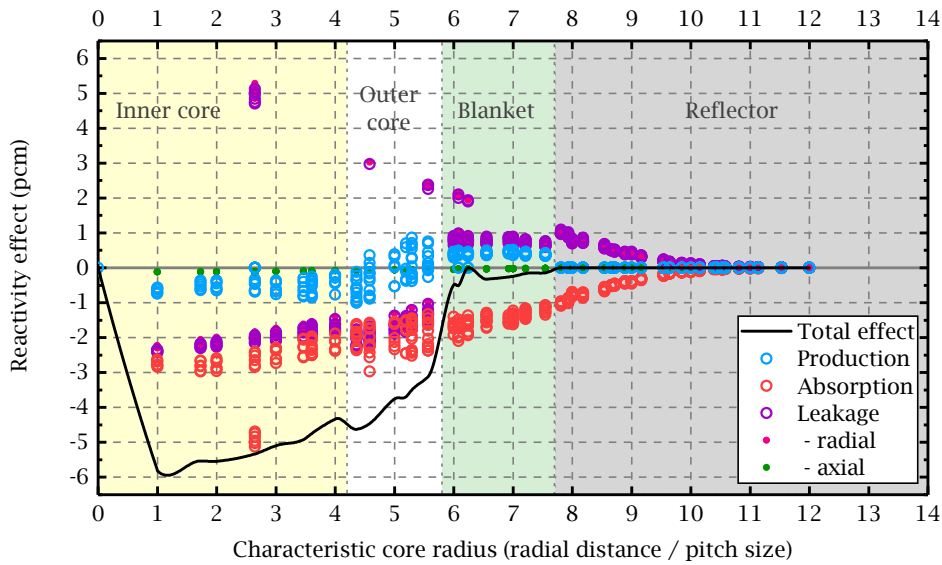
<i>OECD/NEA large oxide core</i>					
Effect	Inner fuel	Outer fuel		Rest of ass.	Full core
<i>Total</i>	-158	+101		0	-428
– Production	+127	-127		0	0
– Absorption	-155	+85		+19	-403
– Leakage	-3	+16		-19	-25
<i>Phenix EOL core</i>					
Reaction	Inner fuel	Outer fuel	Blanket	Rest of ass.	Full core
<i>Total</i>	-483	-24	0	0	-507
– Production	-35	+35	0	0	0
– Absorption	-244	-125	-72	-62	-503
– Leakage	-204	+66	+72	+62	-4

Similarly to the axial expansion effect, in case of the radial expansion, the increased absorption rate on full core level is the dominant contributor to the negative feedback. In the OECD/NEA core, the local radial leakage effects are likewise negligible, while in the more “leaky” Phenix core the radial leakage plays an important role.

Fig. 3.15 presents the radial decomposition of radial expansion effect for both refer-



(a) OECD/NEA core



(b) Phenix EOL core

Figure 3.15: Radially decomposed radial expansion effect at 1.00% radial core expansion.

3.6. Modeling of thermal expansions – Summary of the results

ence cores. It is seen that the absorption rates of inside assemblies are increased, and contributing strong negative reactivity values. For the OECD/NEA core the slightly positive absorption term is compensated with stronger reduction in production rate. While the leakage effects in the OECD/NEA core remains small (Fig. 3.15a), in the Phenix EOL core a strong radial leakage is observed from the fissile into the blanket and reflector area (Fig. 3.15b). The latter strongly increases the absorption rates in the outer regions.

The radial diagrid expansion widens the inter-assembly gap, therefore, strengthening the axial neutron streaming. Figs. 3.16 and 3.17 present an increased axial leakage from the active core region towards the lower and upper part of the core. In the mean time the absorption and production rates are reduced. In the plena, axial reflectors and blankets, the leakage effect is positive demonstrating an increased neutron inflow. This is compensated by the enhanced absorption, as shown in Figs. 3.16 and 3.17.

The wider inter-assembly gap means a larger coolant to fuel ratio resulting a softer neutron spectrum, i.e. higher absorption rates in the ^{238}U (Sun et al., 2011). This effect is notable at the top and bottom nodes of the active core (Fig. 3.16), and in case of the Phenix core also in the blankets (Fig. 3.17).

The radial “leakiness” of the Phenix core is also seen in the axial decomposition of the averaged non-fuel assemblies (Fig. 3.17, bottom), especially, when it is compared to one of the OECD/NEA core (Fig. 3.16, bottom). The presence of strong positive radial leakage component indicates a significantly increased neutron inflow rate in the Phenix core periphery, whereas this effect is negligible in the OECD/NEA core. At the end, the extra influx of neutrons is counterbalanced with increased absorption.

3.6 Modeling of thermal expansions – Summary of the results

In SFR system analyses, the thermal expansion effects play a major role in the evolution of the transients. In order to model local expansion effects and asymmetric core behavior, 3D spatial kinetics codes with thermal expansion treatment are needed. The nodal diffusion code DYN3D was extended by the author with new thermal expansion models to account for axial and radial core expansions. The axial expansion model is based on the XS “mixing” approach and capable of modeling non-uniform core

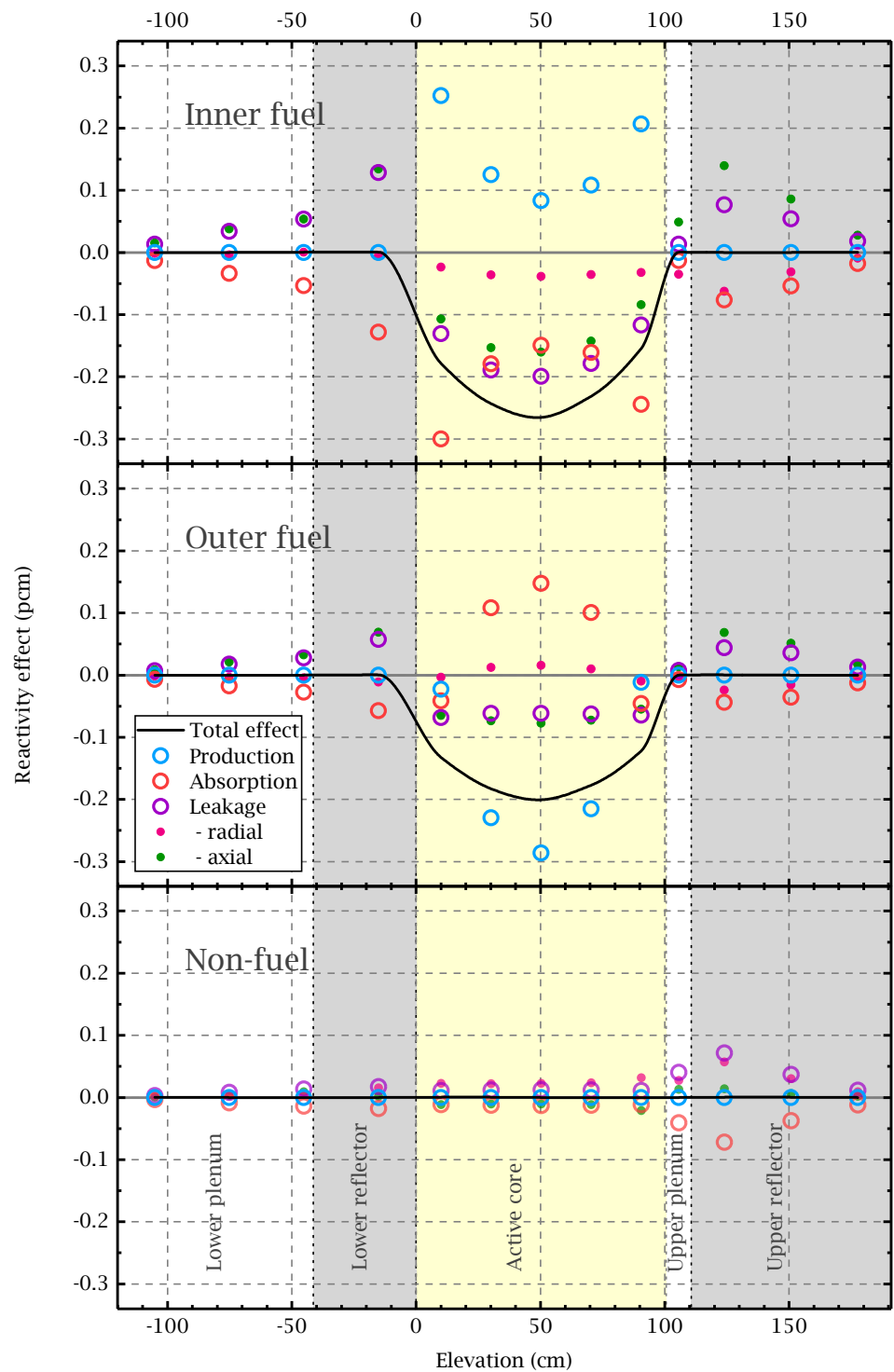


Figure 3.16: Axially decomposed radial expansion effect of the region-wise averaged assemblies in OECD/NEA core.

3.6. Modeling of thermal expansions – Summary of the results

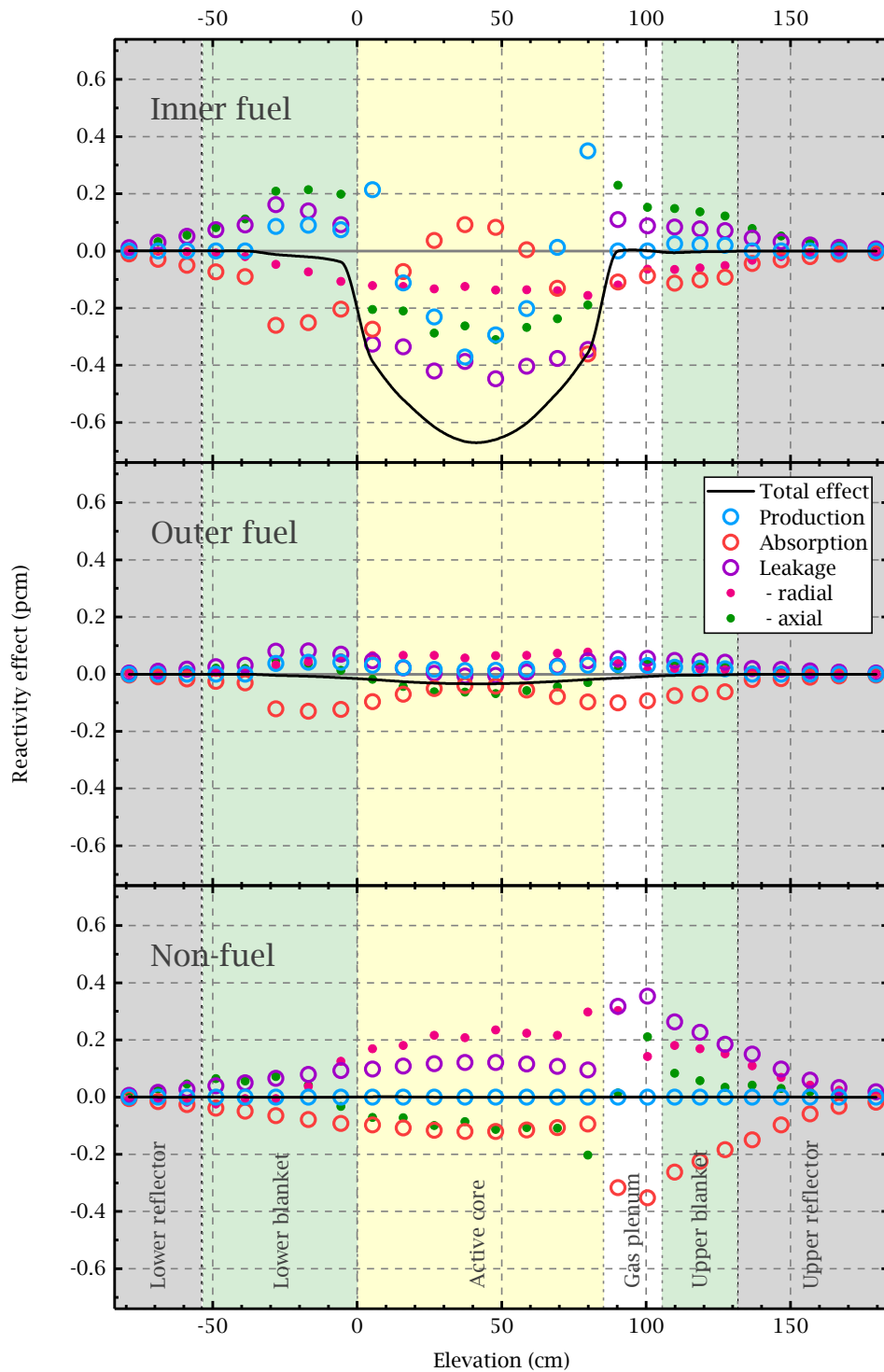


Figure 3.17: Axially decomposed radial expansion effect of the region-wise averaged assemblies in Phenix EOL core.

Chapter 3. Modeling of thermal expansions

expansions by using the spatial temperature distribution of the fuel rods. The radial diagrid expansion model can account for a uniform radial expansion driven by the average inlet sodium temperature.

The axial expansion model was verified for radially uniform axial expansions using the large 3600 MWth oxide core from the OECD/NEA benchmark and the smaller 350 MWth oxide core from the Phenix EOL experiments. The results were in a very good agreement with the reference MC Serpent solution showing a sufficiently good prediction of the axial expansion reactivity effect. This confirms that the XS “mixing” based model is a simple and flexible way of handling the axial fuel rod expansion, which allows for an independent treatment of each fuel assembly based on local TH conditions. The concept of using uniformly expanding radial mesh in the diagrid model for the core radial expansion was also verified based on steady-state analyses of the reference cores.

A spatial reactivity decomposition procedure was introduced for the DYN3D solution based on the neutron balance method. Beside the node-wise decomposition of the reactivity feedback, the reaction-wise share of the effect can be calculated in each node. Currently, the reactivity feedback due to the local change in absorption rates and directional leakage components can be obtained. This method provides the means to gain a better understanding of thermal expansion effects on the neutronic core behavior. Both reference cores were assessed with the reactivity decomposition method in this chapter.

The expansion models are further assessed and validated, as presented in Chapter 4, with the help of the selected IAEA benchmarks on the Phenix EOL experiments: steady-state analysis of the CR shift test and transient calculations of the unprotected stage of the natural circulation test. It should be noted that the latter test is of particular importance, because in this case, the both models are applied to simulate dynamically changing axial and radial core dimensions.

4 Overall verification and validation of the extended DYN3D code

Before permanent shutdown of the Phenix reactor, several tests were performed in order to gain additional knowledge on SFR behavior. From these experiments, two tests were selected for international code benchmarking by the IAEA: (1) the control rod withdrawal tests (IAEA, 2014) and (2) the natural circulation test (IAEA, 2013). In this chapter, several parts of these benchmarks were selected for V&V in order to demonstrate the feasibility of using DYN3D for SFR analyses.

Section 4.1 focuses on the calculations of the CR withdrawal tests, while Section 4.2 is dedicated to the simulation of the unprotected stage of the natural circulation test. The selected tests are described in the beginning of each section. The specifics on computational modeling with DYN3D are presented for each selected test in subsections 4.1.2 and 4.2.2. The numerical results obtained with DYN3D are presented in subsections 4.1.3 and 4.2.3, respectively. Finally, each section concludes with a short summary of the results.

4.1 Phenix EOL control rod withdrawal tests

This section focuses on the verification and validation of the extended version of DYN3D against the IAEA benchmark on the control rod (CR) withdrawal tests from the end-of-life experiments conducted at the Phenix reactor (IAEA, 2014). The selected benchmark was designed to assess the capability of neutronic codes, used for SFR analyses, to model deformations in radial power distribution due to the various asymmetric arrangements of CRs. In order to take a full advantage of the available experimental data, the benchmark tasks were solved by DYN3D in two different ways:

Chapter 4. Overall verification and validation of the extended DYN3D code

(1) neutronic solution without feedbacks, and (2) coupled solution with thermal-hydraulic and thermal-mechanical feedbacks. The first one was obtained using the fixed core geometry while the dimensions of the fuel assemblies and other core components were explicitly expanded based on the average temperatures provided in the benchmark specifications. In contrast to the previous case, the second solution was obtained by invoking the thermal expansion models to obtain the actual core dimensions based on the temperatures provided by the thermal-hydraulic module. In this study, the first solution was used to validate the few-group XS generation methodology and neutronic performance of DYN3D in general, while the second one served to demonstrate and assess the overall capabilities of the extended DYN3D version.

4.1.1 Description of the control rod withdrawal tests

In the control rod withdrawal tests, a series of steady-state measurements were conducted with four different CRs arrangements (hereafter referred to as the CR shift tests). The main goal of the test was to investigate deformations of the radial power shape due to the asymmetric axial positioning of the shifted CRs. At the reference state, all six primary CRs were kept on equivalent level of elevation (so-called “rod bank” position). In three additional steps, CR #1 and #4 shown in Fig. 4.1 were either withdrawn or inserted relatively to the “rod bank” according to the sequence presented in Fig. 4.2. The rod bank position was adjusted to keep the reactor at constant power of about 335 MWth. The total sodium flow rate remained constant along all steps.

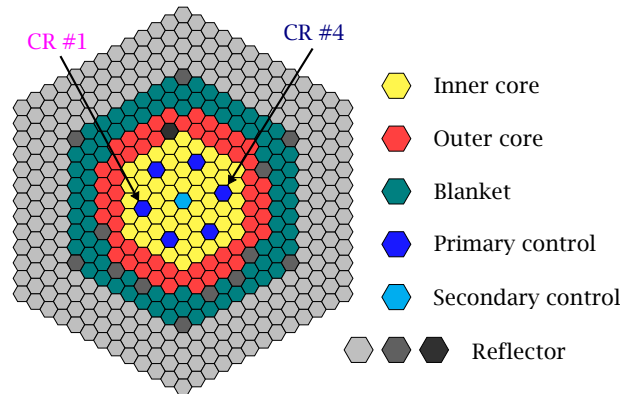


Figure 4.1: Phenix EOL core: radial core layout and location of the shifted CRs.

During the CR shift test, the sodium temperature was measured at the core outlet. Thermocouples were positioned at the head of each assembly located in the first seven assembly rows of the core starting from the core center (120 thermocouples in total).

Using these, the sodium heating (temperature difference between inlet and outlet) was measured assembly-wise at each step. The heat transfer between assemblies was assumed to be insignificant. Moreover, the change in the flowrate distribution due to the change of sodium heating was also assumed negligible. Based on these assumptions, the radial distribution of the relative power deviations in respect to the reference state was calculated for each step from the variation of sodium heating (IAEA, 2014):

$$\delta_{\text{rel}} P_i = \frac{P_i - P_i^{\text{ref.}}}{P_i^{\text{ref.}}} \approx \frac{Q c_P (\Delta T_i - \Delta T_i^{\text{ref.}})}{Q c_P \Delta T_i^{\text{ref.}}} = \delta_{\text{rel}} (\Delta T_i), \quad (4.1)$$

where P is the assembly power, Q is the sodium mass flowrate, c_P is the assembly-average specific heat capacity, and ΔT is the sodium heating in the assembly i . The ref. index denotes the values taken from the reference state. In this study, the deviation in radial power distribution estimated from the temperature measurements for Steps 1-3 were used for the validation of the DYN3D code.

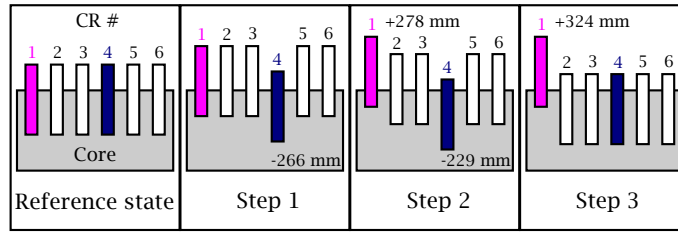


Figure 4.2: CR shift sequence.

The reactivity worth of the two involved CRs was measured before the CR shift test. The balancing method was used to acquire the integral rod worth over the full range of withdrawal (S-curve) for the CR #1 and #4. The test was initiated at critical low power state (~ 50 kW), where CR #1 and CR #4 was in complete inserted and withdrawn position, respectively. By using a succession of elementary steps, the CR #4 was moved from bottom to top, while the CR #1 in the opposite direction.

As presented in Fig. 4.3, the CR #4 was firstly moved downwards by a small increment (Step I in Fig. 4.3) and secondly the CR #1 was withdrawn to compensate the negative change of reactivity (Step II in Fig. 4.3). Between each elementary CR displacement, the differential worth was measured for each CR based on the application of the inverse kinetics method. When the CR #4 had been totally withdrawn to the top and CR #1 inserted to the bottom (Step N in Fig. 4.3), the full S-curves were obtained for both rods.

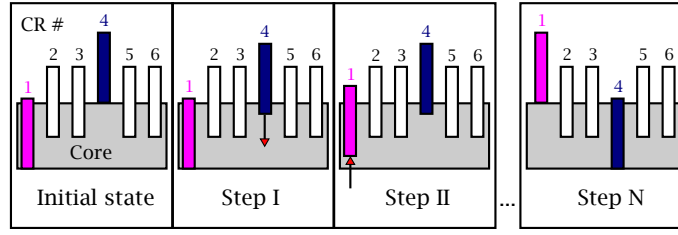


Figure 4.3: Schematic representation of the balancing method.

4.1.2 Computational methodology

The calculations were done in a two-step approach using the Serpent-DYN3D codes sequence. In the first step, the homogenized few-group XS were generated on lattice level with Serpent, and in the second step, the full core nodal calculations were performed with DYN3D.

Generation of parametrized cross section libraries

A parameterized cross section library was generated for DYN3D that covers the full range of reactor conditions of the CR shift tests and the natural circulation test. In this way, the same library was utilized in all calculations presented in this chapter.

The XS were calculated with Serpent at different fuel temperatures, coolant temperatures, axial expansion and radial diagrid expansion states. Table 4.1 presents the selected states that span the parameter space of the XS library. In Table 4.1, the temperature-dependent expansion coefficients are defined according to Eq. (3.3). In this case, the correlation for the temperature-dependent linear expansion coefficients was provided in the benchmark specification.

Table 4.1: Conditions used for cross section parametrization.

Fuel temperature (K)	Coolant temperature (K)	Axial expansion	Radial expansion
523	523	$\epsilon(523)$	$\epsilon(523)$
900			
1500			
1800	900	$\epsilon(1200)$	$\epsilon(900)$

The coolant density effect was implicitly considered in the coolant temperature varia-

tion. In case of the axial expansion effect, the change of dimensions and densities was considered for both fuel and cladding. Furthermore, the radial expansion of the pins, the reduction in the liquid sodium amount between the pins, and the temperature effect of the cladding were taken into account. The axial expansion relies on a closed gap hypothesis and is assumed to be driven by the cladding temperature, which is directly calculated by the internal thermal-hydraulic module of DYN3D.

The JEFF-3.1 based homogenized XS were obtained in the 24-group energy structure as suggested in (Fridman and Shwageraus, 2013). For further improvement of the nodal diffusion solution, the SPH method was applied for blanket and non-multiplying regions adjacent to the fuel nodes. The XS of the Phenix core were generated as described in Section 2.3.

DYN3D model

The Phenix EOL core model was constructed in DYN3D based on the data provided in the corresponding IAEA benchmark report. By using the homogenized XS generated with Serpent, the full core nodal diffusion solution was obtained with DYN3D for all four states of the test. The calculations were repeated in two different ways:

- *Case A* – Pure neutronic calculations by employing the fixed uniform temperatures specified in the benchmark. This approach was adopted by the majority of the benchmark participants.
- *Case B* – Coupled neutronic thermal-hydraulic (N/TH) calculations by employing the newly implemented axial fuel rod expansion model, where the axial expansion of the fuel rods was driven by local cladding temperatures.

Since *Case A* comprises only steady-state neutronic calculations, the nodal mesh was expanded explicitly without applying the thermal expansion models. The following uniform temperatures were used in the CR shift test: 1500 K for the fuel, 900 K for the blanket, and 721 K for structural, coolant, and absorber materials. The latter temperature was used to uniformly expand the core in the axial direction. In the radial direction, the core was expanded according to the inlet temperature of 646 K.

In *Cases B*, the initial core dimensions were set according to the isothermal state of 250°C. During calculations, the fuel rods were expanded using local cladding temperatures provided by the thermal-hydraulic module of DYN3D. The diagrid radial

Chapter 4. Overall verification and validation of the extended DYN3D code

expansion model was applied to automatically obtain the actual assembly pitch corresponding to the specified inlet coolant temperature. In order to ensure a more consistent comparison between the two cases, the gas gap conductance in the fuel rods was adjusted to reproduce the specified core-average fuel temperature of 1500 K. For all reactor states of the CR shift test, the total power and the boundary conditions (i.e. the inlet coolant temperature and the mass flow rate distribution) were set according to the benchmark specification.

The control rod S-curves of CR #1 and #4 were obtained with DYN3D by simulating the balancing method applied in the experiment (see Fig. 4.3). Since the core temperatures were not provided for this measurement, but the test was done in the low power state, it was assumed that the core resides in the isothermal condition (250°C). The simulation comprises a succession of steady-state calculations by using the approach of *Case A*, where all the temperatures were fixed at 250°C. The DYN3D calculations were executed as follows:

1. The CR #1 and #4 were fixed in the totally inserted and withdrawn position, respectively. The rest of the CRs were moved together until critical state was achieved with DYN3D.
2. CR #4 was inserted further by one-ninth of full range of withdrawal, which corresponds to 100 mm at cold state (20°C). This is equivalent to Step I in Fig. 4.3.
3. CR #1 was withdrawn further by one-ninth of full range of withdrawal. This corresponds to Step II in Fig. 4.3.
4. Step 2 and 3 were repeated with DYN3D until the final state was reached (Step N in Fig. 4.3).

The differential rod worth of each elementary displacement was obtained for both CRs. The S-curves were obtained by cumulative summation of the differential rod worths.

4.1.3 Numerical results

Case A – Neutronic calculations

The DYN3D results were compared with the full core MC solution of Serpent and the measurements. The calculated core reactivity values are presented in Table 4.2. In all steps, the codes noticeably overestimate the reactivity by about 430 to 600 pcm. Nevertheless, the Serpent and DYN3D results are very close and agree within about 160 pcm. Moreover, the reactivity swings between the steps remain below 15 pcm for both codes. The Serpent and DYN3D results are consistent with the results of the benchmark participants (IAEA, 2014, p. 175-6) that presented a reactivity bias of around +730 pcm compared to the critical state. Such discrepancies do not only come from nuclear data and measurement uncertainties, but from the averaged description of the reactor core.

Table 4.2: Calculated core reactivity at all states.

(pcm)	Case A			Case B
	Serpent	DYN3D	DYN3D vs. Serpent	DYN3D
Ref. state	584 ± 2	421	-162	463
Step 1	592 ± 2	436	-157	436
Step 2	596 ± 2	436	-161	455
Step 3	596 ± 2	432	-165	474

The radial power distributions of all states calculated with Serpent are presented in Fig. 4.4, top, and the comparison with DYN3D in Fig. 4.4, bottom. The Serpent power distributions were obtained by the averaging the results of the 20 independent Serpent calculations each of which was executed with an overall 960 million neutron generations (i.e. 1500 active and 200 skipped cycles with 640,000 neutrons per generation). As compared to Serpent, the power predicted with DYN3D does not exceed 1.5% for any state, while the average power deviation remains around 0.5%.

The power deviation profiles obtained with Eq. (4.1) from the DYN3D solutions are presented in Fig. 4.5a. The maximal positive and negative power deviations of all steps are compared against the Serpent results and the experimental values in Table 4.3. It is clearly seen that the maximal distortion of the power shape is achieved when the CRs #1 and #4 are shifted in opposite directions (i.e. at Step 2). In this step, according

Chapter 4. Overall verification and validation of the extended DYN3D code

to the experimental data, the power is increased by 12.1% and reduced by 10.9% around the extracted and inserted CRs, respectively. At Step 1 and 3, when only one CR is shifted relatively to the bank, a compensation effect can be observed on the opposite side of the involved CR which is caused by keeping the core on constant power (Pascal et al., 2013).

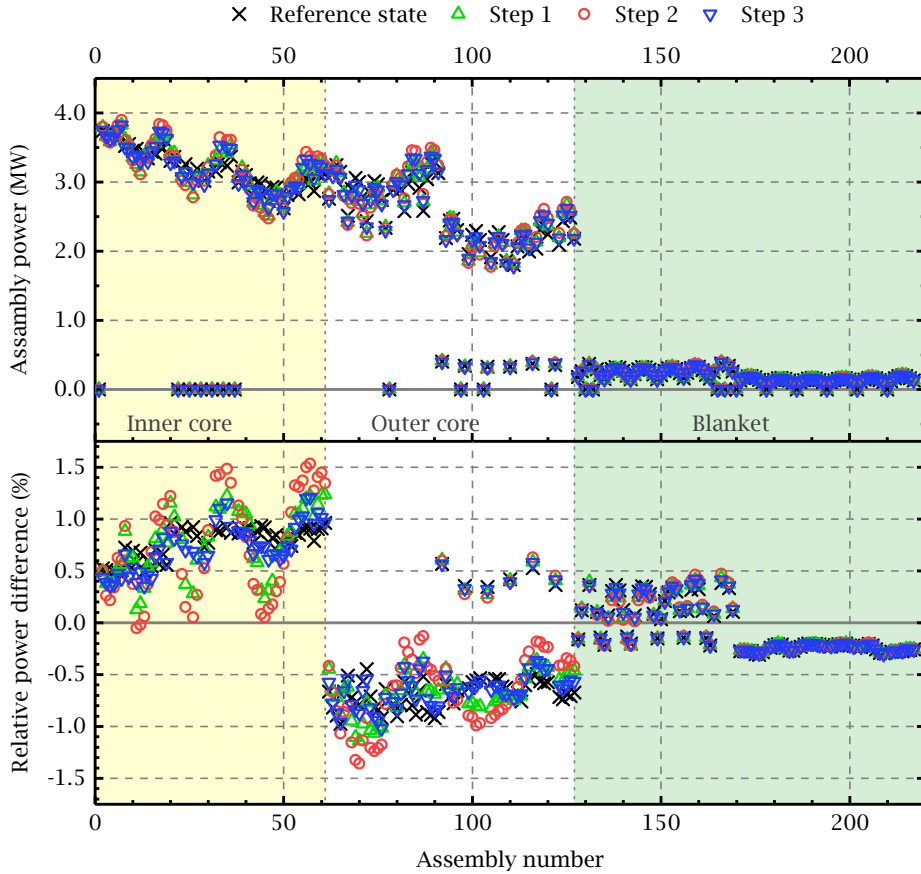


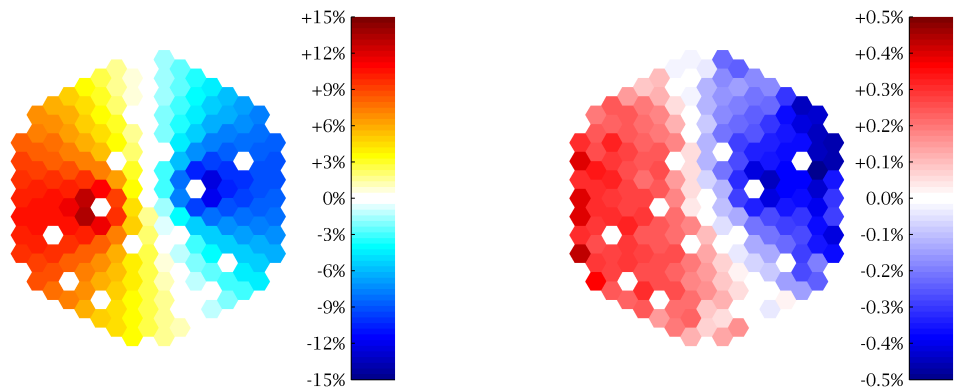
Figure 4.4: Radial power distribution calculated with Serpent for all states (*top*), and the relative difference in power between DYN3D and Serpent (*bottom*). Standard deviation of Serpent values is $<0.025\%$.

As compared to the experimental data, the codes consistently overestimate the effect of the CR shift and predict considerably higher limits in the assembly-wise power deviation distributions (Table 4.3). Nevertheless, a very good agreement is observed between the MC and nodal diffusion methods. The discrepancy in power deviations does not exceed 0.5%, even in the second step, as demonstrated in Fig. 4.5b. The average difference between the codes is $\pm 0.1/0.2/0.1\%$ for Step 1/2/3 respectively.

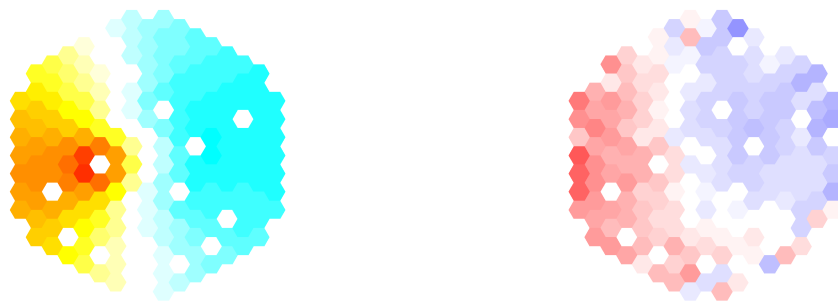
Step 1



Step 2



Step 3



(a) Power deviations calculated with
DYN3D

(b) Difference in power deviations,
DYN3D vs. Serpent

Figure 4.5: Radial distribution of the power deviations (with respect to the reference state) for all steps (a), and the difference between DYN3D and Serpent results (b).

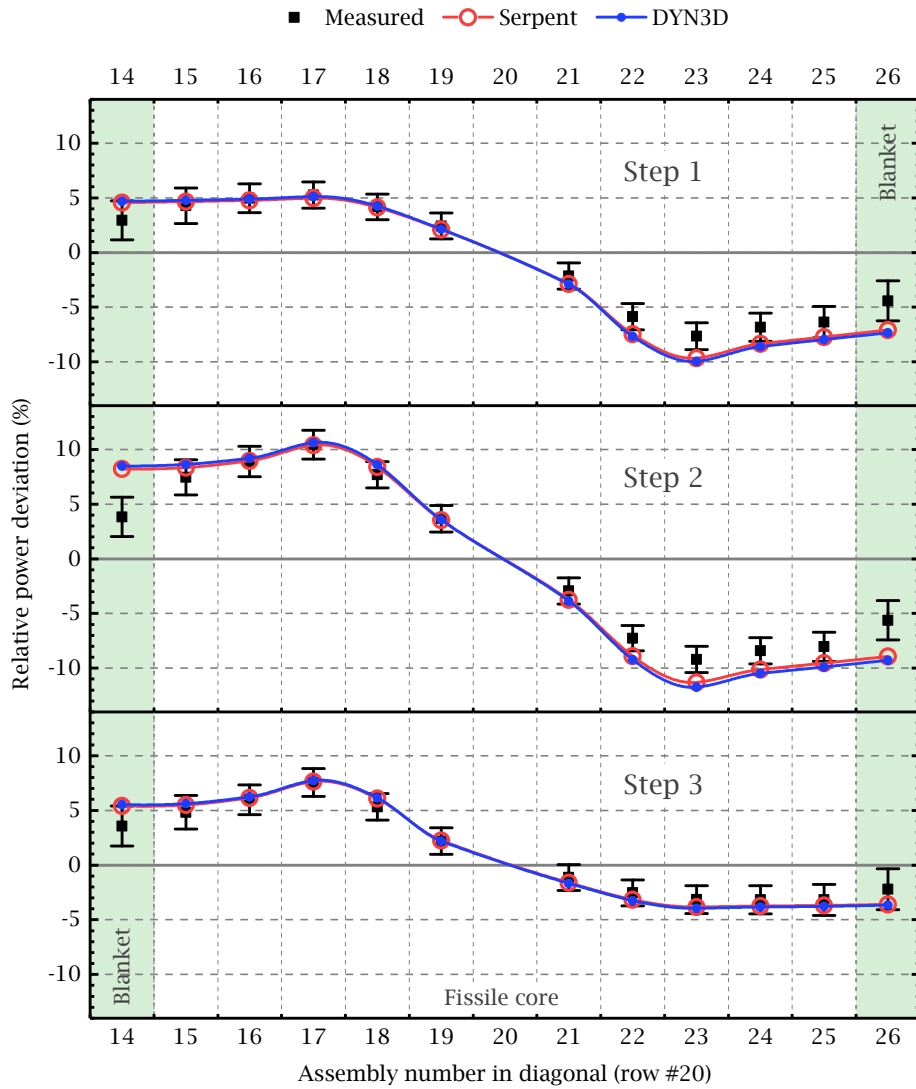


Figure 4.6: Comparison of radial deviation profiles along the diagonal closest to CRs #1 and #4 (*Top to bottom*: Step 1 to Step 3). DYN3D results are from *Case A*. Standard deviation of Serpent values is $<0.035\%$.

4.1. Phenix EOL control rod withdrawal tests

Table 4.3: Comparison of maximal power deviations at all steps.

(%)		Max. positive deviation	Max. negative deviation
<i>Step 1</i>	Experiment	na	-9.5 ± 1.3
	Serpent [*]	5.8	-11.2
	DYN3D	6.0	-11.5
<i>Step 2</i>	Experiment	12.1 ± 1.4	-10.9 ± 1.3
	Serpent [*]	13.0	-12.4
	DYN3D	13.3	-12.8
<i>Step 3</i>	Experiment	9.1 ± 1.4	na
	Serpent [*]	9.5	-3.9
	DYN3D	9.6	-4.0

^{*}Standard deviation of Serpent values is <0.035%.

The calculated power deviations, extracted from the core diagonal closest to CR #1 and #4, were compared with each other and the measurements in Fig. 4.6. The power deviation profiles predicted by DYN3D are in a very good agreement with MC solutions while the maximal differences in the order of the steps are about 0.3%, 0.4% and 0.1%. While the computational results remain within the experimental uncertainty band at the center of the core and around the withdrawn CR, higher discrepancies are observed in the blanket assemblies and around the inserted CR (Fig. 4.6). The highest deviation between DYN3D and the measurement occurs at Step 2, where the maximal differences are around 2.6% and 4.7% in the fissile core and blanket, respectively. Although the discrepancies between DYN3D and the measurement are significant, the DYN3D solution remains within the range of results provided by all other benchmark participants (IAEA, 2014, p. 209-11).

In general, all codes applied in the benchmark overestimate the power deviations. The discrepancies observed between the experiment and the computational results presented in this paper and the benchmark report are mainly caused by measurements problems explained by (Pascal et al., 2013). Some of the thermal-hydraulic effects were disregarded that lead to an overestimation in the peripheral assemblies. The neglected phenomena were the heat transfer between the fertile and fissile assemblies, and the turbulent mixing between the sodium streams of these assemblies and the hot plenum. Still, the systematic overestimation along the whole core is mainly associated with uncertainties of the provided CR positions. These were obtained during the test

Chapter 4. Overall verification and validation of the extended DYN3D code

with the help of empirical models that considered the relative thermal expansions of the core, vessel and CRs.

Table 4.4: Measured and calculated control rod worths for CR #1 and #4.

(pcm)	DYN3D	Serpent	Experiment	DYN3D vs. Serpent	DYN3D vs. Experiment
CR #1	1332	1266 ± 3	1257	66	75
CR #4	1262	1209 ± 3	1238	53	24

Additionally to the CR shift test, the balancing method was simulated with DYN3D and Serpent to obtain the S-curves for CR #1 and #4. The Serpent simulation followed the same procedure as described for DYN3D in subsection 4.1.2. The statistical uncertainty of the Serpent reactivities was kept under 2 pcm. The calculated and measured (IAEA, 2014, p. 18) S-curves of both CRs are compared in Fig. 4.7. The total rod worths are summarized in Table 4.4. The DYN3D overestimates both the Serpent rod worths by 66 and 53 pcm and the measured ones by 75 and 24 pcm for CR #1 and #4, respectively. Nevertheless, the computational results are in a very good agreement with the experimental data while the S-curves are well aligned with each other.

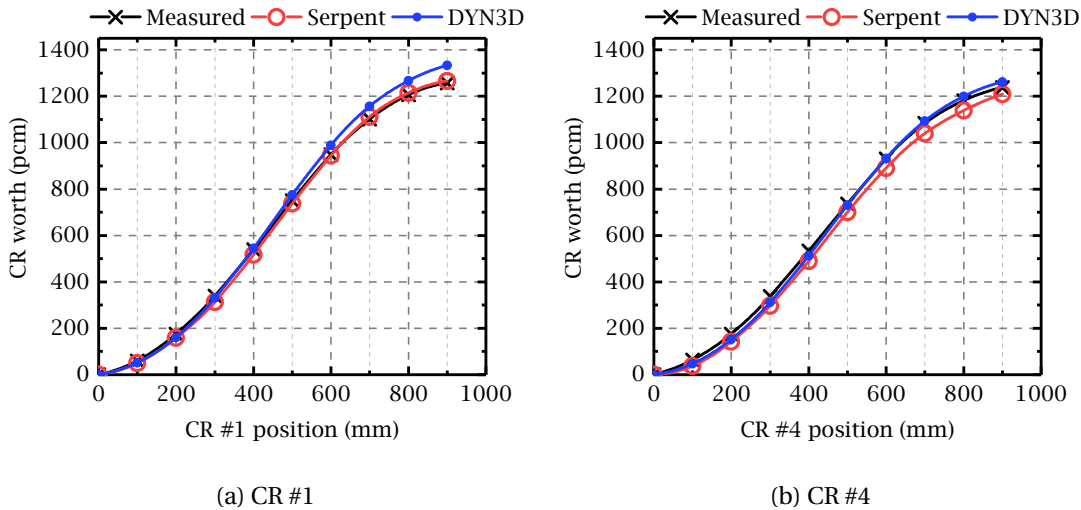


Figure 4.7: Comparison of control rod S-curves. Standard deviation of Serpent values is 3 pcm.

Case B – Coupled neutronic thermal-hydraulic calculations

Beside the *Case A* results, Table 4.2 also contains the reactivity values obtained with DYN3D in the coupled neutronic thermal-hydraulic calculation mode. For *Case B*, the reactivity remains overestimated by ~430-470 pcm.

The impact of using coupled N/TH analysis instead of the pure neutronic calculation with uniform temperature profiles was assessed by comparing the obtained radial power deviation profiles against the measured ones. Fig. 4.8 presents the discrepancies between DYN3D and the experiment for all steps obtained as:

$$\Delta(\delta_{\text{rel}}P)_i = \delta_{\text{rel}}P_i^{\text{C}} - \delta_{\text{rel}}P_i^{\text{E}}, \quad (4.2)$$

where $\delta_{\text{rel}}P$ is the relative power deviation obtained with Eq. (4.2) for each assembly i from the experiment (E) and DYN3D calculations (C). The results of the coupled calculations (*Case B*) are almost aligned with the pure neutronic solution (*Case A*), but a slight reduction of discrepancies is observed in the coupled case (Fig. 4.8).

In *Case B*, a more realistic expansion of each fuel assembly was modeled with DYN3D by using the cladding temperature distribution. Fig. 4.9 presents axial expansion profile of the core calculated for Step 2 with DYN3D. The profile is obtained as the difference in height between the expanded and reference state (20°C):

$$\Delta L = L_{\text{exp}} - L_{\text{ref}}. \quad (4.3)$$

The expansion profile reveals that, while the central assemblies become larger, the assemblies on the periphery remain smaller than in case of uniform expansion. Furthermore, Fig. 4.9 shows that the expansion of an assembly is following the axial sodium heat-up, i.e. the upper nodes expand more than the lower ones. DYN3D uses these self-calculated node-wise expansion profiles to obtain the correct XS with the mixing approach as described in details in Section 3.2.

As compared to the experiment in general, the results demonstrated a competent performance of the coupled code. Although the more realistic expansion profile obtained from the new thermal-mechanical model did not affect the steady-state results notably, the application of this new model can be important in transient and accident analyses where the significantly higher temperature variations can be expected.

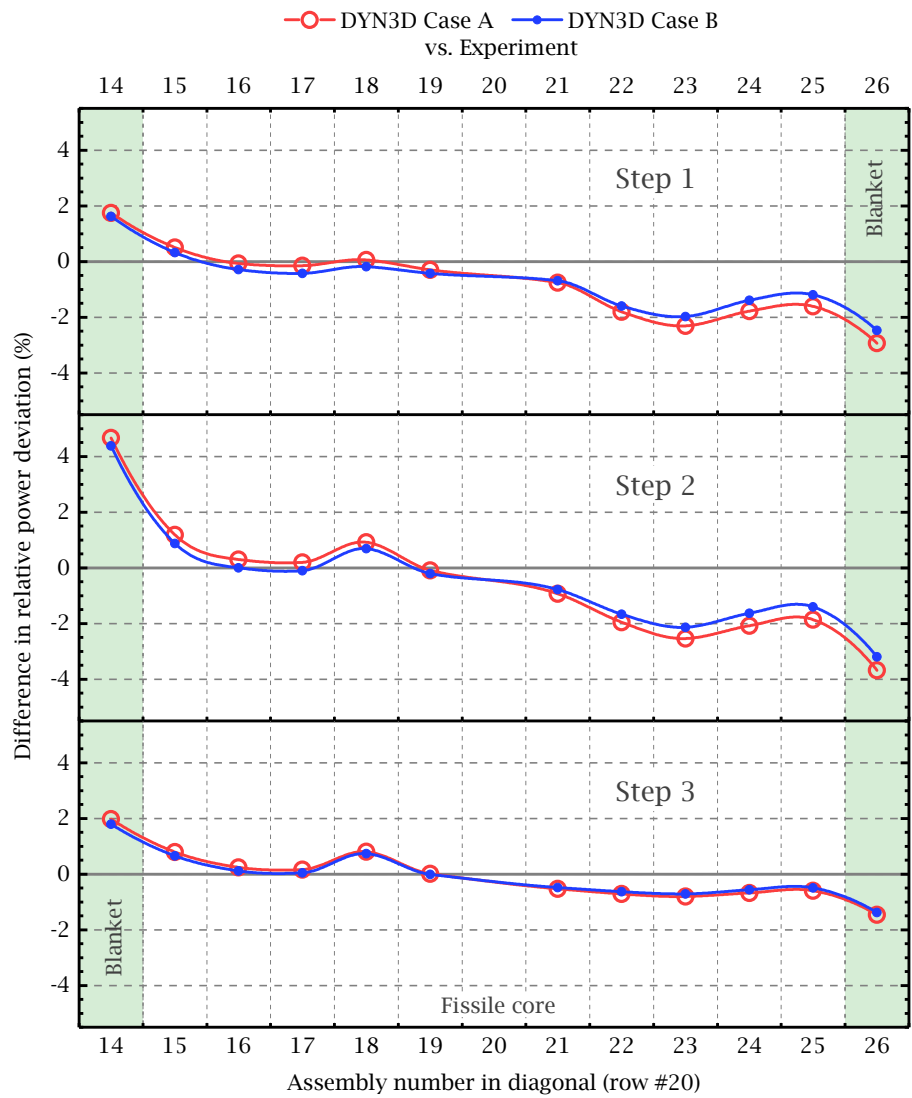


Figure 4.8: Difference in power deviation profiles between DYN3D and the experiment (*Top to bottom*: Step 1 to Step 3). The results are depicted along the diagonal closest to CRs #1 and #4.

4.1. Phenix EOL control rod withdrawal tests

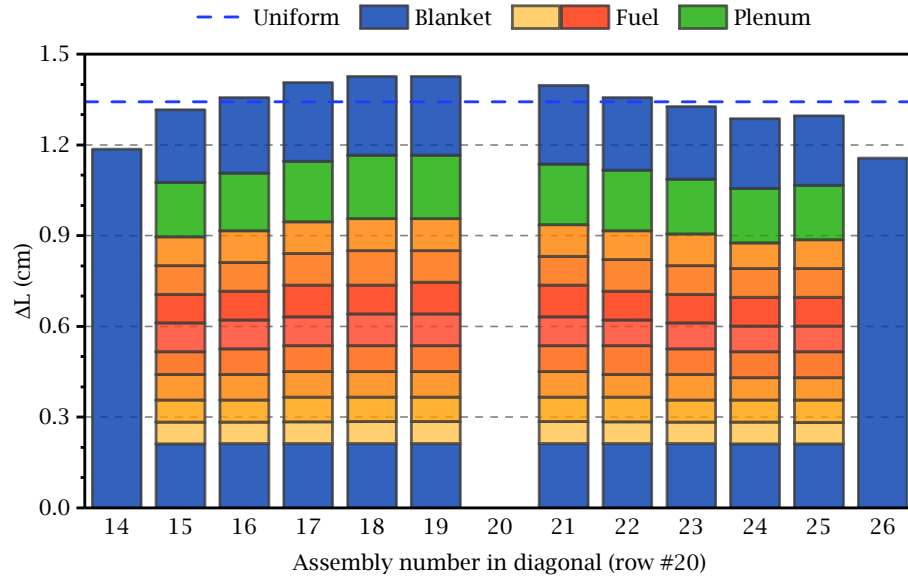


Figure 4.9: Absolute axial expansion profile of assemblies along the diagonal closest to CRs #1 and #4 (Step 2). Calculated with DYN3D.

4.1.4 Control rod withdrawal tests – Summary of the results

This section presented the V&V of the extended version of DYN3D against the Phenix EOL control rod withdrawal benchmark. The benchmark tasks were solved with DYN3D in two different ways: (1) pure neutronic calculations without feedbacks, and (2) coupled N/TH calculations with consideration of local thermal expansion effects. In both cases the homogenized XS were generated with Serpent. The obtained DYN3D results are summarized as follows:

- By using the first method the CR shift test and the CR S-curve measurements were modeled with DYN3D. These solutions were used to validate the few-group XS generation methodology and neutronic performance of DYN3D in general:
 - The DYN3D results are in very good agreement with the full core MC solution of Serpent and they are consistent with the numerical solutions of the benchmark participants.
 - Similarly to the benchmark participants, significant discrepancies were observed between the DYN3D solutions and the experimental data. These were explained with the aforementioned benchmark deficiencies (e.g., the averaged core descriptions and the uncertainties of the provided CR

positions).

- The integral CR worths and the S-curves are in good agreement with the Serpent solution as well as with the experimental data.
- In the second case, only the CR shift test was modeled to demonstrate and assess the overall capabilities of the extended DYN3D version:
 - The coupled N/TH calculations presented an adequate performance of the code, while predicting realistic thermal expansion profiles of the fuel assemblies. The results were not significantly different from the solution where the core-average temperature was used to uniformly expand the core.
 - It is worth noting that in more severe cases, when the local temperature variations are higher, the selection between uniform and non-uniform axial thermal expansion modeling can be more influential on the results.

4.2 Phenix EOL natural circulation test

This section focuses on validation of DYN3D against a transient scenario taken from the IAEA benchmark on the Phenix EOL natural circulation test (IAEA, 2013). Initially, the benchmark targeted sodium capable thermal-hydraulic system codes utilizing point kinetics models for validation. However, by combining this benchmark with the detailed core description of the CR withdrawal benchmark, the point kinetics model can be exchanged with a spatial neutron kinetics code for a more detailed evaluation of the test, as it was also done in (Chenu et al., 2012).

Similarly in this work, the unprotected stage of the natural convection test was calculated with DYN3D using the 3D nodal diffusion solver together with the intrinsic thermal-hydraulic model and the new thermal-mechanical models. This section provides an assessment of DYN3D for coupled neutron kinetics thermal-hydraulics (NK/TH) transient analyses of SFR cores in general, and presents the impact of using uniform axial expansion profiles instead of simulating a more realistic non-uniform core expansion for this particular test.

4.2.1 Description of the unprotected stage of the transient

The natural circulation test (IAEA, 2013) was dedicated to investigate the onset and development of natural circulation in pool-type SFR systems. In the framework of the benchmark, the experimental data were made available for qualification and validation of thermal-hydraulic system codes that are aimed at modeling liquid sodium systems.

The test was initiated by manual dry out of the two steam generators at the reduced power of 120 MWth. This caused a loss of heat removal from the secondary, and consequently, from the primary side. After the initial phase, which lasted 458 seconds, the reactor was manually scrammed. Eight seconds later, the primary pumps were tripped and the characteristics of natural circulation were measured in the primary system.

In the unprotected stage, while the total mass flow rate remained constant, the core inlet temperature has increased by ~ 40 K. As a result, the total power has dropped from 120 MWth to 50 MWth, and the inner core outlet temperature by ~ 10 K, as shown in Fig. 4.10. The power reduction driven by the core reactivity was initiated by the thermal expansion of the core diagrid. The further development of the total reactivity (Fig. 4.10) was mainly influenced by the thermal expansion of the diagrid and fuel rods, the Doppler effect, and the relative CR movement caused by the simultaneous expansion of the core, CR drivelines and vessel. The measured core characteristics, shown in Fig. 4.10, include time-dependent inlet and outlet coolant temperatures, reactivity, and total power.

The temperature increase of the core inlet is mainly driven by the loss of heatsink in the steam generators. The small and slow change of the outlet coolant temperature has only a minor influence on the core inlet during the unprotected stage. Therefore, to a certain extent, the core thermal-hydraulic behavior may be considered decoupled from the primary circuit, and can be modeled with a core simulator by using the inlet temperature curve as time-dependent boundary condition (Fig. 4.10, top). In this section, the unprotected stage of the test was calculated in such way with DYN3D, and the numerical results were compared with the experimental data provided by the benchmark specification (IAEA, 2013).

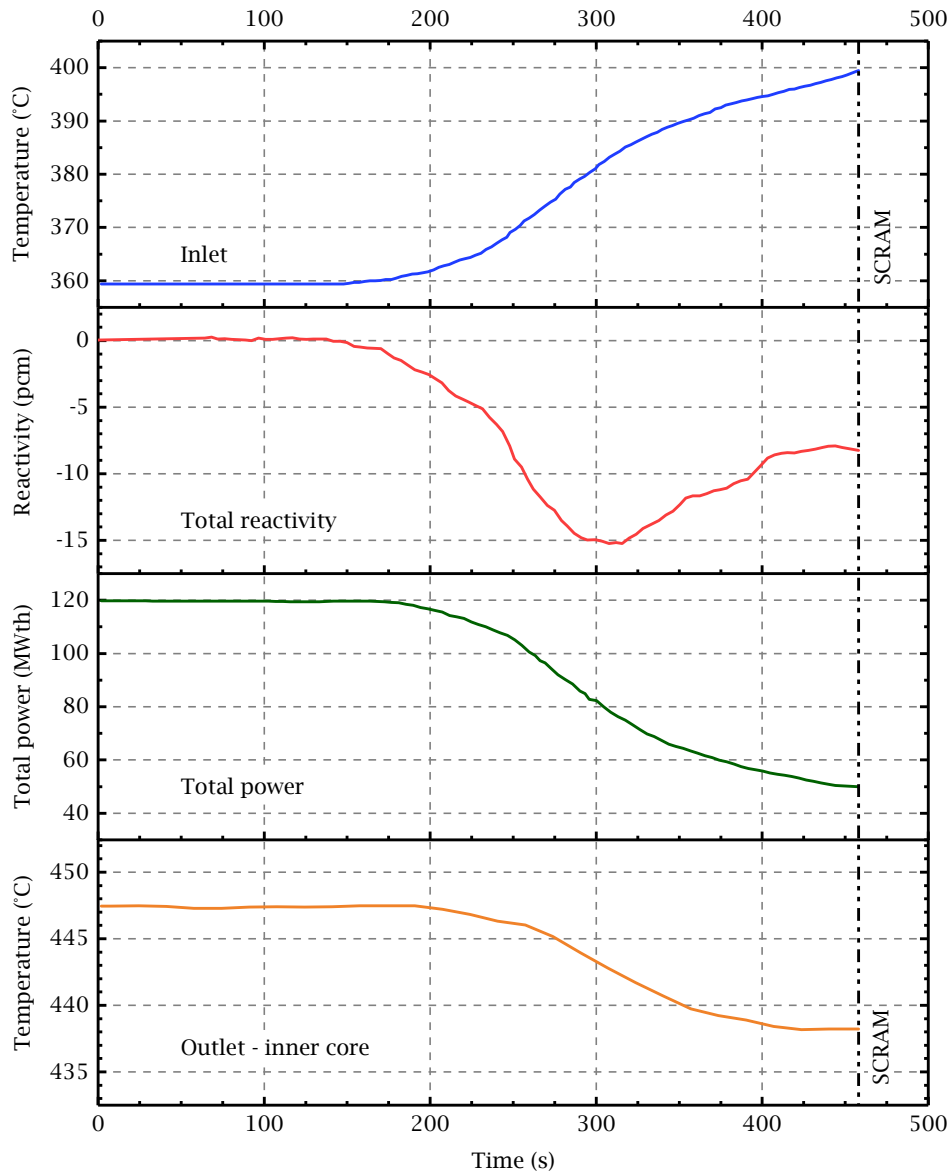


Figure 4.10: Measurements in the unprotected stage of the natural convection test. *Top to bottom:* inlet coolant temperature, reactivity, total thermal power, outlet coolant temperature of the inner core. Data are extracted from the benchmark report.

4.2.2 Computational methodology

The calculations were done in a two-step approach using the Serpent-DYN3D codes sequence. In the first step, the homogenized few-group cross sections (XS) were generated on lattice level with Serpent, and in the second step, the full core nodal calculations were performed with DYN3D.

Generation of parametrized cross section libraries

Identical XS library was applied in this transient calculation as was used for the CR withdrawal tests (Section 4.1). For a detailed description of the XS library see subsection 4.1.2.

DYN3D model

The Phenix EOL core model was constructed in DYN3D based on the data provided in the benchmark reports of the CR shift test and the natural circulation test. The fuel rods were modeled as described in the benchmark, but instead of modeling 90% of the fuel rods in a closed gas gap condition (linked fuel) and 10% in open gas gap condition (free fuel), all fuel pins were considered as linked in the DYN3D model. This approximation is based on the fact that the positions of the linked and free fuel pins are not available in the specification, since the natural circulation benchmark was aimed at system analyses by not modeling spatial neutronics and mechanics.

At the core inlet, a constant mass flow rate and a time-dependent coolant temperature boundary condition was defined. The inlet flow resistance coefficients of the assemblies were set to reproduce the zone-wise mass flow rate distribution given by the benchmark specification. Within the zones, the total mass flow rate of the zone was evenly distributed between the assemblies. The total mass flow rate of the core had to be adjusted, in order to match the initial coolant temperature measured at the outlet of the inner core (Fig. 4.10, bottom). In DYN3D, the total mass flow rate was set to 1275 kg/s instead of 1254 kg/s, which is still within the 5% of reported measurement uncertainty. Furthermore, it is assumed that the diagrid expansion in the Phenix reactor is directly driven by the average sodium inlet temperature without significant delay, since the thermal inertia of the diagrid heat-structure is very small (Chenu et al., 2012).

Chapter 4. Overall verification and validation of the extended DYN3D code

The unprotected stage of the test was computed with DYN3D by using the Serpent-generated parametrized XS library and the newly implemented thermal-mechanical models of thermal expansion. The calculation was repeated twice with different treatments of axial fuel rod expansion:

- *Case A*: The newly implemented axial fuel rod expansion model was employed, where the axial expansion of the fuel rods was driven by local cladding temperatures. Hereafter referred to as the non-uniform expansion model.
- *Case B*: The same mixing based model (Section 3.2) as in *Case A*, but the layer-average cladding temperature is used to expand the sections of the fuel rods located in the same layer. Hereafter referred to as the layer-uniform expansion model.

The solution of *Case A* is considered as the reference solution of DYN3D. *Case B* is a simplified approach of *Case A*, since the radial averaging of thermal expansions covers up the local effects. Nevertheless, the layer-uniform expansion model can be a compromise for other spatial neutronic codes that also utilize a regular axial grid, and prefer an explicit expansion of the mesh.

4.2.3 Numerical results

Before the transient analyses, the reactivity coefficients obtained by DYN3D were compared with values provided by the benchmark specification. The feedback parameters are in good agreement as show in Table 4.5.

Table 4.5: Reactivity coefficients of the Phenix EOL core.

	Doppler effect (pcm)	Diagrid expansion (pcm/K)	Fuel axial expansion (pcm/K)	Coolant temperature (pcm/K)
Benchmark spec.	−680	−1.21	−0.31	−0.02
DYN3D	−661	−1.00	−0.29	−0.05

Case A – Non-uniform thermal expansion modeling

The calculated total reactivity, power and core outlet temperature evolutions over time are presented in Fig. 4.11, along with the measured data. The power and core outlet temperature curves are completely aligned with experimental data, while the calculated values remain within measurement uncertainties. In the first 300 s the calculated reactivity remains in a good agreement with measurements, whereafter the DYN3D underestimates the total reactivity, and reaches 7 pcm discrepancy at the end of the transient. The underestimation can be explained with the missing model of vessel expansion. After 300 s, the increasing sodium temperature of the cold pool warms up enough to induce vessel expansion, which acts as a relative extraction of the control rods (IAEA, 2013). By modeling the vessel expansion effect, the discrepancy can be reduced, as it was demonstrated by (Chenu et al., 2012).

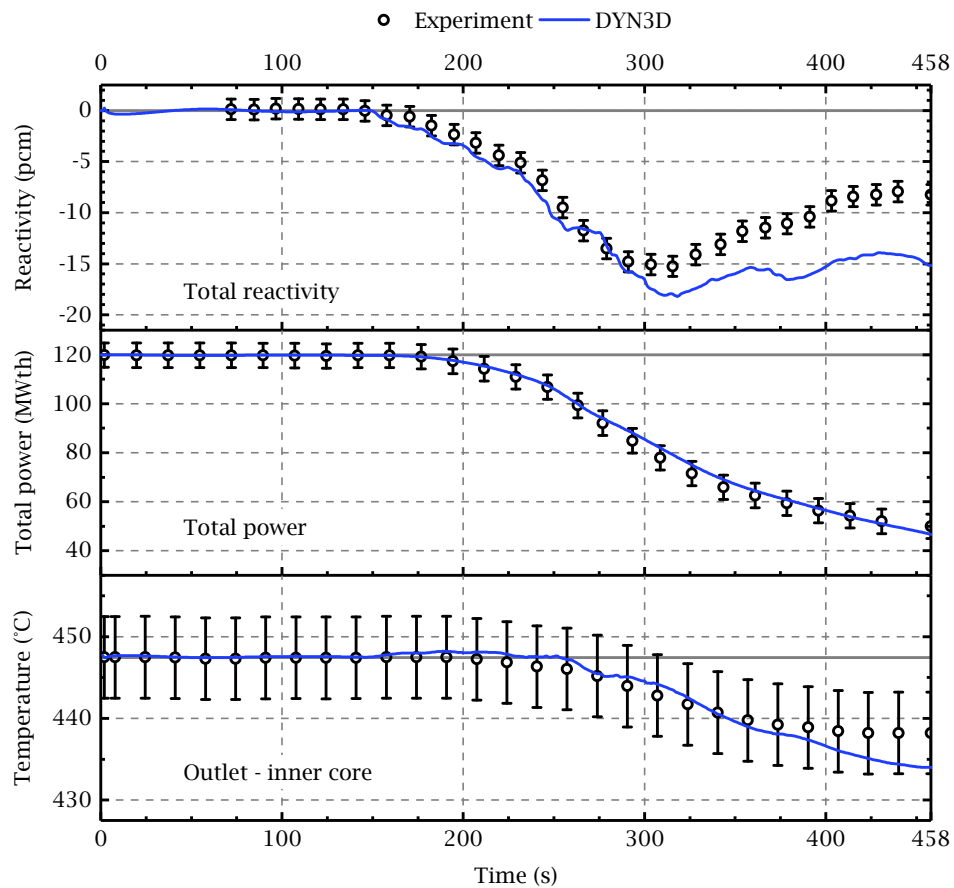


Figure 4.11: DYN3D results on the unprotected stage of the natural circulations test (compared with the experimental results). *Top to bottom*: reactivity, total thermal power, outlet coolant temperature of the inner core.

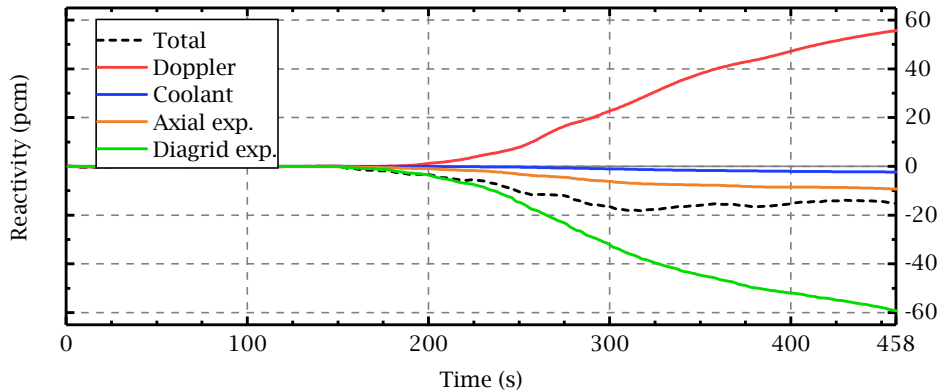


Figure 4.12: Total reactivity decompositions with DYN3D.

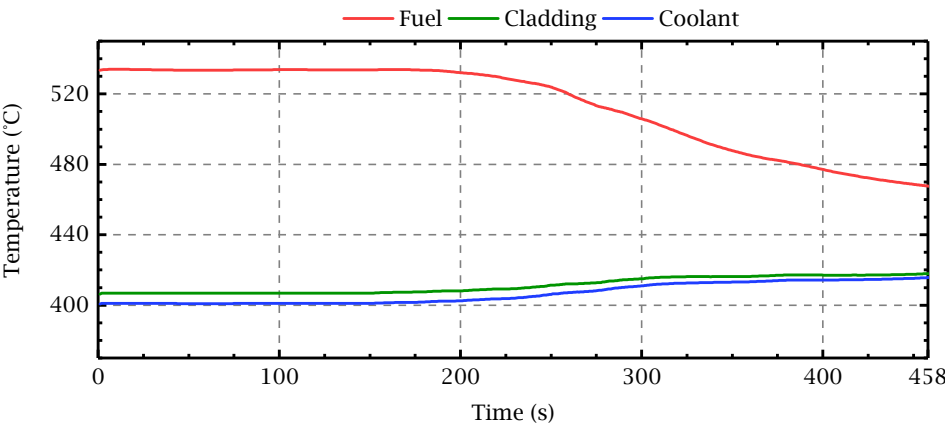


Figure 4.13: Averaged fuel rod temperature evolution in fissile core.

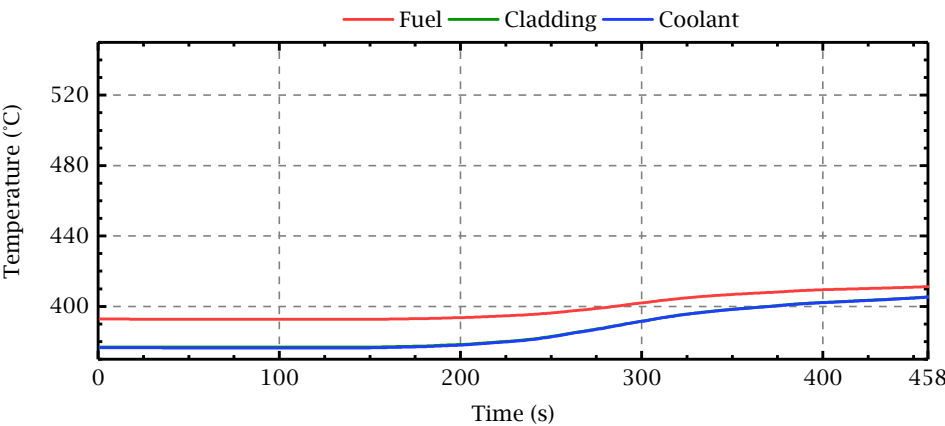


Figure 4.14: Averaged fuel rod temperature evolution in radial blanket.

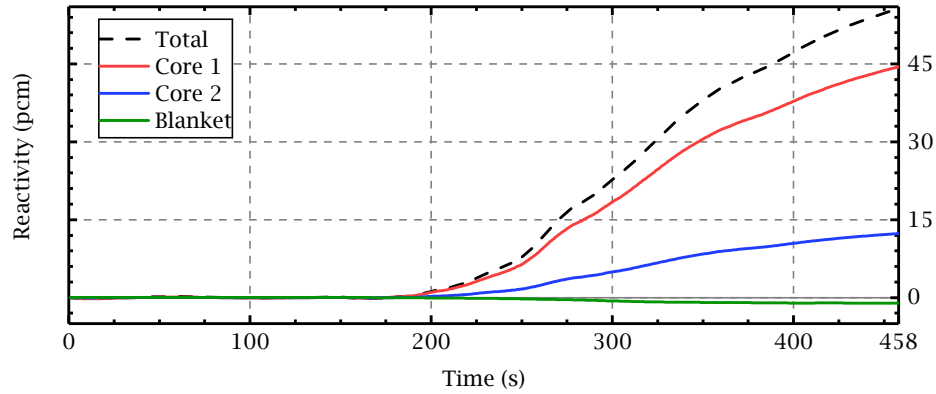


Figure 4.15: Doppler effect decompositions with DYN3D.

As it is presented in Fig. 4.12, the two main contributors to the reactivity evolution are the diagrid expansion and the Doppler effect. The increase of the inlet temperature triggers the diagrid expansion, which initiates the power reduction. The fuel temperature of the fissile zone is decreasing (Fig. 4.13) due the power reduction, while the blanket temperature of the fertile zone is increasing (Fig. 4.14) due to the sodium heat-up. In total, the observed positive Doppler reactivity (Fig. 4.12) is actually the combination of the dominant positive effect from the fissile core and the slightly negative effect from the blanket region, as shown in Fig. 4.15. An overall temperature rise in fuel rod cladding is observed (Figs. 4.13 and 4.14), causing a moderate negative reactivity contribution by axially expanding the fuel rods, as seen in Fig. 4.12. The coolant temperature effect remains insignificant during the whole transient.

Case B – Layer-uniform thermal expansion modeling

The transient calculation was repeated once more with the layer-uniform expansion model. The differences between the results of *Case A* and *B* are summarized in Fig. 4.16. In *Case B*, the DYN3D predicts at the end a lower power of ~ 2 MW, which corresponds to 1.7% of the initial state. This reduction in power is caused by the larger axial expansion reactivity effect (Fig. 4.16, bottom) that is somewhat compensated by the Doppler effect, and yielding a 1 pcm lower reactivity in total (Fig. 4.16, center).

The overestimation of axial expansion effect can be explained by comparing the evolution of the radial profiles of the assembly expansions, as presented in Fig. 4.17. With the layer-uniform model, all assemblies expand by additional 0.038% during

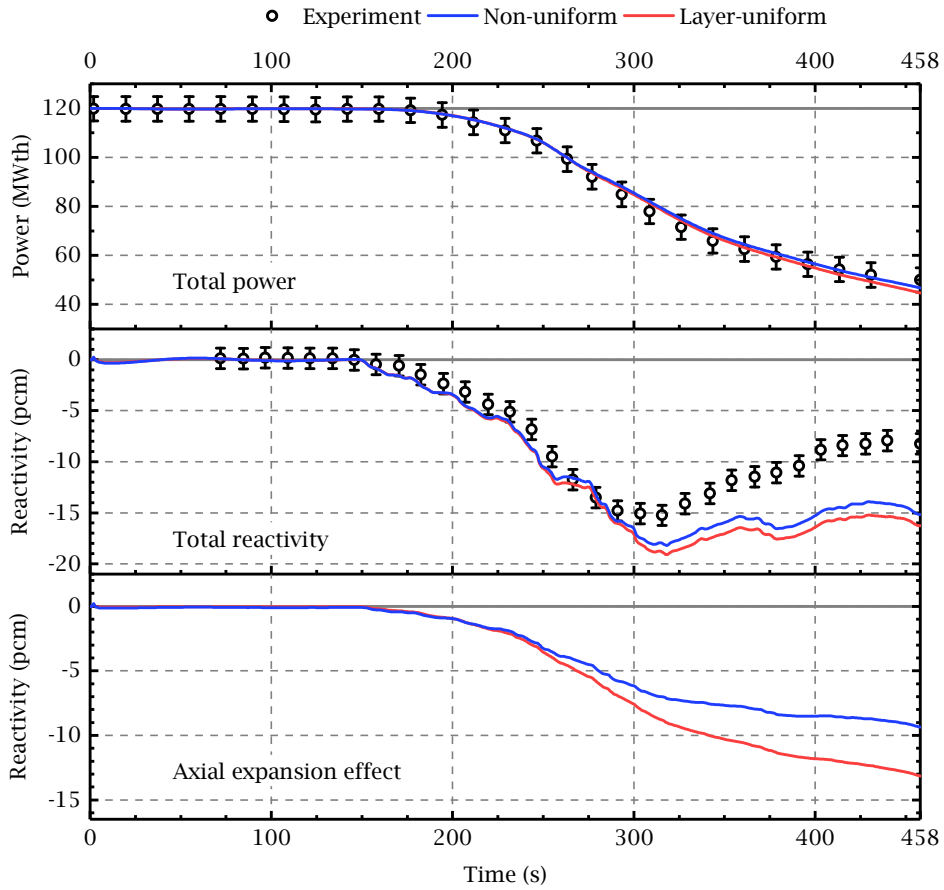


Figure 4.16: Difference in the results by using non-uniform and layer-uniform expansion models. *Top to bottom*: total power, total reactivity, and axial expansion effect.

the transient, while with the non-uniform model by only 0.023% in average. Since the transient is driven by a radially uniform heat-up of the coolant, the non-uniform profiles flattens out in time, and even would become uniform if transient would continue without external interaction. In this core-symmetric transient scenario, the discrepancies seen in the results can be originated from the differences of expansion profiles present at the beginning.

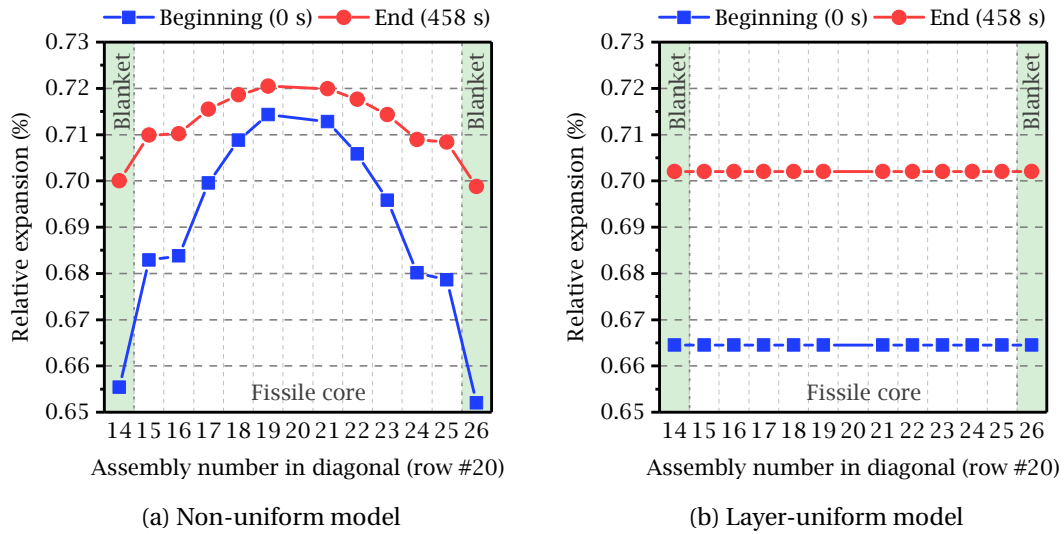


Figure 4.17: Change of the axial expansion profile between the beginning and the end of the transient. The profiles are depicted along the diagonal closest to CRs #1 and #4.

4.2.4 Natural circulation test – Summary of the results

This section presented the validation of the extended version of DYN3D against the unprotected stage of natural circulation test from the Phenix EOL experiments. The test was simulated with the Serpent-DYN3D codes sequence, i.e. the parametrized cross section library was generated with Serpent and the coupled NK/TH time-dependent solution was obtained with DYN3D. The numerical results were compared against the experimental data. The following conclusions can be made from the validation study:

- In general, the DYN3D solutions were in very good agreement with the experimental data indicating the feasibility of using DYN3D in coupled NK/TH transient analyses of SFR cores.

- The deviations from the measurements were only observed when out-of-core thermal expansion effects, such as vessel expansion, start to influence the CR position relatively to the core. In order to account for the correct magnitude and time delay of such relative CR movements, the change in thermal-mechanical conditions of the supporting structures has to be modeled. The development of thermal-mechanical models for the supporting structures is an ongoing research topic at HZDR that will be based on a coupling of DYN3D with a thermal-hydraulic system code capable of sodium flow modeling.
- The study demonstrated that by utilizing the newly implemented fuel rod thermal expansion model, the non-uniform thermal expansion effects can be modeled in transient simulations. As compared to the layer-uniform fuel rod expansion modeling, the discrepancies between the numerical results and the measurements did not change significantly. This can be attributed to a relatively small variation in sodium heat-up over the course of transient (about 40 K). In more severe cases (e.g. accident scenarios with significantly higher or/and asymmetric sodium heat-up) the selection of one thermal expansion model over the other can lead to much higher deviations in the results.
- This study also demonstrated that the MC code Serpent can be successfully applied to generate few-group XS for transient analyses of SFR cores.

5 Summary and future work

The purpose of the present doctoral research was to extend the capabilities of the Light Water Reactor core simulator DYN3D to perform three-dimensional reactor simulations of Sodium cooled Fast Reactor cores. The supplementary methods and models developed in this dissertation make DYN3D feasible to do steady-state and transient calculations on reactor core level. These extensions were verified and validated on both numerical and experimental SFR benchmarks.

The SFR-related DYN3D developments are summarized in the following while the recommendations for further research are provided at the end.

5.1 Thesis summary

By utilizing the Monte Carlo neutron transport code Serpent, a methodology was developed to create homogenized few-group cross sections for more realistic and detailed SFR core configurations. This method is capable of providing group constants to practically any deterministic 3D full core simulator. It is based on lattice-level models, which is favorable in respect to the computation time and memory usage while maintaining an adequate MC statistics. Such is particularly important in branching calculations, when a complete parametrized XS library is prepared for transient simulations. This research demonstrated that the Serpent-DYN3D codes sequence can be used for static neutronic as well as time-dependent N/TH analyses of SFR cores.

In order to support the cross section generation method, the Super-homogenization technique was applied for the first-neighbor regions to the fuel assemblies. This method demonstrated a consistent improvement in the nodal diffusion solution

Chapter 5. Summary and future work

of SFR cores, as compared to full core Monte Carlo results. The highest positive impact was achieved by using the SPH factors on the non-multiplying regions that are surrounded by the fissile core, such as the control and diluant assemblies. The SPH method in combination with the lattice approach of XS generation proved to be an efficient way to improve the nodal diffusion solution of the SFRs.

In order to perform coupled N/TH simulations with DYN3D, the implementation of new thermal expansion models was necessary. In this research, DYN3D was extended with new models to account for time-dependent axial and radial core expansions in the neutronic behavior. The axial expansion model is capable of modeling non-uniform core expansions by using the spatial temperature distribution of the fuel rods. This model allows for an independent treatment of each fuel assembly based on local thermal-hydraulic conditions. The radial diagrid expansion model can account for a uniform radial expansion of the core driven by the average inlet sodium temperature. The verification of these models was carried out in this research based on steady-state analyses of two reference cores, namely the large oxide OECD/NEA benchmark core and the smaller Phenix EOL core.

In the process of verification, and for a better understanding of the reactor behavior during core expansions, a spatial- and reaction-wise reactivity decomposition technique was introduced in this dissertation. The method was especially developed to obtain decomposed thermal expansion feedbacks from the solutions of any nodal diffusion code. This procedure allows in a simple manner to quantify the relation between the change in nodal absorption and leakage rates while locating the regions of significance when the core expands.

Finally, the capability of the extended version of DYN3D to perform steady-state and transient analyses of SFR cores was validated using selected tests from the end-of-life experiments conducted at the Phenix reactor. Firstly, the IAEA benchmark on the control rod withdrawal tests was used to validate the neutronic performance of DYN3D. Then the simulation of the initial stage of the natural convection test was used to validate DYN3D for coupled NK/TH transient calculations. Both tests have also served for the validation of the few-group XS generation methodology for SFR analyses.

In general, all DYN3D benchmark solutions were in good agreement with the experimental data indicating the feasibility of using DYN3D in static and time-dependent analyses of SFR cores. Significant discrepancies between DYN3D and the measure-

ments were only observed when out-of-core thermal expansion effects started to influence the control rod position in the core. However, the modeling of such thermal expansions was beyond the scope of this study.

5.2 Recommendations for further research

The introduced developments make DYN3D capable of calculating steady-states and transients in SFR cores by applying proper boundary conditions. The core level simulation is an important step to use DYN3D in full scale safety analyses of SFR systems. Nevertheless, the standalone application is limited to transients with very short time duration or very slow progression, where the change of core outlet sodium has no time to influence the coolant parameters at core inlet or the relative control rod positions. In order to overcome the current simulation boundaries, several research directions are proposed in the following.

Coupling with a thermal-hydraulic system code capable of sodium flow modeling

The DYN3D can be coupled with a thermal-hydraulic system code in order to scale up the simulation capabilities from core to system level. This will open the possibility to model the primary sodium loop in a closed system, and so to account for the NK feedback on the thermal-hydraulic properties at the core inlet. Such development will overcome the limitations of the standalone DYN3D, and it will serve as a first step for simulating longer transient scenarios.

From the list of system codes that were coupled with DYN3D, the ATHLET code (Lerchl et al., 2012) is considered the most promising candidate as to be used in SFR system analyses. While still under validation, the recent implementations of the sodium models and correlations (since ATHLET 3.0) are specifically aimed to model SFR systems.

Thermal expansion models for out-of-core system components

The relative control rod position in respect to the core is strongly influenced by the differential thermal expansion of the out-of-core system components. In order to predict the control rod positions during transients, the thermal expansion of three main system components has to be accounted for. These are the control rod drive

lines, the core supporting strongback and the reactor vessel.

With the help of a system code, the temperatures of these heat structures can be obtained in real time, and so the thermal expansion of these components. By implementing the missing thermal expansion models, the actual control rod position can be calculated and applied in the DYN3D core simulator. With this approach, the time delays in thermal expansion between different system components will be implicitly considered. With this kind of codes system, the simulation of the whole Phenix EOL natural circulation tests becomes possible.

Non-uniform radial core expansion modeling

The current diagrid model is capable of uniformly expanding the core in radial direction while assuming that all assemblies remain vertical. By developing a model that can expand each axial layer independently while keeping the nodal mesh fixed, the DYN3D can gain the possibility to model layer-uniform assembly bowing, i.e. the uniform core flowering effect. In general, the core flowering is an important effect to consider, since it caused several extremely fast and highly oscillating transients and consequent reactor shutdowns in the Phenix reactor, as reported by (Fontaine et al., 2011). Nevertheless, the assembly bowing is considered as one the most challenging thermal expansion effect to model, especially with nodal diffusion codes that apply regular computational meshes.

Few-group cross section generation methodology for transient analyses of SFRs

In DYN3D, the state-dependent few-group XS are provided in multi-dimensional table format that covers the full parametric space of the given problem. To acquire the XS of a current state, a multi-dimensional interpolation of XS is performed between the available states. Although this method implicitly accounts for the correlations between state variables, the XS generation for multiple state points with Serpent and the on-the-fly interpolations may add significant computational burden. The reduction of the parametric space of the XS can lead to an overall time reduction of the simulations. This can be done by reducing the number of points for each state variable or the energy group structure to an optimal level, i.e. reducing the XS library without degrading the numerical results.

Furthermore, other approximation methods is advised to be tested with the focus

5.2. Recommendations for further research

to perform transient SFR calculations. Simplifications like considering the state variable independence, opens up the possibility to calculate the XS at given state by linear combination of properly selected state derivatives. Such approach is currently used in PARCS of the FAST codes system (Mikityuk et al., 2005), which can be also adopted in DYN3D. A comparison of both methods with the same code will assess the interdependency of selected state variables and the type of dependency (e.g., linear, logarithmic, etc.) of each state derivative.

Further verification and validation

At last but not least, acquiring further experimental data on SFRs will be beneficial for additional validation of the extended version of DYN3D. In May of 2017, the IAEA endorsed a new Coordinated Research Project: the Benchmark Analysis of FFTF Loss of Flow Without Scram Test (IAEA, 2018a). This benchmark will offer experimental data acquired during ULOF tests that were conducted between 1980 and 1992. The participation in the CRP is encouraged, since it will provide an unique opportunity to fully develop the DYN3D/ATHLET codes system and validate it against real measurements.

Beside the comparison against experiments, further application of the code in numerical benchmarks can also reveal model limitations as well as the course for further developments. For instance, the new axial expansion model, together with the spatial kinetics solver of DYN3D, has the potential to improve the simulation of core-asymmetric transients such as a peripheral control rod withdrawal in an UTOP scenario or a single pump failure in an ULOF accident. Even by calculating such postulated cases, the actual benefit of the model can be assessed in comparison to simplified modeling such as point kinetics.

Bibliography

- G. Aliberti, G. Palmiotti, M. Salvatores, J. Lebrat, J. Tommasi, and R. Jacqmin. Methodologies for Treatment of Spectral Effects at Core-Reflector Interfaces in Fast Neutron Systems. In *PHYSOR 2004 – The Physics of Fuel Cycles and Advanced Nuclear Systems: Global Developments Chicago, Illinois, USA, 2004*.
- L. Andriolo, A. Rineiski, B. Vezzoni, F. Gabrielli, X.-N. Chen, W. Maschek, F. Delage, and E. Merle-Lucotte. An Innovative Methodology for Evaluating Core Thermal Expansion. In *ICAPP 2015*, pages 504–512, Nice, France, 2015.
- H. D. Baehr and K. Stephan. *Heat and Mass Transfer*. Physics and Astronomy. Springer Berlin Heidelberg, Berlin, Heidelberg, 2 edition, 2006. ISBN 978-3-540-29526-6. doi:10.1007/3-540-29527-5.
- S. Baier, E. Fridman, S. Kliem, and U. Rohde. Extension and application of the reactor dynamics code DYN3D for Block-type High Temperature Reactors. *Nuclear Engineering and Design*, 271:431–436, may 2014. ISSN 00295493. doi:10.1016/j.nucengdes.2013.12.013.
- D. Baldova, E. Fridman, and E. Shwageraus. High conversion Th–U233 fuel for current generation of PWRs: Part II – 3D full core analysis. *Annals of Nuclear Energy*, 73: 560–566, nov 2014. ISSN 03064549. doi:10.1016/j.anucene.2014.05.018.
- T. Beck, V. Blanc, J.-M. Esclaine, D. Haubensack, M. Pelletier, M. Phelip, B. Perrin, and C. Venard. Conceptual design of ASTRID fuel sub-assemblies. *Nuclear Engineering and Design*, 315:51–60, apr 2017. ISSN 0029-5493. doi:10.1016/J.NUCENGDES.2017.02.027.
- T. Beck, N. Chapoutier, J.-M. Esclaine, L. Gauthier, D. Occhipinti, B. Perrin, and C. Venard. Conceptual design of ASTRID radial shielding sub-assemblies.

Bibliography

- Nuclear Engineering and Design*, 330:129–137, apr 2018. ISSN 0029-5493. doi:10.1016/J.NUCENGDES.2018.01.040.
- P. Bergeonneau, M. Vanier, M. Favet, J. De Antoni, K. Essig, and J. P. Adam. Analysis of the dynamic behavior of the core. *Nuclear Science and Engineering*, 106(1):69–74, 1990. ISSN 00295639.
- D. Blanchet, L. Buiron, S. Nicolas, T. K. Kim, and T. Taiwo. AEN - WPRS Sodium Fast Reactor Core Definitions (version 1.2). Technical report, CEA Cadarache and Argonne National Laboratory US-DOE, OECD/NEA, 2011. URL <https://www.oecd-neo.org/science/wprs/sfr-taskforce/WPRS-AEN-SFR-Cores-V1.2.pdf>.
- F. B. Brown. On the Use of Shannon Entropy of the Fission Distribution for Assessing Convergence of Monte Carlo Criticality Calculations. In *PHYSOR-2006 American Nuclear Society's Topical Meeting on Reactor Physics Organized and hosted by the Canadian Nuclear Society*, volume 836, pages 1–6, 2006. ISBN 0894486977.
- T. Burke. Summary of FY 1997 work related to JAPC-U.S. DOE contract study on improvement of core safety - study on GEM (III). Technical report, DOE Technical Exchange, Tokyo, Japan, 1998. URL https://inis.iaea.org/search/search.aspx?orig_q=RN:30039909.
- J. Cahalan, R. Wigeland, G. Friedel, G. Kussmaul, P. Royle, J. Moreau, and M. Perks. Performance of metal and oxide fuels during accidents in a large liquid metal cooled reactor. In *International topical meeting on fast reactor safety*, Snowbird, UT (USA), 1990. URL http://www.iaea.org/inis/collection/NCLCollectionStore/_Public/21/076/21076260.pdf.
- J. Cahalan, T. Ama, G. Palmiotti, T. Taiwo, and W. Yang. Development of a coupled dynamics code with transport theory capability and application to accelerator driven systems transients. In *PHYSOR 2000*, Pittsburgh, PA, USA, 2000. URL https://inis.iaea.org/search/search.aspx?orig_q=RN:31049253.
- B. Chanaron. Overview of the NURES SAFE European Project. *Nuclear Engineering and Design*, 321:1–7, sep 2017. ISSN 00295493. doi:10.1016/j.nucengdes.2017.09.001.
- B. Chanaron, C. Ahnert, N. Crouzet, V. Sanchez, N. Kolev, O. Marchand, S. Kliem, and A. Papukchiev. Advanced multi-physics simulation for reactor safety in the framework of the NURES SAFE project. *Annals of Nuclear Energy*, 84:166–177, oct 2015. ISSN 0306-4549. doi:10.1016/J.ANUCENE.2014.12.013.

- C. Chauliac, J.-M. Aragonés, D. G. Cacuci, N. Crouzet, F.-P. Weiss, and M. A. Zimmermann. NURESIM – A European simulation platform for nuclear reactor safety: Multi-scale and multi-physics calculations, sensitivity and uncertainty analysis. *Nuclear Engineering and Design*, 241(9):3416–3426, sep 2011. ISSN 0029-5493. doi:10.1016/J.NUCENGDES.2010.09.040.
- T. Chawla, D. Graff, R. Borg, G. Bordner, D. Weber, and D. Miller. Thermophysical properties of mixed oxide fuel and stainless steel type 316 for use in transition phase analysis. *Nuclear Engineering and Design*, 67(1):57–74, oct 1981. ISSN 00295493. doi:10.1016/0029-5493(81)90155-2.
- A. Chenu, K. Mikityuk, and R. Chawla. A coupled 3D neutron kinetics/thermal-hydraulics model of the generation IV sodium-cooled fast reactor. In *International Congress on Advances in Nuclear Power Plants 2010, ICAPP 2010*, volume 2, pages 1331–1337, jan 2010.
- A. Chenu, K. Mikityuk, and R. Chawla. Analysis of selected Phenix EOL tests with the FAST code system – Part II: Unprotected phase of the Natural Convection Test. *Annals of Nuclear Energy*, 49:191–199, nov 2012. ISSN 03064549. doi:10.1016/j.anucene.2012.05.035.
- S. Choi, K. S. Smith, H. Kim, T. Tak, and D. Lee. On the diffusion coefficient calculation in two-step light water reactor core analysis. *Journal of Nuclear Science and Technology*, 54(6):705–715, 2017. ISSN 0022-3131. doi:10.1080/00223131.2017.1299648.
- T. Courau, M. Cometto, E. Girardi, and N. Schwartz. Elements of validation of pin-by-pin calculations with the future EDF calculation scheme based on APOLLO2 and COCAGNE codes. In *International Conference on Advances in Nuclear Power Plants, ICAPP 2008*, volume 4, pages 2439–2448, 2008. ISBN 9781605607870. URL http://inis.iaea.org/Search/search.aspx?orig_q=RN:42094773.
- J. Crank and P. Nicolson. A practical method for numerical evaluation of solutions of partial differential equations of the heat-conduction type. *Advances in Computational Mathematics*, 6(1):207–226, 1996. ISSN 1572-9044. doi:10.1007/BF02127704.
- A. Dall’Osso. Reducing Rod Cusping Effect in Nodal Expansion Method Calculations. In *PHYSOR 2002*, Seoul, 2002.

Bibliography

- K. L. Derstine. DIF3D: A Code to Solve One-, Two-, and Three-Dimensional Finite Difference Diffusion Theory Problems, apr 1984. URL https://inis.iaea.org/search/search.aspx?orig_q=RN:16014547.
- K. Devan, M. Alagan, A. Bachchan, P. Mohanakrishnan, P. Chellapandi, and S. Chetal. A comparative study of FARCOB and ERANOS-2.1 neutronics codes in predicting the Phenix control rod withdrawal end-of-life experimental results. *Nuclear Engineering and Design*, 245:89–98, apr 2012. ISSN 00295493. doi:10.1016/j.nucengdes.2012.01.007.
- T. J. Downar, Y. Xu, V. Seker, and N. Hudson. PARCS v3.0 - U.S. NRC Core Neutronics Simulator. Theory Manual. Technical report, University of Michigan, 2010. URL <http://pbadupws.nrc.gov/docs/ML1016/ML101610117.pdf>.
- S. Duerigen, U. Rohde, Y. Bilodid, and S. Mittag. The reactor dynamics code DYN3D and its trigonal-geometry nodal diffusion model. *Kerntechnik*, 78(4):310–318, aug 2013. ISSN 0932-3902. doi:10.3139/124.110382.
- ESNII Task Force. *A contribution to the EU Low Carbon Energy Policy: Demonstration Programme for Fast Neutron Reactors*. The Sustainable Nuclear Energy Technology Platform, 2010. URL <http://www.snetp.eu/publications/>.
- T. Fanning, T. H. Brunett, and A. J. Sumner. The SAS4A/SASSYS-1 Safety Analysis Code System, 2017. URL https://wiki.anl.gov/sas/Code_Manual.
- T. Fei, E. Shwageraus, and M. J. Driscoll. A cost-effective U-235 once-through startup mode for SFRs. In *Transactions of the American Nuclear Society*, volume 104, pages 734–735, 2011.
- C. Fiorina, I. Clifford, M. Aufiero, and K. Mikityuk. GeN-Foam: a novel Open-FOAM® based multi-physics solver for 2D/3D transient analysis of nuclear reactors. *Nuclear Engineering and Design*, 294:24–37, dec 2015. ISSN 00295493. doi:10.1016/j.nucengdes.2015.05.035.
- G. Fiorini and A. Vasile. European Commission – 7th Framework Programme. *Nuclear Engineering and Design*, 241(9):3461–3469, sep 2011. ISSN 00295493. doi:10.1016/j.nucengdes.2011.01.052.
- B. Fontaine, G. Prulhière, A. Vasile, P. Masoni, P. Barret, D. Rochwerger, J. Gros, R. Dupraz, N. Moussallam, and M. Chassignet. Description and preliminary results

- of PHENIX core flowering test. *Nuclear Engineering and Design*, 241(10):4143–4151, oct 2011. ISSN 00295493. doi:10.1016/j.nucengdes.2011.08.041.
- E. Fridman and J. Leppänen. On the use of the Serpent Monte Carlo code for few-group cross section generation. *Annals of Nuclear Energy*, 38(6):1399–1405, jun 2011. ISSN 03064549. doi:10.1016/j.anucene.2011.01.032.
- E. Fridman and E. Shwageraus. Modeling of SFR cores with Serpent-DYN3D codes sequence. *Annals of Nuclear Energy*, 53:354–363, mar 2013. ISSN 03064549. doi:10.1016/j.anucene.2012.08.006.
- E. Fridman, S. Duerigen, Y. Bilodid, D. Kotlyar, and E. Shwageraus. Axial discontinuity factors for the nodal diffusion analysis of high conversion BWR cores. *Annals of Nuclear Energy*, 62:129–136, dec 2013a. ISSN 03064549. doi:10.1016/j.anucene.2013.06.006.
- E. Fridman, J. Leppänen, and C. Wemple. Comparison of serpent and HELIOS-2 as applied for the PWR few-group cross section generation. *M&C 2013*, pages 693–703, 2013b. URL <http://www.scopus.com/inward/record.url?eid=2-s2.0-84883317165&partnerID=tZOtx3y1>.
- E. Fridman, R. Rachamin, and E. Shwageraus. Generation of SFR few-group constants using the Monte Carlo code serpent. In *International Conference on Mathematics and Computational Methods Applied to Nuclear Science and Engineering, M and C 2013*, volume 4, pages 2978–2985, 2013c. ISBN 9781627486439.
- B. Gallet and R. Venot. Fuel assembly support column for a nuclear reactor diagrid, 1977. URL <https://www.google.de/patents/US4016035>.
- G. Geffraye, O. Antoni, M. Farvacque, D. Kadri, G. Lavialle, B. Rameau, and A. Ruby. CATHARE 2 V2.5_2: A single version for various applications. *Nuclear Engineering and Design*, 241(11):4456–4463, nov 2011. ISSN 00295493. doi:10.1016/j.nucengdes.2010.09.019.
- J. C. Gehin. *A quasi-static polynomial nodal method for nuclear reactor analysis*. Ph.d., Massachusetts Institute of Technology, 1992. URL <http://hdl.handle.net/1721.1/17309>.
- M. Gentili, B. Fontaine, and G. Rimpault. Deformed Core Reactivity Evaluation with Mesh Projection-Based Method. *Nuclear Technology*, 192(1):11–24, 2015. doi:dx.doi.org/10.13182/NT14-123.

Bibliography

- L. K. Ghasabyan. *Use of Serpent Monte-Carlo code for development of 3D full-core models of Gen-IV fast-spectrum reactors and preparation of group constants for transient analyses with PARCS/TRACE coupled system*. Master's thesis, KTH, Physics, 2013. URL <http://urn.kb.se/resolve?urn=urn:nbn:se:kth:diva-118072>.
- A. M. Gomez-Torres, V. H. Sanchez-Espinoza, K. Ivanov, and R. Macian-Juan. DYN SUB: A high fidelity coupled code system for the evaluation of local safety parameters – Part I: Development, implementation and verification. *Annals of Nuclear Energy*, 48:108–122, 2012. ISSN 03064549. doi:10.1016/j.anucene.2012.05.011.
- G. Grasso, C. Petrovich, D. Mattioli, C. Artioli, P. Sciora, D. Gugiu, G. Bandini, E. Bubelis, and K. Mikityuk. The core design of ALFRED, a demonstrator for the European lead-cooled reactors. *Nuclear Engineering and Design*, 278:287–301, oct 2014. ISSN 0029-5493. doi:10.1016/J.NUCENGDES.2014.07.032.
- U. Grundmann and S. Mittag. Super-homogenisation factors in pinwise calculations by the reactor dynamics code DYN3D. *Annals of Nuclear Energy*, 38(10):2111–2119, oct 2011. ISSN 03064549. doi:10.1016/j.anucene.2011.06.030.
- U. Grundmann, U. Rohde, S. Mittag, and S. Kliem. *DYN3D version 3.2 - Code for calculation of transients in light water reactors (LWR) with hexagonal or quadratic fuel elements - description of models and methods*. Wissenschaftlich-Technische Berichte, Forschungszentrum Rossendorf, Dresden, Germany, 2005. URL <https://www.hzdr.de/publications/Publ-7586>.
- A. Hall, Y. Xu, A. Ward, T. Downar, K. Shirvan, and M. Kazimi. Advanced neutronics methods for analysis of the RBWR-AC. In *Transactions of the American Nuclear Society*, volume 108, pages 771–774. American Nuclear Society, 2013. URL <http://www.scopus.com/inward/record.url?eid=2-s2.0-84896535910&partnerID=tZOtx3y1>.
- M. L. Hamilton, D. S. Genes, G. D. Johns, and W. F. Brown. Fabrication Technological Development of the Oxide Dispersion Strengthened Alloy MA957 for Fast Reactor Applications. Technical report, U.S. Department of Energy, 2000.
- A. Hebert and P. Benoist. A consistent technique for the global homogenization of a pressurized water reactor assembly. *Nuclear Science and Engineering*, 109:360–372, 1991. URL http://inis.iaea.org/Search/search.aspx?orig_q=RN:23059575.

- A. Hebert and G. Mathonniere. Development of a third-generation superhomogenisation method for the homogenization of a pressurized water reactor assembly. *Nuclear Science and Engineering*, 115:129–141, 1993. URL http://inis.iaea.org/Search/search.aspx?orig_q=RN:25018811.
- W. Heo and Y. Kim. A new Monte Carlo-Deterministic two-step method for fast reactor diffusion analysis. In *Physor 2014*, Kyoto, 2014.
- B. R. Herman and E. Shwageraus. Application of axial discontinuity factors for high conversion water reactors. In *Transactions of the American Nuclear Society*, volume 105, pages 855–857, 2011.
- L. Holt, U. Rohde, M. Seidl, A. Schubert, P. Van Uffelen, and R. Macián-Juan. Two-way coupling between the reactor dynamics code DYN3D and the fuel performance code TRANSURANUS at assembly level. In *22nd International Conference on Nuclear Engineering (ICONE22)*, Prague, Czech Republic, 2014. ASME. doi:10.1115/ICONE22-30812.
- L. Holt, U. Rohde, M. Seidl, A. Schubert, P. Van Uffelen, and R. Macián-Juan. Development of a general coupling interface for the fuel performance code TRANSURANUS – Tested with the reactor dynamics code DYN3D. *Annals of Nuclear Energy*, 84: 73–85, 2015. ISSN 03064549. doi:10.1016/j.anucene.2014.10.040.
- L. Holt, U. Rohde, S. Kliem, S. Baier, M. Seidl, P. Van Uffelen, and R. Macián-Juan. Investigation of feedback on neutron kinetics and thermal hydraulics from detailed online fuel behavior modeling during a boron dilution transient in a PWR with the two-way coupled code system DYN3D-TRANSURANUS. *Nuclear Engineering and Design*, 297:32–43, 2016. ISSN 00295493. doi:10.1016/j.nucengdes.2015.11.005.
- H. H. Hummel and D. Okrent. *Reactivity coefficients in large fast power reactors*. Monograph series on nuclear science and technology. American Nuclear Society, United States, 1970.
- M. Hursin, A. Vasiliev, H. Ferroukhi, and A. Pautz. Comparison of SERPENT and CASMO-5M for pressurized water reactors models. In *International Conference on Mathematics and Computational Methods Applied to Nuclear Science and Engineering, M&C 2013*, Sun Valley, 2013.

Bibliography

- IAEA. *Fast Reactor Database 2006 Update*. International Atomic Energy Agency, Vienna, 2006. ISBN 92-0-114206-4. URL <http://www-pub.iaea.org/books/IAEABooks/7581/Fast-Reactor-Database-2006-Update>.
- IAEA. *Status of Fast Reactor Research and Technology Development, IAEA-TECDOC-1691*. International Atomic Energy Agency, Vienna, Austria, 2012. ISBN 978-92-0-130610-4.
- IAEA. *Benchmark Analyses on the Natural Circulation Test Performed During the PHENIX End-of-Life Experiments, IAEA-TECDOC-1703*. International Atomic Energy Agency, Vienna, Austria, 2013. ISBN 978-92-0-139610-5.
- IAEA. *Benchmark Analyses on the Control Rod Withdrawal Tests Performed during the PHENIX End-of-Life Experiments, IAEA-TECDOC-1742*. International Atomic Energy Agency, Vienna, Austria, 2014. ISBN 978-92-0-105314-5.
- IAEA. *Fast Reactors and Related Fuel Cycles: Safe Technologies and Sustainable Scenarios (FR13)*. Proceedings Series. International Atomic Energy Agency, Vienna, 2015. ISBN 978-92-0-104114-2.
- IAEA. *Benchmark Analysis of EBR-II Shutdown Heat Removal Tests*. INTERNATIONAL ATOMIC ENERGY AGENCY, Vienna, 2017a. ISBN 978-92-0-105517-0. URL <http://www-pub.iaea.org/books/IAEABooks/12247/Benchmark-Analysis-of-EBR-II-Shutdown-Heat-Removal-Tests>.
- IAEA. *Nuclear Power Reactors in the World*. Number 2 in Reference Data Series. International Atomic Energy Agency, Vienna, 2017b. ISBN 978-92-0-104017-6. URL <https://www-pub.iaea.org/books/IAEABooks/12237/Nuclear-Power-Reactors-in-the-World-2017-Edition>.
- IAEA. Benchmark Analysis of FFTF Loss Of Flow Without Scram Test (I32011), 2018a. URL <https://www.iaea.org/newscenter/news/new-crp-benchmark-analysis-of-fftf-loss-of-flow-without-scram-test-i32011>.
- IAEA. Power Reactor Information System, 2018b. URL <http://www.iaea.org/pris>. Accessed: 2018-08-07.
- G. Ilas and F. Rahnema. A Monte Carlo based nodal diffusion model for criticality analysis of spent fuel storage lattices. *Annals of Nuclear Energy*, 30(10):1089–1108, jul 2003. ISSN 03064549. doi:10.1016/S0306-4549(03)00037-9.

- U. Imke, D. Struwe, H. Niwa, I. Sato, F. Camous, and D. Moxon. Status of the SAS4A-code development for consequence analysis of core disruptive accidents. In *Proceedings of an International Topical Meeting on Sodium Cooled Fast Reactor Safety*, Obninsk, Russia, 1994.
- A. Kavenoky. The SPH Homogenization Method. In *A Specialists' Meeting on Homogenization Methods in Reactor Physics, IAEA-TECDOC-231*, Lugano, 1978.
- S. Kliem, Y. Kozmenkov, T. Höhne, and U. Rohde. Analyses of the V1000CT-1 benchmark with the DYN3D/ATHLET and DYN3D/RELAP coupled code systems including a coolant mixing model validated against CFD calculations. *Progress in Nuclear Energy*, 48(8):830–848, 2006. ISSN 01491970. doi:10.1016/j.pnucene.2006.06.008.
- S. Kliem, A. Gommlich, A. Grahn, U. Rohde, J. Schütze, T. Frank, A. Gomez, and V. Sanchez. Development of multi-physics code systems based on the reactor dynamics code DYN3D. *Kerntechnik*, 76(3):160–165, jul 2011. ISSN 0932-3902. doi:10.3139/124.110146.
- S. Kliem, Y. Kozmenkov, J. Hadek, Y. Perin, F. Fouquet, F. Bernard, A. Sargeni, D. Cuervo, A. Sabater, S. Sanchez-Cervera, N. Garcia-Herranz, O. Zerkak, H. Ferroukhi, and P. Mala. Testing the NURESIM platform on a PWR main steam line break benchmark. *Nuclear Engineering and Design*, 321:8–25, sep 2017. ISSN 0029-5493. doi:10.1016/J.NUCENGDES.2017.05.028.
- M. Knebel, L. Mercatali, V. Sanchez, R. Stieglitz, and R. Macian-Juan. Validation of the Serpent 2-DYNSUB code sequence using the Special Power Excursion Reactor Test III (SPERT III). *Annals of Nuclear Energy*, 91:79–91, may 2016. ISSN 03064549. doi:10.1016/j.anucene.2016.01.005.
- K. Koebke. A new approach to homogenization and group condensation. Technical report, IAEA-TECDOC-231, 1978. URL https://inis.iaea.org/search/search.aspx?orig_q=RN:12619334.
- T. Kozlowski and T. Downar. PWR MOX/UO₂ Core Transient Benchmark. Technical report, OECD/NEA, 2007. URL https://www.oecd-neo.org/science/wprs/MOX-UOX-transients/benchmark_documents/final_report/mox-uo2-bench.pdf.
- Y. Kozmenkov, Y. Orekhov, U. Grundmann, S. Kliem, U. Rohde, and A. Seidel. Development and benchmarking of the DYN3D/RELAP5 code system. In *Annual*

Bibliography

- meeting on nuclear technology 2001*, 2001. URL http://inis.iaea.org/Search/search.aspx?orig_q=RN:32052345.
- Y. Kozmenkov, S. Kliem, and U. Rohde. Validation and verification of the coupled neutron kinetic/thermal hydraulic system code DYN3D/ATHLET. *Annals of Nuclear Energy*, 84:153–165, 2015. ISSN 03064549. doi:10.1016/j.anucene.2014.12.012.
- A. Lázaro, L. Ammirabile, G. Bandini, G. Darmet, S. Massara, P. Dufour, A. Tosello, E. Gallego, G. Jimenez, K. Mikityuk, M. Schikorr, E. Bubelis, A. Ponomarev, R. Kruessmann, and M. Stempniewicz. Code assessment and modelling for Design Basis Accident Analysis of the European sodium fast reactor design. Part I: System description, modelling and benchmarking. *Nuclear Engineering and Design*, 266:1–16, jan 2014a. ISSN 00295493. doi:10.1016/j.nucengdes.2013.10.019.
- A. Lázaro, M. Schikorr, K. Mikityuk, L. Ammirabile, G. Bandini, G. Darmet, D. Schmitt, P. Dufour, A. Tosello, E. Gallego, G. Jimenez, E. Bubelis, A. Ponomarev, R. Kruessmann, D. Struwe, and M. Stempniewicz. Code assessment and modelling for Design Basis Accident analysis of the European Sodium Fast Reactor design. Part II: Optimised core and representative transients analysis. *Nuclear Engineering and Design*, 277:265–276, oct 2014b. ISSN 00295493. doi:10.1016/j.nucengdes.2014.02.029.
- C. Lee and W. S. Yang. MC2-3: Multigroup Cross Section Generation Code for Fast Reactor Analysis. *Nuclear Science and Engineering*, 187(3):268–290, sep 2017. ISSN 0029-5639. doi:10.1080/00295639.2017.1320893.
- K. B. Lee, H. G. Joo, B.-o. Cho, and S.-q. Zee. Correction of the Control Rod Cusping Effect Using One-Dimensional Fine Mesh Flux Profiles. In *Korean Nuclear Society autumn meeting*, Seoul, 1998.
- E. Lemarchand, M. Klein, I. Pasichnyk, K. Velkov, and W. Zwermann. Pin-by-pin calculations with QUABOX/CUBBOX using the super homogenization method. In *Annual meeting on nuclear technology 2012*, Stuttgart, Germany, 2012. URL http://inis.iaea.org/Search/search.aspx?orig_q=RN:43117170.
- J. Leppänen. *Development of a New Monte Carlo reactor physics code*. PhD thesis, Helsinki University of Technology, 2007. ISBN 978-951-38-7019-5.
- J. Leppänen and R. Mattila. Validation of the Serpent-ARES code sequence using the MIT BEAVRS benchmark – HFP conditions and fuel cycle 1 sim-

- ulations. *Annals of Nuclear Energy*, 96:324–331, oct 2016. ISSN 03064549. doi:10.1016/j.anucene.2016.06.014.
- J. Leppänen, R. Mattila, and M. Pusa. Validation of the Serpent-ARES code sequence using the MIT BEAVRS benchmark – Initial core at HZP conditions. *Annals of Nuclear Energy*, 69:212–225, jul 2014. ISSN 03064549. doi:10.1016/j.anucene.2014.02.014.
- J. Leppänen, M. Pusa, T. Viitanen, V. Valtavirta, and T. Kaltiaisenaho. The Serpent Monte Carlo code: Status, development and applications in 2013. *Annals of Nuclear Energy*, 82:142–150, sep 2015. ISSN 03064549. doi:10.1016/j.anucene.2014.08.024.
- J. Leppänen, M. Pusa, and E. Fridman. Overview of methodology for spatial homogenization in the Serpent 2 Monte Carlo code. *Annals of Nuclear Energy*, 96:126–136, oct 2016. ISSN 03064549. doi:10.1016/j.anucene.2016.06.007.
- G. Lerchl, H. Austregesilo, P. Schöffel, D. von der Cron, and F. Weyermann. *ATHLET Mod 3.0 Cycle A. User's Manual, GRS - P - 1 / Vol. 1 Rev. 6*. GRS, Garching bei München, Germany, 2012.
- M. Marchetti. *Neutronics Methods for Transient and Safety Analysis of Fast Reactors*. PhD thesis, Karlsruher Institut für Technologie (KIT), 2017. ISBN 9783731506119. doi:10.5445/KSP/1000063691.
- R. Michal. Fifty years ago in December: Atomic reactor EBR-I produced first electricity. *Nuclear News*, 44(12):28–29, 2001. ISSN 0029-5574. URL <http://www2.ans.org/pubs/magazines/nn/docs/2001-11-2.pdf>.
- K. Mikityuk and A. Shestopalov. FRED fuel behaviour code: Main models and analysis of Halden IFA-503.2 tests. *Nuclear Engineering and Design*, 241(7):2455–2461, jul 2011. ISSN 00295493. doi:10.1016/j.nucengdes.2011.04.033.
- K. Mikityuk, S. Pelloni, P. Coddington, E. Bubelis, and R. Chawla. FAST: An advanced code system for fast reactor transient analysis. *Annals of Nuclear Energy*, 32(15):1613–1631, oct 2005. ISSN 03064549. doi:10.1016/j.anucene.2005.06.002.
- K. Mikityuk, E. Girardi, J. Krepel, E. Bubelis, E. Fridman, A. Rineiski, N. Girault, F. Payot, L. Buligins, G. Gerbeth, N. Chauvin, C. Latge, and J.-C. Garnier. ESFR-SMART: new Horizon-2020 project on SFR safety. In *FR17 - International Conference on Fast Reactors and Related Fuel Cycles: Next Generation Nuclear Systems for Sustainable Development*, Yekaterinburg, Russian Federation, jun 2017.

Bibliography

- T. E. Narasimhan. Kalpakkam Prototype Fast Breeder Reactor to go critical by end of 2016. *Business Standard*, apr 2016. URL <http://mybs.in/2TDtBAJ>.
- NEA. *Nuclear Energy Outlook (NEO)*. OECD Publishing, 2008. ISBN 978-92-64-05410-3. URL <https://www.oecd-neo.org/pub/2008/6436-nuclear-energy-outlook-2008.pdf>.
- NEA. *Technology Roadmap Update for Generation IV Nuclear Energy Systems*. OECD Publishing, 2014. URL <https://www.gen-4.org/gif/upload/docs/application/pdf/2014-03/gif-tru2014.pdf>.
- NEA. Benchmark for Neutronic Analysis of Sodium-cooled Fast Reactor Cores with Various Fuel Types and Core Sizes, NEA/NSC/R(2015)9. Technical Report February, OECD Nuclear Energy Agency, 2016a. URL <https://www.oecd-neo.org/science/docs/2015/nsc-r2015-9.pdf>.
- NEA. *Uranium 2016: Resources, Production and Demand*. OECD Publishing, 2016b. ISBN 9789264268449. doi:[dx.doi.org/10.1787/uranium-2016-en](https://doi.org/10.1787/uranium-2016-en).
- NERAC and GIF. A Technology Roadmap for Generation IV Nuclear Energy Systems. Technical report, Issued by the US-DOE Nuclear Energy Research Advisory Committee (NERAC) and the Generation IV International Forum (GIF), 2002. URL https://www.gen-4.org/gif/jcms/c_40481/technology-roadmap.
- K. Okumura, Y. Oka, and Y. Ishiwatari. Nuclear Reactor Calculations. In Y. Oka, editor, *Nuclear Reactor Design, An Advanced Course in Nuclear Engineering*, chapter 2, pages 49–126. Springer Japan, 2014. ISBN 978-4-431-54897-3. doi:[10.1007/978-4-431-54898-0_2](https://doi.org/10.1007/978-4-431-54898-0_2).
- G. Palmiotti, J. Rieunier, C. Gho, and M. Salvatores. BISTRO Optimized Two Dimensional Sn Transport Code. In *Topical Meeting on Advances in Reactor Physics, Mathematics and Computation*, Paris, France, 1987.
- G. Palmiotti, E. E. Lewis, and C. B. Carrico. VARIANT: VARIational Anisotropic Nodal Transport for Multidimensional Certesian and Hexagonal Geometry Calculation, oct 1996. URL https://inis.iaea.org/search/search.aspx?orig_q=RN:27049245.
- V. Pascal, G. Prulhière, M. Vanier, and B. Fontaine. Interpretation of the Control Rod Withdrawal Test in the Sodium-Cooled Fast Reactor Phénix. *Nuclear Science and Engineering*, 175(2):109–123, oct 2013. ISSN 0029-5639. doi:[10.13182/NSE12-19](https://doi.org/10.13182/NSE12-19).

- C. Patricot, D. Broc, E. Hourcade, and K. Ammar. APOLLO3 based method for 3D warped cores calculations – Application to flowering tests of Phenix. In *Physor 2014*, Kyoto, Japan, 2014.
- C. Patricot, A.-M. Baudron, O. Fandeur, and D. Broc. Neutronic calculation of deformed cores: Development of a time-dependent diffusion solver in CAST3M, a mechanics dedicated finite element code. In *PHYSOR 2016*, volume 1, pages 583–592, 2016.
- S. Pelloni and K. Mikityuk. A new cross-section generation model in the FAST code system and its application to gas- and sodium-cooled Generation IV fast reactors. *Annals of Nuclear Energy*, 38(1):1–13, jan 2011. ISSN 03064549. doi:10.1016/j.anucene.2010.08.009.
- V. V. Petrochenko, S. A. Grigoriev, O. G. Komlev, A. V. Kondaurov, and G. I. Toshinsky. SVBR Project : status and possible development. In *International Conference on Fast Reactors and Related Fuel Cycles: Next Generation Nuclear Systems for Sustainable Development (FR17)*, Yekaterinburg, Russian Federation, 2017. IAEA. URL <https://www.iaea.org/sites/default/files/fr17-programme.pdf>.
- H. P. Planchon, R. M. Singer, D. Mohr, E. E. Feldman, L. K. Chang, and P. R. Betten. The experimental breeder reactor II inherent shutdown and heat removal tests — results and analysis. *Nuclear Engineering and Design*, 91(3):287–296, 1986. ISSN 00295493. doi:10.1016/0029-5493(86)90082-8.
- A. Ponomarev. *Improved methodologies for evaluation of severe transient conditions of sodium-cooled fast systems*. PhD thesis, Karlsruhe Institut für Technologie, 2017. doi:10.5445/IR/1000069106.
- A. Ponomarev and V. Sanchez. Modeling of reactivity effects and non-uniform axial expansion of SFR core on basis of neutronics model with constant calculation mesh. In *International Congress on Advances in Nuclear Power Plants, ICAPP 2014*, pages 1184–1190, 2014.
- J. Pounders, F. Rahnema, and G. Ilas. CANDU core calculations with Monte Carlo based homogenized cross sections. In *Transactions of the American Nuclear Society*, volume 92, pages 525–527, 2005.
- R. Rachamin, C. Wemple, and E. Fridman. Neutronic analysis of SFR core with HELIOS-2, Serpent, and DYN3D codes. *Annals of Nuclear Energy*, 55:194–204, may 2013. ISSN 03064549. doi:10.1016/j.anucene.2012.11.030.

Bibliography

- A. Rais, D. Siefman, M. Hursin, A. Ward, and A. Pautz. Neutronics modeling of the CROCUS reactor with SERPENT and PARCS codes. In *M&C 2017 - International Conference on Mathematics & Computational Methods Applied to Nuclear Science & Engineering*, Jeju, Korea, 2017. ISBN 9789790971424. doi:10.2527/jas2012-5761.
- E. L. Redmond. *Multigroup cross section generation via Monte Carlo methods*. PhD thesis, Massachusetts Institute of Technology, 1997. URL <http://hdl.handle.net/1721.1/10405>.
- M. Reed, K. Smith, and B. Forget. The “Virtual Density” Theory of Neutronics: A Generic Method For Geometry Distortion Reactivity Coefficients. In *PHYSOR 2014*, pages 1–20, Kyoto, Japan, 2014.
- G. Rimpault, P. Ribon, M. Grimstone, C. Dean, B. Thom, and C. Cavarec. Validation of new sub-group algorithms for resonance self-shielding in heterogeneous structures, 1989. URL https://inis.iaea.org/search/search.aspx?orig_q=RN:22032416.
- G. Rimpault, D. Plisson, J. Tommasi, R. Jacqmin, J.-M. Rieunier, D. Verrier, and D. Biron. The ERANOS code and data system for fast reactor neutronic analyses. In *Physor 2002*, Seoul, Korea, 2002.
- A. Rineiski and J.-Y. Doriath. Time-dependent Neutron Transport with Variational Nodal Method. In *M&C '97 International Conference*, Saratoga Springs, NY, USA, 1997.
- U. Rohde. The modeling of fuel rod behaviour under RIA conditions in the code DYN3D. *Annals of Nuclear Energy*, 28(13):1343–1363, 2001. ISSN 03064549. doi:10.1016/S0306-4549(00)00128-6.
- U. Rohde, S. Kliem, U. Grundmann, S. Baier, Y. Bilodid, S. Duerigen, E. Fridman, A. Gommlich, A. Grahn, L. Holt, Y. Kozmenkov, and S. Mittag. The reactor dynamics code DYN3D – models, validation and applications. *Progress in Nuclear Energy*, 89: 170–190, 2016. ISSN 01491970. doi:10.1016/j.pnucene.2016.02.013.
- J. Rouault, P. Chellapandi, B. Raj, P. Dufour, C. Latge, L. Paret, P. L. Pinto, G. H. Rodriguez, G.-M. Gautier, G.-L. Fiorini, M. Pelletier, D. Gosset, S. Bourganel, G. Mignot, F. Varaine, B. Valentin, P. Masoni, P. Martin, J.-C. Queval, D. Broc, and N. Devictor. Sodium Fast Reactor Design: Fuels, Neutronics, Thermal-Hydraulics, Structural

- Mechanics and Safety. In D. G. Cacuci, editor, *Handbook of Nuclear Engineering*, pages 2321–2710. Springer US, Boston, MA, 2010. ISBN 978-0-387-98149-9. doi:10.1007/978-0-387-98149-9_21.
- J. Rouault, E. Abonneau, D. Settimo, J.-M. Hamy, H. Hayafune, R. Gefflot, R.-P. Bernard, O. Mandement, T. Chauveau, G. Lambert, P. Audouin, H. Mochida, T. Iitsuka, M. Fukuie, J. Molyneux, and J.-L. Mazel. ASTRID, The SFR GENIV Technology Demonstrator Project: Where Are We, Where Do We Stand For? In *ICAPP 2015*, pages 824–831, Nice, France, 2015.
- J. M. Ruggieri, J. Tommasi, J. F. Lebrat, C. Suteau, D. Plisson-Rieunier, C. De Saint Jean, G. Rimpault, and J. C. Sublet. ERANOS 2.1: International code system for GEN IV fast reactor analysis. In *Proceedings of the 2006 International Congress on Advances in Nuclear Power Plants, ICAPP'06*, pages 2432–2439, Reno, 2006.
- M. Schneider. Fast Breeder Reactors in France. *Science & Global Security*, 17(1):36–53, jun 2009. ISSN 0892-9882. doi:10.1080/08929880902953013.
- H. Schulz. Configuration of the HPC clusters at the HZDR, 2017. URL <https://www.hzdr.de/db/Cms?pOid=29813&pNid=1615>. Accessed: 2017-07-21.
- SCK•CEN. MYRRHA: Multi-purpose hybrid research reactor for high-tech applications, 2016. URL <http://myrrha.sckcen.be/>. Accessed: 2016-08-03.
- S. B. Shikhov. Perturbation theory formulas for the effect of the dimensions on the critical mass in a fast reactor. *The Soviet Journal of Atomic Energy*, 6(2):90–94, sep 1960. ISSN 1063-4258. doi:10.1007/BF01836107.
- D. J. Siefman, G. Girardin, A. Rais, A. Pautz, and M. Hursin. Full Core modeling techniques for research reactors with irregular geometries using Serpent and PARCS applied to the CROCUS reactor. *Annals of Nuclear Energy*, 85:434–443, nov 2015. ISSN 0306-4549. doi:10.1016/j.anucene.2015.05.004.
- K. Smith. Assembly homogenization techniques for light water reactor analysis. *Progress in Nuclear Energy*, 17(3):303–335, 1986. ISSN 01491970. doi:10.1016/0149-1970(86)90035-1.
- K. Smith. Nodal diffusion methods: Understanding numerous unpublished details. In *PHYSOR 2016*, Sun Valley, ID, 2016.

Bibliography

- K. S. Smith. *Spatial homogenization methods for light water reactor analysis*. PhD thesis, Massachusetts Institute of Technology, 1980. URL <http://hdl.handle.net/1721.1/16042>.
- M. A. Smith, C. Adams, W. S. Yang, and E. E. N. E. D. Lewis. VARI3D & PERSENT: Perturbation and Sensitivity Analysis. Technical report, Argonne National Laboratory (ANL), United States, aug 2013.
- N. Soppera, M. Bossant, and E. Dupont. JANIS 4: An Improved Version of the NEA Java-based Nuclear Data Information System. *Nuclear Data Sheets*, 120:294–296, jun 2014. ISSN 00903752. doi:10.1016/j.nds.2014.07.071.
- R. Stainsby, K. Peers, C. Mitchell, C. Poette, K. Mikityuk, and J. Somers. Gas cooled fast reactor research in Europe. *Nuclear Engineering and Design*, 241(9):3481–3489, sep 2011. ISSN 0029-5493. doi:10.1016/J.NUCENGDES.2011.08.005.
- R. J. J. Stammler and M. J. Abbate. *Methods of steady-state reactor physics in nuclear design*. Academic Press, London, 1983. URL https://inis.iaea.org/search/search.aspx?orig_q=RN:14807060.
- K. Sun, J. Krepel, K. Mikityuk, S. Pelloni, and R. Chawla. Void reactivity decomposition for the Sodium-cooled Fast Reactor in equilibrium fuel cycle. *Annals of Nuclear Energy*, 38(7):1645–1657, jul 2011. ISSN 03064549. doi:10.1016/j.anucene.2011.02.018.
- T. Takeda. Improvement of Neutronics Calculation Methods for Fast Reactors. *Progress in Nuclear Science and Technology*, 2:289–293, oct 2011. ISSN 2185-4823. doi:10.15669/pnst.2.289.
- T. Takeda, H. Imai, T. Kitada, H. Nishi, J. Ishibashi, and A. Kitano. Development of 3-D Detailed FBR Core Calculation Method Based on Method of Characteristics. In *Mathematics and Computation, Supercomputing, Reactor Physics and Nuclear and Biological Applications*, Palais des Papes, Avignon, France, 2005.
- D. Tenchine, R. Baviere, P. Bazin, F. Ducros, G. Geffraye, D. Kadri, F. Perdu, D. Pialla, B. Rameau, and N. Tauveron. Status of CATHARE code for sodium cooled fast reactors. *Nuclear Engineering and Design*, 245:140–152, apr 2012. ISSN 00295493. doi:10.1016/j.nucengdes.2012.01.019.
- G. Van den Eynde, E. Malambu, A. Stankovskiy, R. Fernandez, and P. Baeten. An updated core design for the multi-purpose irradiation facility MYRRHA. *Journal*

- of Nuclear Science and Technology*, 52(7-8):1053–1057, aug 2015. ISSN 0022-3131. doi:10.1080/00223131.2015.1026860.
- S. S. Van der Marck, J. C. Kuijper, and J. Oppe. Homogenized group cross sections by Monte Carlo. In *PHYSOR-2006 - American Nuclear Society's Topical Meeting on Reactor Physics*, Vancouver, 2006. ISBN 0894486977 | 9780894486975.
- C. Venard, T. Beck, B. Bernardin, A. Conti, D. Gentet, P. Lamagnere, P. Sciora, D. Lorenzo, A. Tosello, M. Vanier, A.-C. Scholer, D. Verrier, F. Barjot, and D. Schmitt. The ASTRID core at the midterm of the conceptual design phase (AVP2). In *ICAPP 2015*, pages 651–659, Nice, France, 2015.
- A. E. Waltar, D. R. Todd, and P. V. Tsvetkov. *Fast Spectrum Reactors*. Springer Science+Business Media, 2012. ISBN 9781441995711. doi:10.1007/978-1-4419-9572-8.
- WNN. Consortium established to build Alfred, 2013. URL <http://www.world-nuclear-news.org/NN-Consortium-established-to-build-Alfred-2012134.htm>. Accessed: 2016-08-03.
- WNN. TerraPower, CNNC team up on travelling wave reactor, 2015. URL <http://www.world-nuclear-news.org/NN-TerraPower-CNNC-team-up-on-travelling-wave-reactor-25091501.html>. Accessed: 2016-07-29.
- WNN. Russia's BN-800 unit brought to minimum controlled power, aug 2016a. URL <http://www.world-nuclear-news.org/NN-Russias-BN-800-unit-brought-to-minimum-controlled-power-04081501.html>.
- WNN. Russia's MBIR gets construction licence, 2016b. URL <http://www.world-nuclear-news.org/NN-Russias-MBIR-gets-construction-licence-15051501.html>. Accessed: 2016-07-28.
- WNN. Russia completes TVS 5 tests, 2016c. URL <http://www.world-nuclear-news.org/NN-Russia-completes-TVS-5-tests-22101401.html>. Accessed: 2016-08-02.

Thesis-related publications

Peer-reviewed journal papers

E. Nikitin and E. Fridman. Extension of the reactor dynamics code DYN3D to SFR applications – Part I: Thermal expansion models. *Annals of Nuclear Energy*, 119: 382–389, sep 2018a. ISSN 03064549. doi:10.1016/j.anucene.2018.05.015.

E. Nikitin and E. Fridman. Extension of the reactor dynamics code DYN3D to SFR applications – Part II: Validation against the Phenix EOL control rod withdrawal tests. *Annals of Nuclear Energy*, 119:411–418, sep 2018b. ISSN 03064549. doi:10.1016/j.anucene.2018.05.016.

E. Nikitin and E. Fridman. Extension of the reactor dynamics code DYN3D to SFR applications – Part III: Validation against the initial phase of the Phenix EOL natural convection test. *Annals of Nuclear Energy*, 119:390–395, sep 2018c. ISSN 03064549. doi:10.1016/j.anucene.2018.05.017.

E. Nikitin, E. Fridman, and K. Mikityuk. Solution of the OECD/NEA neutronic SFR benchmark with Serpent-DYN3D and Serpent-PARCS code systems. *Annals of Nuclear Energy*, 75:492–497, jan 2015a. ISSN 03064549. doi:10.1016/j.anucene.2014.08.054.

E. Nikitin, E. Fridman, and K. Mikityuk. On the use of the SPH method in nodal diffusion analyses of SFR cores. *Annals of Nuclear Energy*, 85:544–551, nov 2015b. ISSN 03064549. doi:10.1016/j.anucene.2015.06.007.

Conference papers

- E. Nikitin and E. Fridman. Axial fuel rod expansion model in nodal code DYN3D for SFR application. In *PHYSOR 2016*, pages 3241–3251, 2016.
- E. Nikitin and E. Fridman. Modeling of Phenix End-of-Life control rod withdrawal tests with the Serpent-DYN3D code system, IAEA-CN-245-18. In *International Conference on Fast Reactors and Related Fuel Cycles: Next Generation Nuclear Systems for Sustainable Development (FR17)*, 2017.

Evgeny Nikitin

Weimarische Str. 18
01127 Dresden, Germany

+49 160 950 69535 | evgeny.nikitin@gmail.com
<https://www.linkedin.com/in/evgenynikitinphd>

EDUCATION

- **Ph.D. in Nuclear Engineering** (2015 - 2019)
École Polytechnique Fédérale de Lausanne, Switzerland.
- **Master in Physics** – specialized in Nuclear Techniques (2011 - 2013)
Budapest University of Technology and Economics, Hungary.
- **Bachelor in Physics** – specialized in Applied Physics (2007 - 2011)
Budapest University of Technology and Economics, Hungary.

PROFESSIONAL EXPERIENCE

- **Scientific researcher** (2017 - 2019 September)
Helmholtz-Zentrum Dresden-Rossendorf, Germany. Computational safety analyses of nuclear reactors and code development. Involved in HORIZON 2020 projects: the European Sodium Fast Reactor Safety Measures Assessment and Research Tools (ESFR-SMART), and the High-Performance Monte Carlo Methods for SAFETY Demonstration (McSAFE).
- **Scientific employee with the possibility of preparation for Ph.D.** (2013 - 2017)
Helmholtz-Zentrum Dresden-Rossendorf, Germany. Extension of the reactor dynamics code DYN3D to SFR applications.
- **Internship** (Summer 2012)
Helmholtz-Zentrum Dresden-Rossendorf, Germany. Neutronic benchmarking with reactor dynamics code DYN3D and FEM-based neutron diffusion code TRIVAC.

TECHNICAL SKILLS

- **Software:** Windows and Linux OS, \LaTeX , Microsoft Office Tools and Visual Studio, Origin.
- **Programming:** ANSI C, Fortran, Matlab, Python.
- **Nuclear reactor analysis tools:** Serpent, DYN3D, TRIVAC, APROS, ANSYS CFX.

LANGUAGE SKILLS

- **Russian:** native speaker.
- **English:** fluent.
- **Hungarian:** native language.
- **German:** good command.

PROFESSIONAL TRAINING

- *Iterative Linear Solvers and Parallelization* (February 2016) High Performance Computing Center Stuttgart (HLRS), Germany.
- *Frédéric Joliot/Otto Hahn Summer School on Nuclear Reactors – Tomorrow's Liquid Metal Fast Reactors: Towards Improved Safety and Performance* (August 2016) Aix-en-Provence, France.
- *EuroTech summer school on Integrated Approaches to Energy Systems* (June 2016) EPFL, Lausanne, Switzerland.
- *Fortran for Scientific Computing* (April 2016) at the High Performance Computing Center Stuttgart (HLRS), Germany.
- *WP5 lab session in the frame of the FREYA project* (February 2016) SCK-CEN, Mol, Belgium.
- *HLRS Parallel Programming Workshop – MPI, OpenMP and Tools* (February 2016) Centre for Information Services and High Performance Computing (ZIH), TU Dresden, Germany.
- *Topical day on generation and use of covariance data in nuclear energy applications* (December 2015) EC-JRC-IRMM, Geel, Belgium.
- *Frédéric Joliot/Otto Hahn Summer School on Nuclear Reactors – Bridging the Gap between Science and Industry* (August 2014) Aix-en-Provence, France.
- *ESNII+ summer school* (May 2014) KTH, Stockholm, Sweden.

